

# UC Irvine

## UC Irvine Electronic Theses and Dissertations

### Title

Mechanisms of non-apoptotic roles for apoptotic proteins in development of the chick auditory brainstem

### Permalink

<https://escholarship.org/uc/item/1sv1b1bv>

### Author

Weghorst, Forrest

### Publication Date

2022

### Copyright Information

This work is made available under the terms of a Creative Commons Attribution License, available at <https://creativecommons.org/licenses/by/4.0/>

Peer reviewed|Thesis/dissertation

UNIVERSITY OF CALIFORNIA,  
IRVINE

Mechanisms of non-apoptotic roles for apoptotic proteins  
in development of the chick auditory brainstem

DISSERTATION

submitted in partial satisfaction of the requirements  
for the degree of

DOCTOR OF PHILOSOPHY

in Biological Sciences

by

Forrest Weghorst

Dissertation Committee:  
Professor Karina Cramer, Chair  
Professor Susana Cohen-Cory  
Professor Leslie Thompson

2022

Figure 0.1 © 2016 Cramer and Rubel.  
Figure 0.3 © 2016 Rotschafer, Allen-Sharpley and Cramer.  
Chapter 1 © 2020 Weghorst, Mirzakhanyan, Samimi, Dhillon, Barzik, Cunningham,  
Gershon and Cramer.  
Chapter 2 © 2022 Weghorst, Mirzakhanyan, Hernandez, Gershon and Cramer.  
All other materials © 2022 Forrest Weghorst.

## DEDICATION

To my wife, Peace, for her undying love and support.  
I'm sorry you don't get to share the "doctor" title.

# TABLE OF CONTENTS

LIST OF FIGURES .....	iv
LIST OF TABLES .....	v
ACKNOWLEDGMENTS .....	vi
VITA .....	viii
ABSTRACT OF THE DISSERTATION .....	ix
Chapter 0 : Introduction.....	1
Chapter 1 : Caspase-3 cleaves extracellular vesicle proteins during auditory brainstem development .....	16
Chapter 2 : Non-apoptotic caspase activity preferentially targets a novel consensus sequence associated with cytoskeletal proteins in the developing auditory brainstem.....	52
Chapter 3 : Caspase activity regulates abundance of the long non-coding RNA CREVASSE in extracellular vesicles of the developing auditory brainstem .....	77
Chapter 4 : Conclusions and Future Directions .....	100
BIBLIOGRAPHY .....	106

# LIST OF FIGURES

Figure 0.1 - Anatomy and physiology of the avian auditory brainstem.....	2
Figure 0.2 - Apoptotic pathway.....	7
Figure 0.3 - The role of caspase-3 activity in development of the chick auditory brainstem.....	10
Figure 1.1 - Experimental workflow for caspase-3 substrate identification.....	19
Figure 1.2 - Caspase-3 is likely the most abundant caspase in the brainstem.....	21
Figure 1.3 - Auditory brainstem caspase substrates are enriched in datasets of known caspase-3 substrates, especially non-apoptotic datasets .....	23
Figure 1.4 - Functional annotation enrichment of auditory brainstem caspase-3 substrates. ....	25
Figure 1.5 - Purity of EV preparation. ....	27
Figure 1.6 - ABC3 substrates are enriched for EV proteins, and vice versa .....	32
Figure 1.7 - Embryonic chick auditory brainstems contain EVs. ....	34
Figure 1.8 - Caspase-3 and its substrates co-localize in the ITD circuit.....	37
Figure 2.1 - Caspase activity prefers a non-canonical consensus sequence in the non-apoptotic chick auditory brainstem .....	56
Figure 2.2 - The P2 position of the non-apoptotic auditory brainstem caspase consensus sequence is associated with substrates enriched for the GO term “Structural Constituent of Cytoskeleton” .....	58
Figure 2.3 - The GD motif is enriched among SCoC substrates in the apoptotic chick auditory brainstem, despite preference for the apoptotic VD motif. ....	61
Figure 2.4 - SCoC-specific motifs in the Degradase represent likely candidates for human non-apoptotic consensus sequences .....	65
Figure 3.1 - A long non-coding RNA is more abundant in EVs from caspase-inhibited brainstem than in EVs from control brainstems.....	79
Figure 3.2 - The transcripts of the caspase-regulated lncRNA do not match its Ensembl annotation.....	82
Figure 3.3 - Secondary structures of the isoforms of CREVASSE .....	83
Figure 3.4 - The four CREVASSE transcripts are expressed in the same proportion in EVs from caspase-inhibited and control brainstems .....	85
Figure 3.5 - EV proteins predicted to interact with CREVASSE are caspase substrates in the chick auditory brainstem .....	86
Figure 3.6 - CREVASSE binds RNAs involved in neural, brainstem, and auditory development .....	88
Figure 3.7 - Model by which caspase activity regulates loading of EVs with CREVASSE.....	92

## LIST OF TABLES

Table 1.1 - Identification of positive and negative EV markers in ABEV proteome .....	30
Table 1.2 - Antibody concentrations .....	51
Table 2.1 - Definition and derivation of variables used in hypergeometric tests for each P4-P2 motif in caspase consensus sequences .....	74

## ACKNOWLEDGMENTS

I extend my deepest gratitude to my advisor, Dr. Karina Cramer, for her scientific expertise, her endless patience, and for always believing in me. I came to UCI specifically so that I could work under her, and I have not been disappointed. I am a better scientist, writer, and person because I have worked in the Cramer lab, and I am endlessly grateful.

I also want to thank the members of my dissertation committee, Drs. Leslie Thompson and Susan Cohen-Cory, along with the members of my advancement committee, Drs. Oswald Stewart and Paul Gershon. Their feedback was invaluable in shaping the course of this project and in making sure I saw the forest through the chlorophyll.

Special thanks to Dr. Gershon and his student Yeva Mirzakhanyan, without whose collaboration this project would not have been possible.

Thanks to Drs. Vivek Swarup and Craig Stark for their instruction in programming, which contributed greatly to Chapters 2 and 3.

Thanks to my labmates, Sima Chokr and Giedre Milinkeviciute, and to my undergraduate students: Kian Samimi, Mehron Dhillon, Alireza Ansari, Avril Stulginski, Kiersten Hernandez, Shawyon Ezzati, and Garrison Faridi. Teamwork makes the dream work!

Chapter 1 of this dissertation is a reprint of the material as it appears in Weghorst et al., 2020, used with permission of the copyright holders (myself and my co-authors) under a [Creative Commons CC-BY license](#) (CC-BY 4.0). The co-authors of this publication are Yeva Mirzakhanyan, Kian Samimi, Mehron Dhillon, Melanie Barzik, Lisa Cunningham, Paul Gershon, and Karina Cramer. Some modifications to the text of the Results and Discussion of the cited article have been made to account for newer findings that have built upon prior ones. Some changes to figures and tables of the cited article were made to facilitate data presentation: Figure 3 and Table 2 of the

cited article were replaced by Figure 1.3 in this dissertation; Figure 4 in the cited article was not included in this dissertation; Figure 7 and Table 4 in the cited article were replaced by Figure 1.6 in this dissertation.

Chapter 2 of this dissertation is a reprint of the material as it appears in Weghorst et al., 2022, used with permission of the copyright holders (myself and my co-authors) under a [Creative Commons CC-BY license](#) (CC-BY 4.0). The co-authors of this publication are Yeva Mirzakhanyan, Paul Gershon, and Karina Cramer.

This work was supported in part by the Division of Intramural Research at the National Institute on Deafness and other Communication Disorders (NIH/NIDCD # ZIA DC000079), NIH SIG grant 1S10OD016328-01, NIH/NIDCD 010796, NIH R01DC010796, NIH 5T32DC010775, NIH F31DC019548, and seed funding from the UCI School of Biological Sciences.

# VITA

## Forrest Weghorst

2016 B.S. in Neuroscience and Behavior, University of Notre Dame  
2017-2019 UCI Center for Hearing Research Training Fellowship  
2018-2020 Teaching Assistant, Developmental Neurobiology  
2021-2022 Ruth L. Kirschstein Individual Predoctoral Fellowship  
2022 Ph.D. in Biological Sciences, University of California, Irvine

## FIELD OF STUDY

Molecular and Developmental Neurobiology

## PUBLICATIONS

**Weghorst**, Mirzakhanyan, Hernandez, Gershon and Cramer (2022). *Non-apoptotic caspase activity preferentially targets a novel consensus sequence associated with cytoskeletal proteins in the developing auditory brainstem*. *Frontiers in Cell and Developmental Biology*.

**Weghorst**, Mirzakhanyan, Samimi, Dhillon, Barzik, Cunningham, Gershon and Cramer (2020). *Caspase-3 cleaves extracellular vesicle proteins during auditory brainstem development*. *Frontiers in Cellular Neuroscience*.

**Weghorst** and Cramer (2019). *The evolution of hearing and balance*. *eLife*.

Mecklenburg, **Weghorst**, Freed and O'Tousa (2018). *Discordant responses to MAPK pathway stimulation include axonal growths in adult Drosophila photoreceptors*. *Frontiers in Molecular Neurosci*.

# ABSTRACT OF THE DISSERTATION

Mechanisms of non-apoptotic roles for apoptotic proteins  
in development of the chick auditory brainstem

by

Forrest Weghorst

Doctor of Philosophy in Biological Sciences

University of California, Irvine, 2022

Professor Karina Cramer, Chair

The auditory brainstem is specialized to localize sounds with extreme temporal precision, which requires highly accurate development of the circuit that facilitates this function. In the embryonic chicken, this circuit is comprised of the axonal projection from the cochlear nucleus (*nucleus magno-cellularis*; NM) to the monolayer coincidence detector *nucleus laminaris* (NL). Our lab has previously shown that formation of this circuit requires non-apoptotic activity of the apoptotic protease caspase-3. Pharmacological inhibition of caspase-3 activity in NM axons results in dual aberrant phenotypes: NM axons that overshoot NL, and NL cells that do not form a monolayer. How does caspase activity mediate auditory brainstem development?

We characterized the proteome of auditory brainstems that had been treated with caspase-3 inhibitor or vehicle, screening for peptides that bore the biochemical signature of caspase proteolysis and that were present in control brainstems but absent in caspase-inhibited brainstems. The 288 proteins with at least one such peptide (i.e. likely caspase-3 substrates) were disproportionately proteins associated with extracellular vesicles (EVs; membrane-bound nanoparticles that carry cargo and information between cells). We purified EVs from chick auditory brainstems and found that their contents were enriched for caspase substrates.

We next sought to determine how caspase activity occurs in the auditory brainstem without inducing apoptosis. One possibility was that caspases cleave proteins at different sites

than during apoptosis. We analyzed the cleavage sites of auditory brainstem caspase substrates and found that they were cleaved at a novel cleavage site: IX(G/R)D instead of DEVD. The proteins with (G/R)D cleavage sites were enriched for proteins associated with the cytoskeleton. The human apoptotic proteomic database Degradbase also showed evidence that specific motifs are associated with cytoskeletal proteins, suggesting that non-apoptotic caspase activity may cleave substrates at sites enriched in cytoskeletal proteins to change cell morphology without killing the cell.

Finally, based on the preponderance of EV proteins and RNA-binding proteins (RBPs) in caspase substrates, as well as the established enrichment of RBPs in EVs, we hypothesized that caspase activity controls the loading of RBPs (and therefore RNAs) into EVs. We sequenced the RNA of EVs derived from brainstems treated with caspase inhibitor or vehicle solution. We found that a highly abundant, long intergenic non-coding RNA (CREVASSE; Caspase-Regulated, Extracellular-Vesicle-Associated, Single-Stranded Effector) was more abundant in EVs from caspase-inhibited brainstems than EVs from control brainstems. We corrected some inconsistencies between the Ensembl annotation for this lncRNA and the annotation indicated by our sequencing data, and we predicted RNA binding partners for the resulting transcripts. Gene Set Enrichment Analysis of the ranked RNA binding partners showed that CREVASSE binds RNAs involved in development and differentiation, especially in the nervous system, auditory system, and brainstem. Together, these data suggest that auditory brainstem caspase activity regulates axon guidance by targeting cytoskeletal proteins, and it facilitates timely intercellular communication leading to neuronal differentiation (likely of NL cells) once caspase activity subsides.

*“Air entered into the nostrils, assuming the form of the sense of smell;*

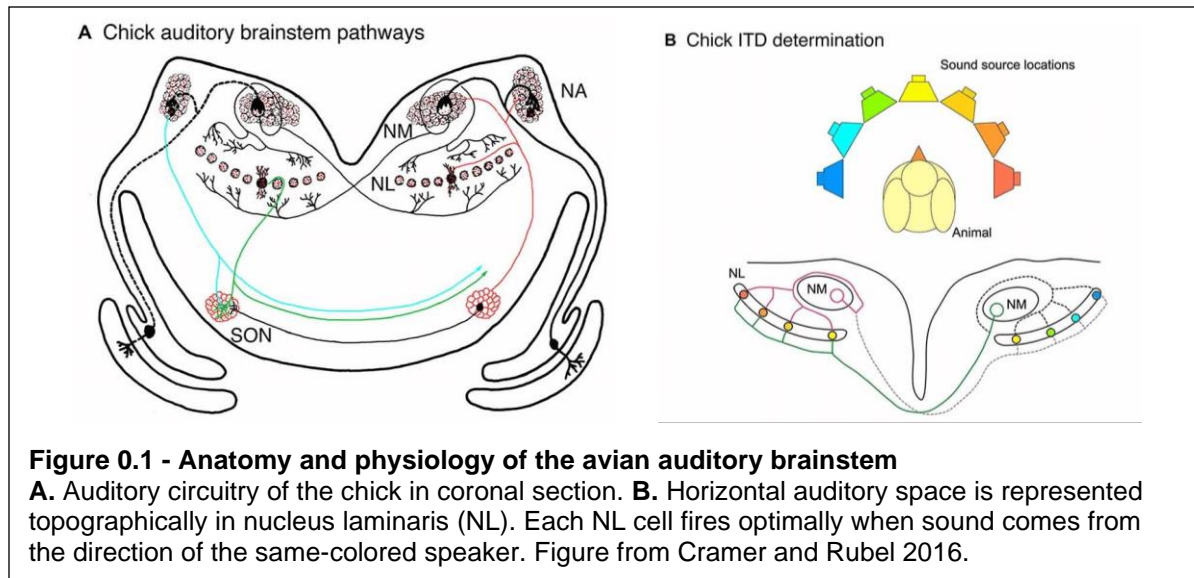
*The Sun entered into the eyes as the sense of sight;*

*The Directions entered into the ears by becoming the sense of hearing.”*

-The Aitareya Upanishad (Hindu creation myth)

## **Chapter 0 : Introduction**

**Auditory System.** Sensory systems allow us to detect the nature, meaning and location of cues in our environment. The auditory system processes the rich landscape of sounds from the frequencies and intensities of sound waves, and it localizes sound sources with specialized circuitry housed in the auditory brainstem, the first stage at which signals from both ears converge on the same cell (Nelken, 2008). This confluence allows the brainstem to integrate differences between the ears in sound intensity (interaural level differences; ILDs) or sound arrival time (interaural time differences; ITDs) into information about a sound source’s horizontal location (Yin, 2002). In birds and some reptiles, ITDs are calculated bilaterally by a neural circuit (Figure 0.1A) resembling the classic Jeffress model (Jeffress, 1948). Neural delay lines carry signals from each ear to coincidence detector cells, which are maximally excited when they receive simultaneous signals from both ears. Because the coincidence detector cells are ordered linearly along the delay lines originating from different ears, each cell only fires when a sound arrives at the ipsilateral ear at a specific time after it arrived at the contralateral ear. The spatial organization of the coincidence detector nucleus therefore corresponds topographically to horizontal auditory space, with each cell firing optimally when sounds originate from a specific direction (Figure 0.1B; Jeffress, 1948; Ashida and Carr, 2011).



**ITD circuit anatomy and physiology.** The anatomy and development of this circuit have been extensively studied in chick embryos because of the wide availability of chicken eggs and the accessibility of chicken embryos for manipulation during the key events of auditory brainstem development (Rubel and Parks, 1988). In chickens, the ITD circuit begins with the basilar papilla, the avian homolog of the organ of Corti in the cochlea (Figure 0.1A, bottom corners). Hair cells deliver glutamatergic input to spiral ganglion cells, whose axons form the auditory portion of the VIII<sup>th</sup> cranial nerve. The VIII<sup>th</sup> nerve projects from the inner ear to the avian cochlear nuclei: *nucleus angularis* (NA), which is involved in sound intensity processing, and *nucleus mesencephalicus profundus* (NM; Ryugo and Parks, 2003). The ITD circuit continues with the projection from NM to the coincidence detector, *nucleus laminaris* (NL), a monolayer of cell bodies with bipolar tufted dendritic arbors that extend dorsally and ventrally (Jhaveri and Morest, 1982a). The NM projection to NL is composed of a branching axon that projects ipsilaterally to dorsal NL and contralaterally to ventral NL. While this circuit approximates the Jeffress model, only the contralateral NM projection is a true delay line; signals from the ipsilateral branches of NM reach their targets almost simultaneously (Overholt et al., 1992; Joseph and Hyson, 1993; Hyson, 2005; Fischer and Seidl, 2014). NL projects to the superior olivary nucleus (SON). The

SO feeds back with GABAergic input on every nucleus mentioned so far, as well as to the lateral lemniscus and the inferior colliculus, where sound and visual information are integrated to form a map of auditory space (Lachica et al., 1994; Westerberg and Schwarz, 1995; Yang et al., 1999).

Interaural computations depend on the faithful transmission and alignment of a sound's temporal profile from each ear, so the utmost precision and sensitivity are required in the development of neural circuits that convey and integrate binaural information. The chick auditory brainstem has evolved multiple adaptations to preserve the temporal information of sound and to ensure that the two branches of NM simultaneously stimulate the cell corresponding to the correct point in space (Ohmori, 2014). These modifications include excess axon length of the ipsilateral NM branch and increased NM axon diameter, myelination, and internode distance of the contralateral branch (Hong and Sanchez, 2018).

Sound frequency is also represented with a high degree of precision throughout the ITD circuit. The characteristic frequency of cells in chicken auditory brainstem nuclei varies from high to low frequency along the rostromedial to caudolateral axis, which runs perpendicular to the representation of horizontal space in NL (Rubel and Parks, 1975). Remarkably, this tonotopy is largely established prior to the onset of hearing due to the combined effort of axon guidance molecule gradients and spatially synchronized spontaneous burst firing that originates in the cochlea (Friauf and Lohmann, 1999). This spontaneous activity allows the axons of cells that are neighbors in the cochlea (and therefore have similar characteristic frequencies) to innervate neighboring target cells in the auditory brainstem by seeking regions that are occupied by axons with similarly timed bursts. The effect of this strategy is the preservation of tonotopy from one nucleus to the next, and only minor refinements of the characteristic frequencies of cells in brainstem auditory nuclei occur after hearing onset (Kandler et al., 2009).

Tonotopic organization is significant to research on neural development because avian auditory nuclei exhibit specialized structural and morphological differences along their tonotopic axis that are thought to optimize the processing of ITDs of different frequencies. A major feature of ITD processing (as well as the reason for the physical upper limit of sound frequency that can be reliably localized with ITDs) is the need for neurons throughout the ITD circuit to fire in phase with a sound wave. To produce rapid firing that approaches the maximum possible rate for neurons, auditory brainstem cells with high characteristic frequencies (>1kHz) have adaptations that shorten their action potentials and ensure their firing is an all-or-none event with little chance for time-consuming integration of signals.

For instance, high- to mid-frequency NM cells are enveloped by a large synaptic terminal of the auditory nerve known as the endbulb of Held (Parks and Rubel, 1978). This endbulb is conserved between birds and mammals, and it elicits large excitatory postsynaptic potentials (EPSPs) in NM cells. In contrast, low-frequency NM cells have smaller somatic synapses and no endbulbs (Köppl, 1994). This distinction mirrors tonotopic gradients in expression of the low-voltage activated potassium channels Kv1.1. High expression of Kv1.1 in high-frequency NM cells effectively lowers their resting membrane potential and raises their threshold for action potential firing (Wang et al., 2017). The large axosomatic endbulbs that deliver enormous amounts of glutamate from a substantial readily releasable pool of synaptic vesicles combined with the low resting potential converts the auditory nerve synapse on high frequency NM neurons into a binary event, where the NM cell is either stimulated to action potential or not stimulated at all. For a similar reason, NL dendrite length varies from shortest at high frequencies to longest at low frequencies. Shorter dendrites mean that EPSPs have less distance to decay, which increases the accuracy of phase locking (Smith and Rubel, 1979). All of these tonotopically varying differences support the notion that different regions of the auditory

brainstem nuclei develop distinctly to optimally process the specific frequency of sound information they receive.

**ITD circuit evolution and development.** The avian ITD circuit is superficially similar to its counterpart in mammals. NL and the mammalian nucleus that detects ITDs, the medial superior olive (MSO), are thought to be completely novel solutions to the problem of interaural time differences. While NL primarily relies on binaural excitation, MSO relies on a balance of binaural excitatory and inhibitory inputs to calculate ITDs (Grothe and Pecka, 2014). Until recently, NM was believed to be homologous to its mammalian counterpart, the anterior ventral cochlear nucleus (AVCN). Genetic fate mapping has now shown that the avian NA shows greater homology to mammalian AVCN, while NM arises from a distinct pool of progenitors. The functional and anatomical similarities between the two nuclei are thus due to convergence, not homology (Lipovsek and Wingate, 2018).

NM and NL derive from cells in the dorsal lip of several rhombomeres, (developmental subdivisions of the hindbrain): rhombomeres 4-6 and 5-8, respectively (Marín and Puelles, 1995; Cramer et al., 2000a). NM cells undergo their final division by embryonic day (E)3, while NL cells are born by E4 (Rubel et al., 2004). In rhombomeres that give rise to cells of both nuclei, cells that will become NM are born in regions distinct from cells that will become NL, suggesting predetermination of cell identity (Cramer et al., 2000a). Future NM and NL cells may remain in distinct locations at E5, when the cells that will form the two nuclei have coalesced into a combined structure, the auditory anlage. From E6 to E9, the anlage separates, and the nuclei can be clearly distinguished by E10 (Hendricks et al., 2006).

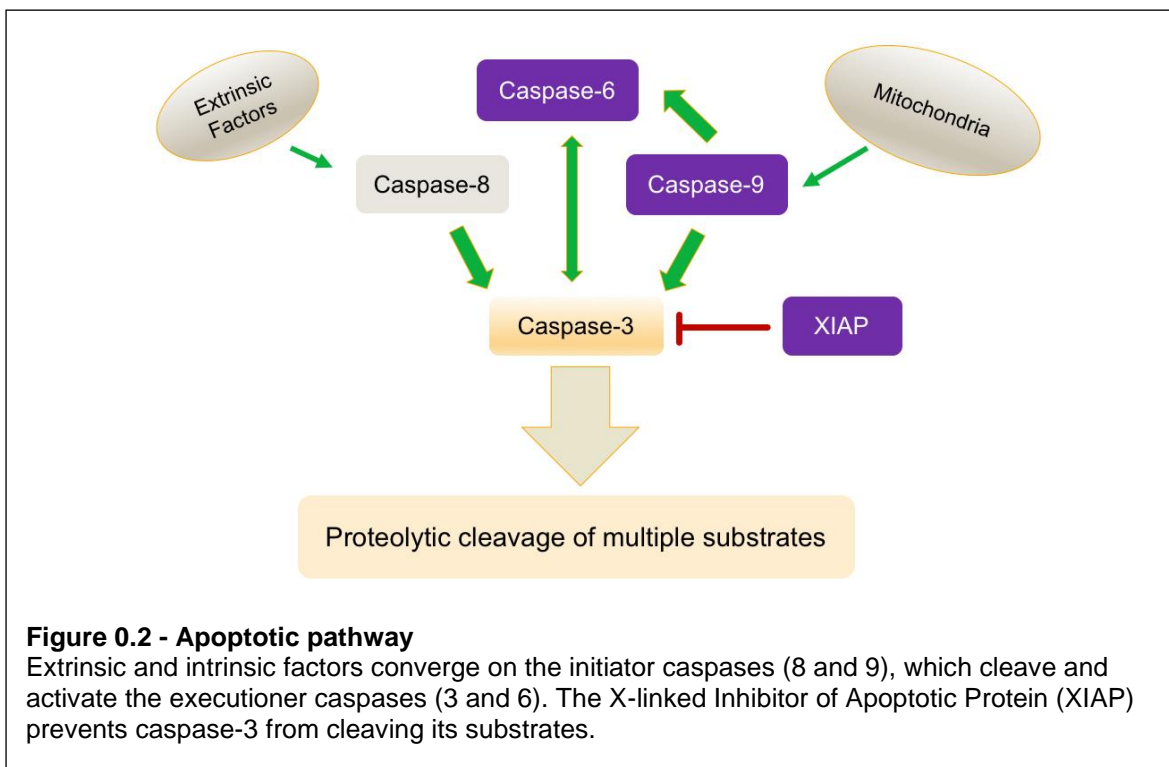
At around E6 or E7, the contralateral branch of NM reaches the ventral side of NL, prior to the arrival of the ipsilateral branch of NM at the dorsal side of NL (Book and Morest, 1990). This axon pathfinding is facilitated by a variety of molecular factors, including EphB2, which

repels NM axons from the midline (Cramer et al., 2006, 2). Around the time that the NM-NL synapse forms, the axon guidance molecule EphA4 is differentially expressed in the dorsal and ventral dendritic fields of NL, which also express EphB2. Disruption of EphA4 or EphB2 produce targeting errors whereby contralateral NM axon branches project into dorsal NL dendritic fields (Cramer et al., 2000b, 2002; Allen-Sharpley et al., 2013). From E9 to E13, NL dendrites undergo extensive proliferation, which is largely reversed by a period of pruning from E14 to E16 until the dendrites adopt a mature morphology by E17 (Smith, 1981).

Meanwhile, VIIIth nerve fibers reach the brainstem by E4 and enter the auditory anlage around E7-8, two full days after NM contacts NL (Book and Morest, 1990; Kubke et al., 1998; Rubel et al., 2004). VIIIth nerve terminals mature from growth-cone-like structures that contact the transient dendrites of NM cells at E10 to a primitive, unramified endbulb at E17, and finally to a fenestrated, mature endbulb by P8 (Jhaveri and Morest, 1982b). These developments are mirrored by changes in NM cells, which begin with multiple dendrites at E7 to a single unbranching dendrite or no dendrites at E17, and finally to a single branching dendrite or no dendrites at P4 (Jhaveri and Morest, 1982c; Parks and Jackson, 1984). All of these changes occur first in high-frequency (rostromedial) regions of NM and later proceed to low-frequency (caudolateral) regions (Smith and Rubel, 1979; Rubel and Parks, 1988). Both the extension of NM axons to NL and the innervation of NL along its tonotopic axis occurs before NM has been penetrated by any auditory nerve fibers. This suggests that NM may be the primary organizational hub of the auditory brainstem, serving as the link between the processes that guide NM axons to the correct isofrequency band of NL and the processes that attract auditory nerve fibers that originate from the correct region of the basilar papilla (Hendricks et al., 2006).

**Caspase pathways.** While some of the molecular mechanisms regulating auditory brainstem development are known, a new potential mechanism depends on non-apoptotic functions for caspases, a family of cysteine-dependent, aspartate-specific proteases best known for their role

in apoptosis (Hengartner, 2000). During normal cell function, caspases exist as inactive proenzymes (Shi, 2004). Pro-death signals can arise either extrinsically through cell-membrane-bound death receptors or intrinsically through intracellular events that lead to mitochondrial outer membrane permeabilization (MOMP). The extrinsic and intrinsic pathways converge on a signaling cascade in which the prodomain is cleaved from the initiator caspases (caspase-8 and -9), allowing them to activate themselves through autoproteolysis. The initiators then cleave and activate executioner caspases (caspase-3, -6, and -7; see Figure 0.2; Gross et al., 1999; Hengartner, 2000; Miura, 2012; Brentnall et al., 2013).



While initiator caspases only have a few dozen known targets, executioner caspases, the architects of apoptosis, cleave hundreds of different proteins. Many caspase-cleaved proteins are likely bystanders whose proteolysis has no biological significance, and there are relatively few known “intended” targets of caspase proteolysis (Julien and Wells, 2017). They include proteins involved in cytoskeleton growth and maintenance, which destabilizes

membrane-cytoskeleton adherence and creates the characteristic blebbing phenotype seen during apoptosis. Other major targets of executioner caspases include the proteasome, signaling molecules such as kinases and phosphatases, and translation machinery (Crawford and Wells, 2011). The destruction of these cellular components facilitates the controlled disassembly of the cell in a manner that avoids inflammatory processes associated with necrosis.

**Non-apoptotic functions of caspases.** Recent developments have shown that cell death is not the only function of caspases, which are now also implicated in neural development and plasticity (Gulyaeva, 2003; Galluzzi et al., 2012; Connolly et al., 2014; Unsain and Barker, 2015; Hollville and Deshmukh, 2017; Mukherjee and Williams, 2017; Nakajima and Kuranaga, 2017; Kellermeyer et al., 2018). As in apoptosis, nonlethal caspase activity often regulates destructive processes such as axonal degeneration, dendritic pruning, and long-term depression (Li et al., 2010; Cusack et al., 2013; Ertürk et al., 2014). More surprisingly, caspases are also responsible for constructive processes such as axonal growth, axon guidance and synaptogenesis. Mice with a double knockout of the apoptosome components Apaf1 and caspase-9 show targeting errors of olfactory axons and deficits in proteolytic cleavage of the membrane-bound axon guidance molecule Sema7a (Ohsawa et al., 2009, 2010). Caspase-3 regulates protein degradation through the proteasome in retinal ganglion cell growth cones, a function required for the growth cones' ability to respond to several chemotropic guidance cues: netrin-1, LPA and Sema3a (Campbell and Holt, 2001, 2003). In the same model system, caspase-3 and caspase-9 act downstream of signaling through the axon guidance molecules Slit and Robo to promote plasticity in branch formation during axonal arborization. (Campbell and Okamoto, 2013).

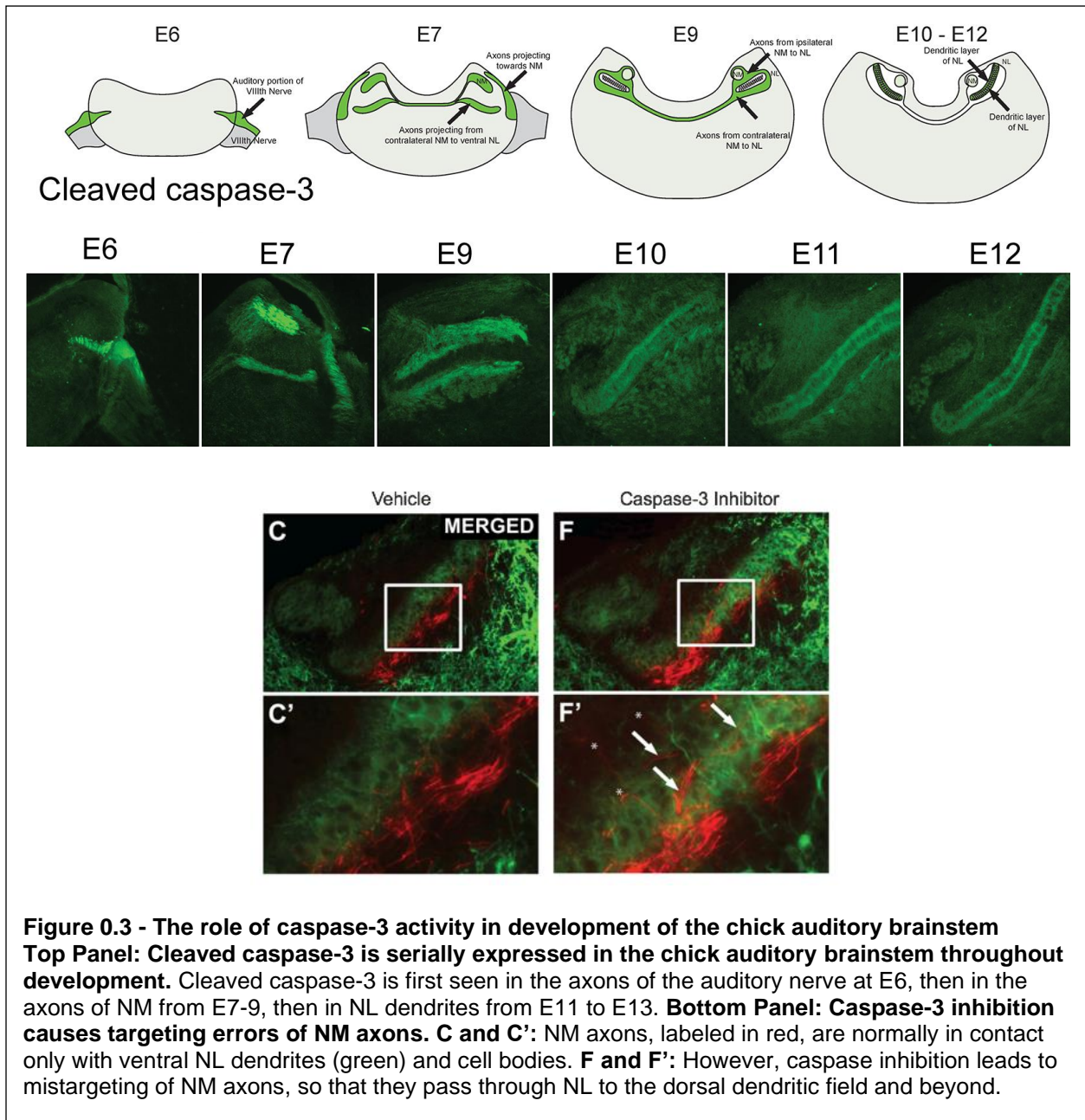
Additionally, recent work in our laboratory has shown that cleaved caspase-3 is serially expressed in neural processes of the ascending chick auditory brainstem during development (Rotschafer et al., 2016). Cleaved caspase-3 is first seen in the auditory nerve and its terminals

at E6 (Figure 0.3, Top Panel). It is then expressed in the axons of NM, the synaptic target of the auditory nerve, from E7 to E10. Finally, cleaved caspase-3 appears in the dendrites of NL, the target of NM axons, from E11 to E12. Each of these transitions in caspase-3 activity occurs as the projections expressing cleaved caspase-3 are nearing their targets and beginning to form synapses (Parks and Rubel, 1975; Jhaveri and Morest, 1982a; Hendricks et al., 2006).

Importantly, it was also shown that inhibition of caspase-3 activity during the developmental period when cleaved caspase-3 is expressed in NM axons results in NM axonal mistargeting (Figure 0.3, Bottom Panel). We have replicated this phenotype by transfecting NM with plasmids that express a dominant-negative caspase-3 transgene, indicating that the effects of z-DEVD-fmk injection are due to the activity of this drug on caspase activity and not to off-target effects. These data suggest that caspase-3 activity is necessary for correct ITD circuit formation in the developing chick auditory brainstem (Rotschafer et al., 2016). However, the mechanism by which caspase-3 mediates auditory circuit development is still unknown.

**Caspase regulation.** A strong candidate for the function of caspase activity in the auditory brainstem is the local proteolytic degradation of cytoskeletal components in response to external guidance cues, a role that is essential for growth cone turning and for the destabilization of neural processes necessary for plasticity (Kellermeyer et al., 2018). This mechanism highlights the fact that the molecular function of caspases in nonapoptotic contexts is similar to that in apoptotic contexts, namely the proteolytic cleavage of specific protein targets, and this process probably only differs from apoptotic contexts by the degree and extent of caspase activation and inhibition. The cell must therefore ensure that caspase activity is tightly regulated so that it does not kill itself by accident.

This regulation can occur through several means. First, neurons are inherently more resistant to apoptotic cell death. This is partially because neurons express lower levels of major



apoptotic components such as Apaf-1 compared to non-neural cells, and because much of caspase activity in neurons occurs far from the nucleus, whose destruction by caspases generally is fatal for a cell (Wright et al., 2004). Mitochondria harbor many of the factors needed to activate caspases, so caspase activity may be regulated by the movement of mitochondria, a process known to occur in stimulated dendritic spines (Loo et al., 2002; Li et al., 2004). Caspase activity can also be spatially restricted by endogenous apoptotic inhibitors, such as the Inhibitor

of Apoptotic Protein (IAP) family, which ubiquitinate initiator caspases and directly bind and sequester the active site of executioner caspases (Figure 0.2; Suzuki et al., 2001; Srinivasula and Ashwell, 2008; Galbán and Duckett, 2010). It has been proposed that transient, hyperlocal activation of caspases may bypass the need for initiator caspases by employing an “IAP clutch” in which IAP sequestering of already-cleaved caspases is briefly inhibited, possibly due to phosphorylation or S-nitrosylation of IAPs (Tsang et al., 2009; Nakhaei et al., 2012). This inhibition of IAPs results in some caspase molecules being freed, but they can be quickly bound again by the IAPs that released them (Mukherjee and Williams, 2017). Thus, active caspases can be rapidly and reversibly inhibited in response to both intracellular and extracellular stimuli.

Additionally, caspase activity may be directed toward certain groups of proteins based on the rate of proteolysis for each potential cleavage site by the caspase in question. During apoptosis, high concentrations of active caspase result in most caspase target sites being cleaved to completion regardless of the degree of preference for each site. In contrast, when low concentrations of active caspase are present, only the mostly highly preferred sites will be cleaved to a biologically relevant extent, while the less preferred sites will largely be left untouched (Julien and Wells, 2017). In this way, the effects of caspases can be limited to specific substrates with minimal danger of catastrophic apoptotic activity.

The preference of each caspase for its suite of substrates is determined by multiple factors, the most important of which is the identity of the amino acid residues N-terminal to the cleavage site. The first amino acid N-terminal to the cleavage site (position P1) has the greatest effect on proteolytic efficiency and is almost invariably an aspartate, glutamate, or phosphoserine residue (D/E/pS, ordered by decreasing proteolytic efficiency; Seaman et al., 2016) It was previously believed that the other three residues (positions P2-4) exercised similar stringency on cleavage rate. For instance, caspase-3 was once thought to only cleave after DXVD, where X is any amino acid. It is now known that the identities of P2-4 vary greatly among

cleavage sites and determine the rate of proteolysis based on the similarity of their properties to those of each caspase's preferred amino acid sequence (Julien et al., 2016).

**Extracellular Vesicles.** My data (Chapter 2) suggest that caspase function in the auditory brainstem is related to extracellular vesicles (EVs). EVs are any nanoparticles with a lipid bilayer that are present outside of cells (Raposo and Stoorvogel, 2013). They are released by every known cell type, are present in every tissue and biological fluid studied so far, and carry proteins, lipids, and nucleic acid cargo between cells, which can have a plethora of effects depending on the specific vesicular content (Maas et al., 2017; van Niel et al., 2018). For instance, mRNAs in EVs can be translated (and miRNAs can similarly inhibit translation) in cells that did not transcribe them. EVs carrying transcription factors can elicit novel transcriptional programs in their recipients. EVs carrying signaling proteins can serve as the impetus for informational transfer between cells as well. The effects of EV-mediated communication range from pro-survival (such as when apoptotic components are jettisoned in EVs from injured cells; Böing et al., 2013) to morphological changes (a likely function of cell adhesion molecules on EVs; Gutwein et al., 2003) to spreading disease (such as when EVs transport A $\beta$  between cells in Alzheimer's brains; Rajendran et al., 2006).

EVs are traditionally divided into microvesicles (also called ectosomes or microparticles) and exosomes. Microvesicles are 100-1000 nm in diameter and bud directly from the plasma membrane of the cell, while exosomes are 30-100 nm in diameter and are released from multivesicular bodies of the endosomal pathway (Raposo and Stoorvogel, 2013). However, an emerging picture of the heterogeneity of populations of EVs, even among populations with the same alleged origin, suggests that this classic view is grossly oversimplified. An EV's origin can rarely be proven unless observed directly, which has led to the use of terms such as "large EVs" instead of microvesicles and "small EVs" instead of exosomes (Gould and Raposo, 2013). Even increasing precision of language cannot change the fact that the use of multiple EV isolation

techniques in tandem (such as iodixanol gradient separation and bind-elute chromatography, or size exclusion and bind-elute chromatography) has shown that classically defined populations of EVs are composed of multiple subpopulations with distinct repertoires of molecular content (Jeppesen et al., 2014; Kowal et al., 2016; Corso et al., 2017; Onódi et al., 2018). This suggests that the “microvesicle-exosome” dichotomy underestimates the diversity of EVs and may not even represent the most important distinction in EV function and composition. The recent discovery of exomeres (extracellular nanoparticles that contain proteins, lipids, and RNA similar to those found in EVs but that have no lipid bilayer) further complicates an already tangled domain of research (Zhang et al., 2018).

Because of the lack of consensus on EV physiology and nomenclature, as well as the abundance of claims purporting the discovery of some new function of “exosomes” or “microvesicles” with no attempt to prove the identity of the EV in question or to rule out contaminating factors, the International Society for Extracellular Vesicles published the first Minimum Requirements for Publications on Extracellular Vesicles in 2014 (MISEV2014; Lötvall et al., 2014). This brief guide specifies that any study claiming to have purified a sample of EVs must demonstrate not only the enrichment of EV-associated transmembrane and cytosolic protein (such as tetraspanins and TSG101, respectively) but also the absence of proteins indicative of cellular contamination (such as histones or the ER-enriched calnexin). Additionally, MISEV2014 suggests that electron microscopy or atomic force microscopy must be used to examine individual vesicles to verify their diameter and the presence of a lipid bilayer, which distinguishes EVs from similarly sized non-membranous particles.

The MISEV2018 provided an updated and much more detailed account of what constitutes sufficient evidence of EV enrichment (Witwer et al., 2017; Théry et al., 2018a). Many of the previous requirements were simply reiterated, and additional requirements were added to increase the rigor and reproducibility of studies on EVs, such as comparisons of and

recommendations for EV isolation methods. These included more specific standards for quantitation, characterization, and reporting of EV physical characteristics, molecular content, and biological function. For instance, while MISEV2014 required studies to report the presence of just one transmembrane protein, one cytosolic protein, and the absence of a cellular contaminant protein to claim that a sample likely contains pure EVs, MISEV2018 also recommends markers for ruling out contaminants that often co-isolate with EVs, such as lipoproteins, secreted proteins, and intracellular vesicles. Additionally, a checklist is provided with guidelines that researchers must follow to claim purity of an EV sample.

**Caspases and Extracellular Vesicles.** There are several documented cases of EVs transporting caspases, other apoptotic signaling molecules, and caspase cleavage products between cells. The most well-characterized EV associated with caspases are apoptotic bodies: large (>500 nm) EVs that bud from the plasma membrane of dying cells. Apoptotic bodies were once believed to contain mostly bulk-loaded, nonspecific protein content, but they are now recognized to play important roles in the inflammatory signaling and debris cleanup that accompany apoptosis (Caruso and Poon, 2018). An intermediate between apoptotic bodies and classically defined EVs are the apoptotic exosome-like vesicles: small, exosome-sized EVs released by dying cells but that were found to contain a unique protein fingerprint compared to exosomes released by healthy cells. Most notably was the presence of sphingosine-1-phosphate receptors that facilitate inflammatory processes in the surrounding tissue (Park et al., 2018). Studies of nonapoptotic spleen dendritic cells have also shown that they release exosomes that contain apoptotic proteins such as Alix and 14-3-3, which are now known to be found almost universally in EVs (Théry et al., 2001, 2018a).

Other work implicates caspase cleavage as a required factor for the loading of proteins into exosomes. For instance, lysyl-tRNA synthetase (KRS) cannot be loaded into exosomes of colorectal carcinoma cells unless it has been cleaved by caspase-8. The KRS-containing

exosomes are then secreted and promote inflammation by attracting macrophages and inducing their expression of TNF (Kim et al., 2017b, 8). Another study found that the antiapoptotic protein Bcl-xL is found on the exterior of exosomes, where it is cleaved by caspase-3. This proteolysis is necessary for the exosomes' uptake by myeloma and lymphoma cells, where the contents of the exosomes contribute to cell growth and proliferation (Vardaki et al., 2016). In addition to playing functional roles downstream of EVs, caspases may be packaged and secreted by cells attempting to avoid apoptosis (Böing et al., 2013). For example, dihydrotestosterone treatment prevents cell death in cultured submandibular gland cells by inducing them to excrete caspase-3 in exosomes (Trokovic et al., 2012). Despite this multitude of functions of caspases and apoptotic proteins in EVs, the role of caspases in EVs of the nervous system, let alone in nervous system development, has yet to be explored.

# Chapter 1 : Caspase-3 cleaves extracellular vesicle proteins during auditory brainstem development

The auditory system depends on specialized neural circuits that faithfully preserve sound information from the ears to higher order auditory structures, processing various aspects of the sound environment along the way. Some auditory features, such as sound frequency, are neurally encoded as soon as sound reaches the cochlea and are thereafter represented topographically throughout the auditory system. Other features, such as the spatial location of sound sources, are instead rapidly calculated by circuits in the auditory hindbrain and midbrain (Nelken, 2008). One such circuit in the auditory brainstem exploits interaural time differences (ITDs), discrepancies in the arrival time of sounds between the ears, to localize sound sources in horizontal space (Carr and Konishi, 1990; Overholt et al., 1992). Many species use this circuit to distinguish sounds arising from sources as close as 1 spatial degree, a feat that requires accurate detection of ITDs of less than 10 microseconds. Such extreme functional precision leaves little room for error in auditory neuroanatomy, which suggests that the auditory system employs high-fidelity systems of axon guidance and synapse formation to ensure that auditory projections innervate the correct targets. However, the molecular mechanisms responsible for assembling these precise circuits remain largely unknown.

We previously reported a requirement for activity of the apoptotic protease caspase-3 for proper chick ITD circuit assembly (Rotschafer et al., 2016). This role was first suggested by the sequential, ascending expression pattern of active caspase-3 in neuronal processes of the chick auditory brainstem throughout embryonic development: First in axons of the auditory nerve (AN) on embryonic days (E) 6-7; then in axons of the AN synaptic target, *nucleus magnocellularis* (NM) on E8-10; and finally in dendrites of the NM synaptic target, *nucleus laminaris* (NL) on E11-13. When caspase-3 activity was inhibited from E6 to E9, examination of E10 brainstems

revealed mistargeting of NM axons and disruption of the laminar structure of NL. Importantly, TUNEL staining revealed no apoptotic cell death until after this timepoint, in accordance with earlier studies showing that the period of developmental cell death in the auditory brainstem begins around E11 (Rubel et al., 1976). Collectively, these findings suggest that caspase-3 influences chick ITD circuit development without causing cell death.

During apoptosis, pro-death signals result in the initiator caspases (i.e. caspase-2, -8, -9, and -10) activating the executioner caspases (i.e. caspase-3, -6, and -7) by cleavage of an inactive zymogen, or procaspase, form (Hengartner, 2000). The executioners then cleave a repertoire of protein substrates, culminating in cell death (Julien and Wells, 2017). Although caspases are typically associated with this role in apoptosis, several non-lethal functions of caspase-3 have been identified in the nervous system. Neurons become increasingly resistant to programmed cell death as they mature (Kole et al., 2013), and robust cellular safeguards allow caspase-3 to carry out other functions without leading to cell death (Holville and Deshmukh, 2017). However, despite numerous examples of the importance of caspase activity in neural development and physiology (Campbell and Holt, 2003; Gulyaeva, 2003; Campbell and Okamoto, 2013; Ertürk et al., 2014; Wang and Luo, 2014; Unsain and Barker, 2015; Nakajima and Kuranaga, 2017), our understanding of non-apoptotic caspase function lags behind our knowledge of apoptotic caspase functions.

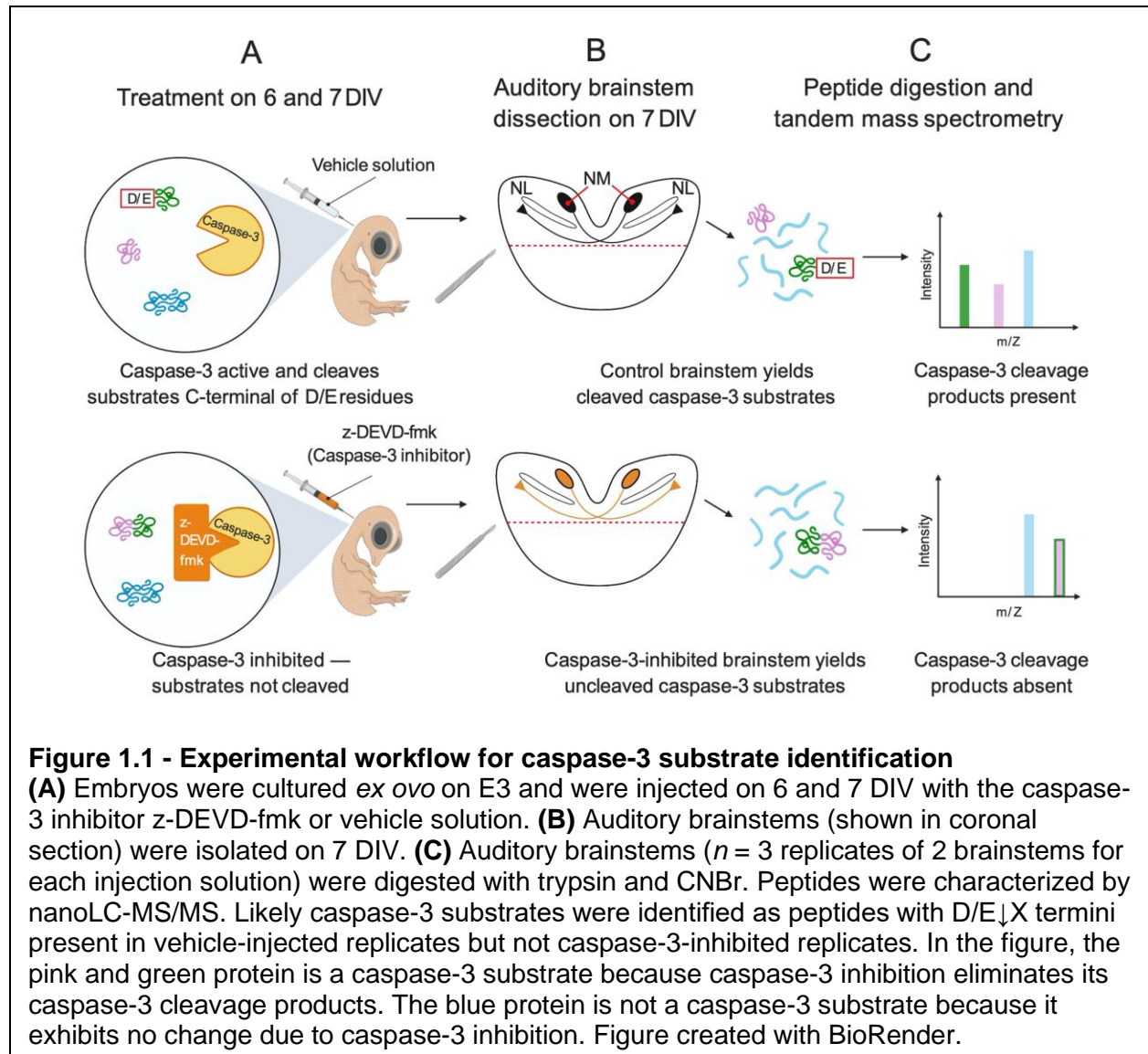
Because of the ease with which apoptosis can be induced in cell culture, hundreds of apoptotic caspase substrates have been experimentally verified (Lüthi and Martin, 2007; Crawford et al., 2012, 2013). Non-apoptotic caspase functions, in contrast, are often more transient and difficult to verify conclusively. Some studies have explored caspase activity in cellular compartments relevant to neural development, such as synaptosomes (Victor et al., 2018), but only a handful of substrates have been demonstrated to be important for non-apoptotic neurodevelopmental functions in living systems (Kellermeyer et al., 2018). An

unbiased investigation of non-apoptotic neurodevelopmental caspase substrates that approximates the depth and breadth of screens for apoptotic substrates has never been accomplished. We therefore aimed to address the following outstanding questions: What are the proteolytic substrates of non-apoptotic caspase-3 activity during axonal guidance in the chick auditory brainstem, and how does the proteolysis of these substrates facilitate proper development of the ITD circuit?

We screened for caspase-3 cleavage events within a shotgun proteome of the auditory brainstem and found that many of the substrates of caspase-3 are associated with extracellular vesicles (EVs), membrane-bound nanoparticles that have important functions in intercellular communication. To verify this finding, we isolated EVs from the chick auditory brainstem and showed that they contain a large proportion of the proteins we identified as caspase-3 substrates. Finally, we found that two caspase-3 substrates associated with axon growth, NCAM and Ng-CAM, are sequentially expressed in axons and dendrites of the ascending auditory brainstem. This discovery parallels our previously published results on cleaved caspase-3 expression dynamics and potentially implicates non-apoptotic caspase-3 activity in the development of multiple structures in the chick auditory brainstem.

## **RESULTS**

**Identification of caspase-3 substrates in the auditory brainstem.** To identify the targets of non-apoptotic caspase-3 activity in the embryonic chick auditory brainstem, we searched for likely caspase product peptides that were abolished by caspase-3 inhibition using the strategy shown in Figure 1.1. Specifically, we performed intraventricular injections of the caspase-3/7 inhibitor z-DEVD-fmk or vehicle solution at developmental stages when cleaved caspase-3 is expressed in NM axons and nowhere else in the auditory brainstem, namely embryonic days (E) 9 and 10, corresponding to Hamburger-Hamilton stages 35 and 36



(Hamburger and Hamilton, 1951; Rotschafer et al., 2016). We then used tandem mass spectrometry to characterize auditory brainstem proteins and peptides. We filtered the peptidomes for peptides likely produced by *in vivo* caspase-3 proteolysis based on two criteria:

- (1) One peptide terminus was a canonical caspase cleavage site, with an aspartate (D) or glutamate (E) residue immediately N-terminal of the cleavage site (Seaman et al., 2016). Caspases represent 9 of the 10 chicken proteases with D/E↓X specificity, where ↓ represents the scissile peptide bond and X represents any amino acid. By contrast, CNBr and trypsin

(which were used to digest the proteome prior to mass spectrometry) exhibit M↓X and R/K↓X and specificity, respectively.

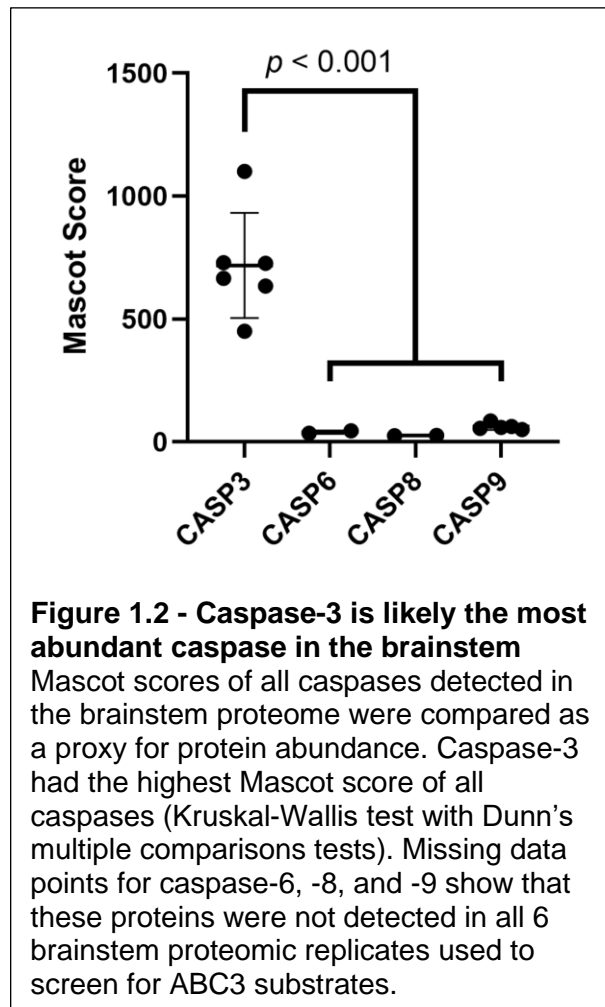
(2) The peptide must have been identified in at least one of the vehicle replicates but in none of the three caspase-3-inhibited replicates, indicating that the caspase-cleaved terminus requires caspase-3 activity. This criterion was adopted on the basis of the mass spectrometry “missing data” rubric, namely the enormously greater prevalence of incomplete proteomic data than of false positive data from a sample under the conditions employed here (Karpievitch et al., 2012; Wei et al., 2018; McGurk et al., 2020). Thus, detection of a peptide in some samples but not in others more likely reflects higher abundance (not false detection) of the peptide in the samples in which it was observed. Our set of substrates was denoted Auditory Brainstem Caspase-3 (ABC3) substrates.

We identified 421 distinct peptides that met both of the above criteria. This set included seven peptide pairs representing opposite sides of the same cleavage site, and three peptide pairs representing variable numbers of missed tryptic cleavages on the same side of the caspase cleavage site. Therefore, the 421 peptides were derived from 411 unique cleavage sites arising from 288 unique proteins, which represented about 5% of the total brainstem proteome of 5653 unique proteins. Of the 288 likely ABC3 substrate proteins, 58 (20%) possessed multiple sites that fulfilled the two criteria for ABC3 cleavage, consistent with previous reports that many caspase substrates are cleaved at multiple sites (Crawford et al., 2013; Seaman et al., 2016).

### **ABC3 substrates were most likely cleaved by caspase-3, not other proteases.**

The inhibitor used in this study, z-DEVD-fmk, is designed to primarily inhibit caspase-3 and caspase-7 by virtue of its similarity to these caspases’ preferred consensus sequence. We detected caspase-3 but not caspase-7 in the chick auditory brainstem, suggesting that all

peptides that fulfilled our criteria for ABC3 substrates are truly produced by caspase-3. However, several studies have shown that other caspases are inhibited by as little as 1  $\mu\text{M}$  of z-DEVD-fmk (Berger et al., 2006; Timmer and Salvesen, 2007; Pereira and Song, 2008; Poręba et al., 2013; McStay, 2016), a concentration less than the inhibitor's  $\text{IC}^{50}$  for caspase-3 (18  $\mu\text{M}$ ) and far below the 50  $\mu\text{M}$  used in this study. Given this promiscuity of caspase inhibition, we considered whether other caspases detected in the auditory brainstem (caspase-6, -8 or -9) may have produced some of the cleavage sites that we attributed to caspase-3 activity. Several lines of evidence suggest that caspase-3 is responsible for the majority of ABC3 substrates. First, caspase-8 and -9 are initiator caspases with just 45 and 10 known substrates, respectively (Rawlings et al., 2010). Only one ABC3 substrate (vimentin) is also a substrate of caspase-8 or -9, so these initiator caspases are likely to be responsible for few, if any, ABC3 substrates. Additionally, though we did not conduct quantitative proteomic analysis, we used protein Mascot score, which correlates moderately with protein abundance (Ishihama et al., 2005), to compare the relative



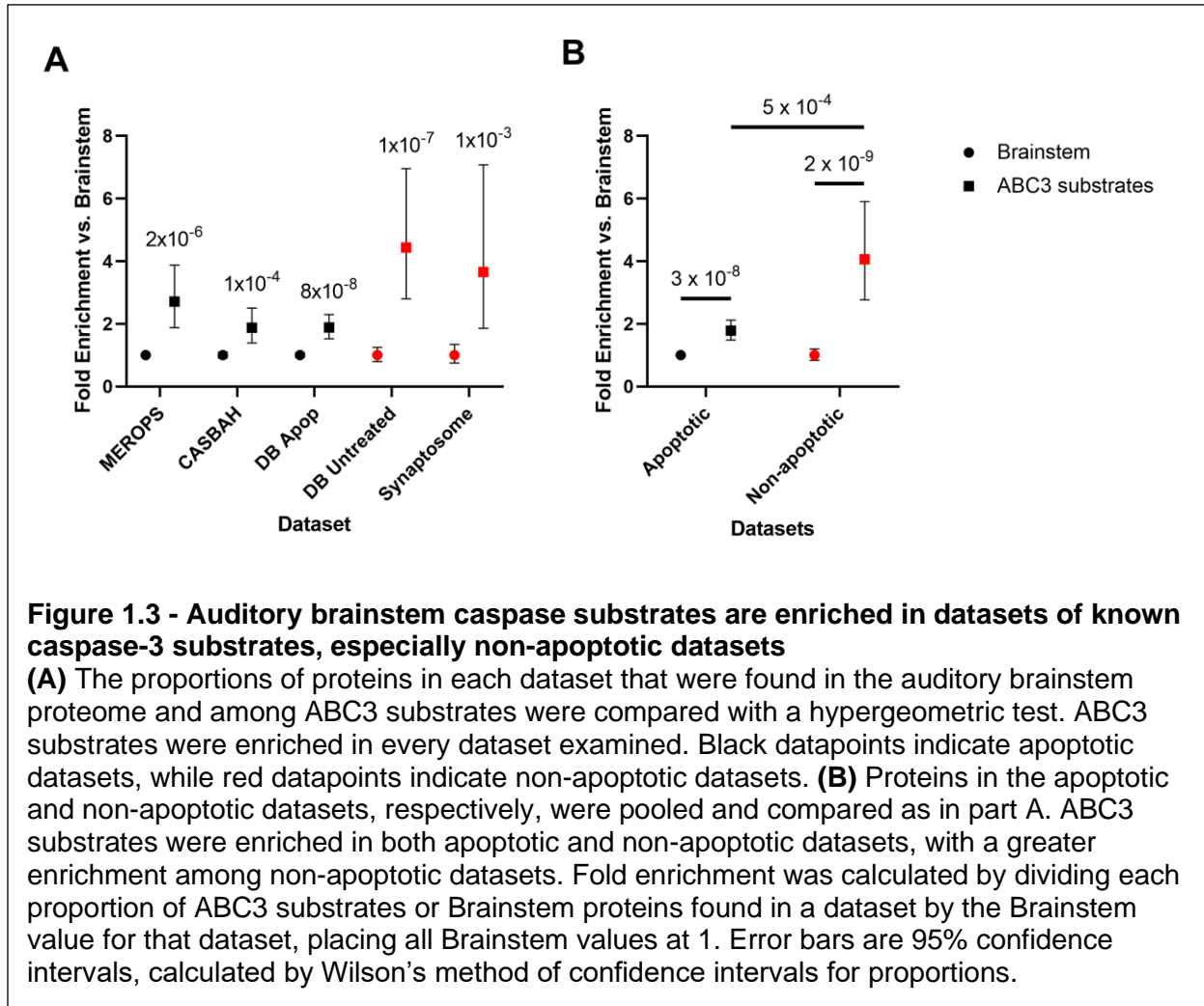
abundance of caspases in the auditory brainstem (Figure 1.2; Welch's ANOVA,  $p = 0.0073$ ). Caspase-3 had a greater Mascot score (mean = 717.8, 95% CI: 493.7 to 942.0) than caspase-6 (mean = 40.0, 95% CI: -23.5 to 103.5; Dunnett's multiple comparisons test,  $p = 0.0006$ ), caspase-8 (mean = 26.5, 95% CI: 20.2 to 32.9;  $p = 0.0005$ ), and caspase-9 (mean = 62.6, 95%

CI: 46.1 to 79.1;  $p = 0.0006$ ), suggesting that caspase-3 is the most abundant caspase in the auditory brainstem. Indeed, the other three caspases were not observed in all six biological replicates used in this study, evidenced by missing Mascot score data. Taken together, these data suggest that inhibition of proteins other than caspase-3 did not contribute significantly to identification of ABC3 substrates.

### **Auditory brainstem caspase-3 activity cleaves both novel and known substrates, especially known substrates observed in non-apoptotic contexts.**

We next investigated whether our ABC3 substrates have been previously reported as caspase-3 substrates and whether they are associated with apoptotic or non-apoptotic caspase activity. We consulted four sources of known caspase-3 substrates: MEROPS (Rawlings et al., 2010), CASBAH (Lüthi and Martin, 2007), DegraBase (Crawford et al., 2013), and Victor *et al.* 2018. We used a hypergeometric test to calculate the probability of obtaining the observed number of proteins that were caspase-3 substrates both in the above databases *and* in our ABC3 dataset, assuming each is randomly selected from a brainstem proteome of 5653 proteins containing 288 caspase-3 substrates. Nearly one third (91) of our 288 ABC3 substrates were present in at least one of the four datasets ( $p = 2.45 \times 10^{-10}$ ), suggesting that caspase-3 cleaves many of the same proteins in the developing auditory brainstem as in other conditions. This enrichment of known caspase-3 targets among ABC3 substrates was observed for all databases examined (Figure 1.3A). Additionally, of the roughly two-thirds (197) of the ABC3 substrates not found in any of the databases, three were chicken-specific proteins, but the remaining 194 have homologs in other species and are thus novel caspase-3 substrates.

Because the ABC3 dataset was obtained from embryonic brainstems not undergoing significant cell death (Rotschafer et al., 2016), we hypothesized that databases representing samples that are primarily apoptotic in nature (MEROPS, CASBAH, and the apoptotic



DegraBase substrates) would contain fewer ABC3 substrates than sets more comparable to the present study insofar as caspase activity is localized to synapses (Victor et al. 2018) or is not associated with apoptosis (untreated DegraBase substrates). Our hypothesis was supported in that the fold-enrichment of ABC3 substrates in apoptosis-only datasets was less than that of non-apoptotic substrates (Figure 1.3B). These results show that the set of ABC3 substrates resembles known sets of caspase-3 substrates, especially those associated with non-apoptotic caspase activity.

**Auditory brainstem caspase-3 activity cleaves proteins associated with extracellular vesicles.** To determine the role of caspase-3 in the auditory brainstem, we next investigated pathways targeted by ABC3 activity. We again used DAVID to analyze functional annotation term enrichment among ABC3 substrates compared to the auditory brainstem proteome. Thirty-three terms were enriched among ABC3 substrates according to our significance criterion. These 33 terms were reduced to 14 terms after clustering of terms with similar protein content. Nine of these terms were related to biological processes and molecular functions of ABC3 substrates, representing 6 categories of pathways targeted by ABC3 activity: Biosynthesis of amino acids, RNA binding, ribosomal proteins, chaperones and protein folding, actin binding, and phosphoproteins (Figure 1.4A). Besides the inclusion of “ribosomal proteins” within “RNA binding,” these 6 categories generally overlapped little with each other, suggesting that ABC3 activity regulates several distinct processes.

Of the 14 post-clustering terms, the remaining 5 terms referred to cellular location of the ABC3 substrates: Myelin sheath, extracellular vesicle, cytoplasm/cytosol, and focal adhesion (Figure 1.4B). Most ABC3 substrates in “myelin sheath” and “focal adhesion” were also found in “extracellular vesicle” and “cytoplasm/cytosol.” The reverse was not true, with many ABC3 substrates found only in “extracellular vesicle” and “cytoplasm/cytosol,” suggesting that these two terms best explain the cellular location of ABC3 substrates. The apparent enrichment of “focal adhesion” and “myelin sheath” proteins is likely a side effect of the similarity of these categories with “extracellular vesicle” and “cytoplasm/cytosol” combined with the substantial overrepresentation of proteins in the latter two terms. While we expected ABC3 substrates to be primarily cytosolic (since caspase-3 activity canonically occurs in the cytosol), we were surprised at the nearly two-fold enrichment of extracellular vesicle (EV) proteins among our ABC3 substrates.

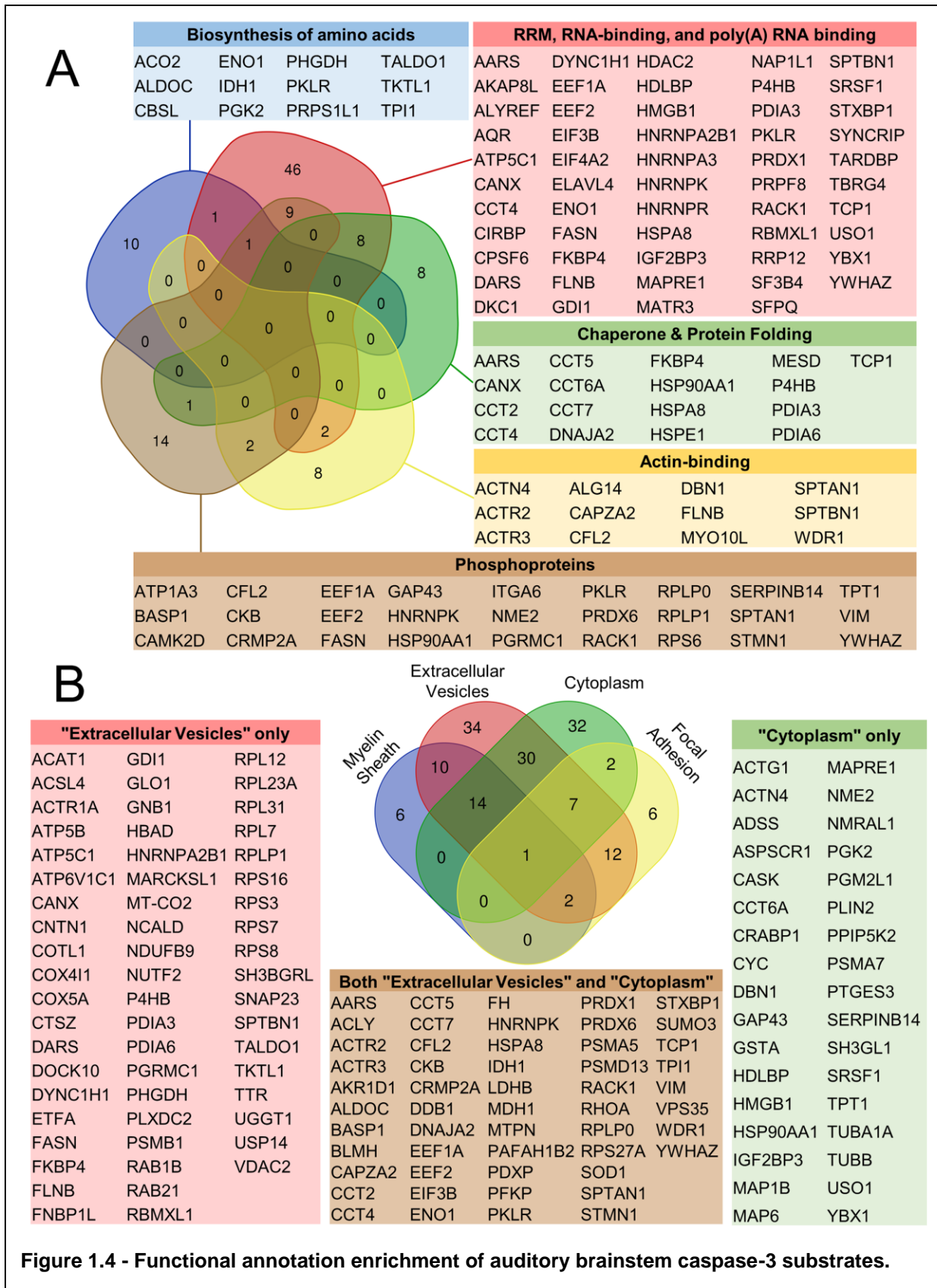


Figure 1.4 - Functional annotation enrichment of auditory brainstem caspase-3 substrates.

To determine the cellular and molecular pathways targeted by caspase-3 activity in the auditory brainstem, DAVID enrichment analysis was used to compare the frequency of functional annotation terms of ABC3 substrates to those of the auditory brainstem proteome. **(A)** ABC3 substrates were significantly enriched for six categories of functional annotation terms related to biological processes or molecular functions. Five of these categories and the gene symbols of their constituent ABC3 substrates are shown along with a Venn diagram depicting the number of ABC3 substrates in the categories and their overlaps. The sixth category, Ribosomal Proteins, contained 20 ABC3 substrates but is not shown due to its large overlap with the RNA binding category. Besides this exception, the ABC3 substrates in each category are generally unique to that category, suggesting that caspase-3 activity regulates several distinct processes during auditory brainstem development. Gene symbols of category members are shown in color-coded tables. Ribosomal proteins are not shown in the “RNA-binding” table but are included in Venn diagram counts. **(B)** ABC3 substrates were significantly enriched for four terms related to cellular location. The Venn diagram shows the number of ABC3 substrates associated with each term. Two of these terms alone, Extracellular Vesicle and Cytoplasm/Cytosol, accounted for the majority of the proteins in the other two categories, suggesting that Extracellular Vesicles and Cytoplasm/Cytosol most parsimoniously describe the cellular location of the majority of ABC3 substrates. The overrepresentation of these categories among ABC3 substrates suggests that caspase-3 preferentially cleaves cytosolic proteins and EV proteins.

Extracellular vesicles are membrane-bound nanoparticles that facilitate intercellular signaling and transport of RNA, proteins, and other cargo between cells (Maas et al., 2017). Their molecular cargoes can induce changes in the recipient cell by altering gene expression with transported transcription factors, silencing translation with transported miRNAs, or other mechanisms (Yáñez-Mó et al., 2015; van Niel et al., 2018). Caspase-mediated cleavage of EV proteins has been previously described (Vardaki et al., 2016; Wang et al., 2016; Kim et al., 2017b). However, EV-associated proteins are rarely exclusive to EVs (De Maio and Vazquez, 2013). Additionally, functional annotation terms like “Extracellular Vesicle” are assigned by DAVID and other annotation tools with varying levels of evidence, many of which are inferential but are given the same weight as direct observation (Balakrishnan et al., 2013). It was therefore possible that ABC3 substrates were enriched in EV proteins even in the absence of any caspase-3 activity associated with EVs or their contents.

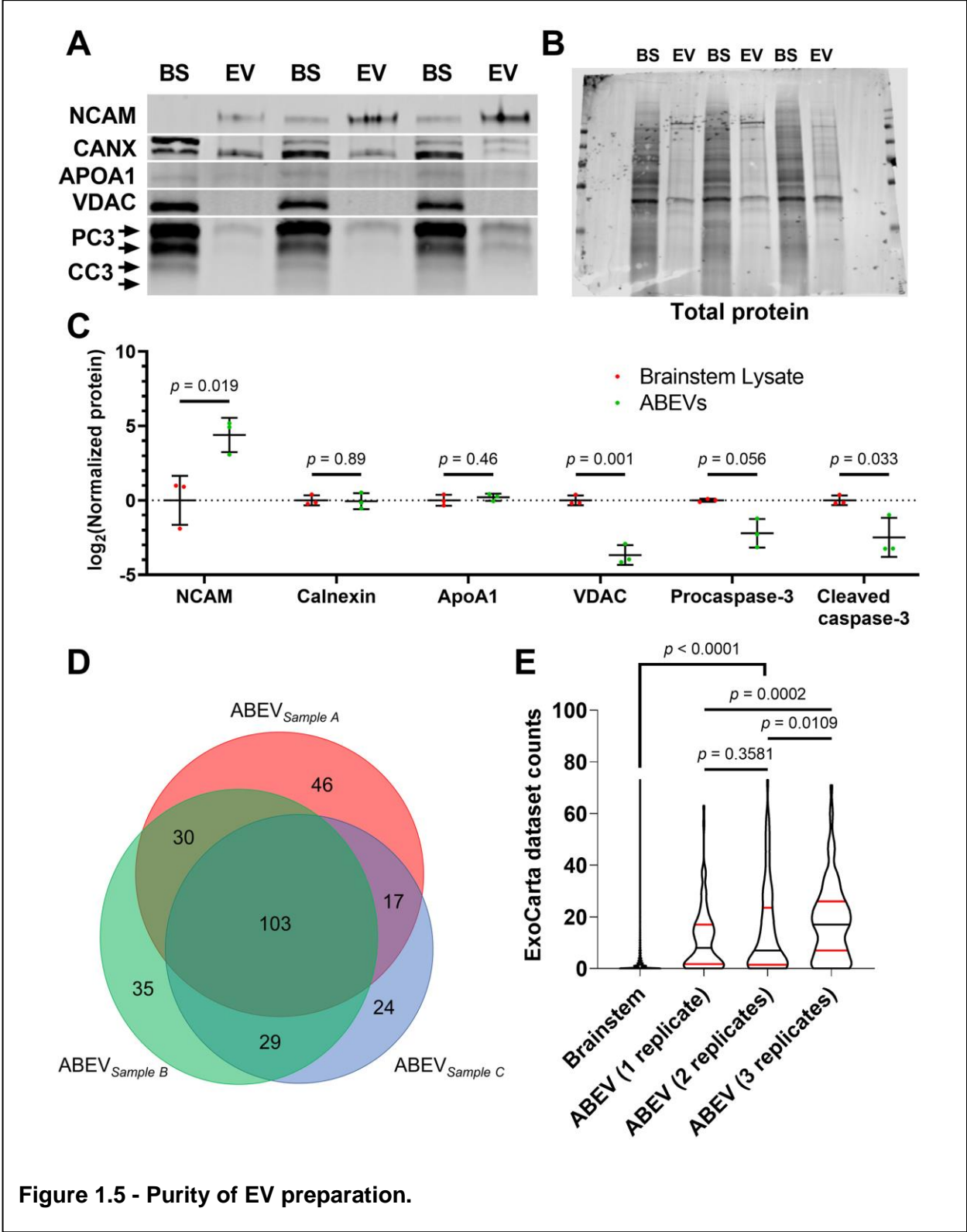


Figure 1.5 - Purity of EV preparation.

**(A)** Western blot comparing protein levels in 3 biological replicates of ABEVs (EV) and crude brainstem lysates (BS). Neural cell adhesion molecule (NCAM), a positive marker for EVs released by neural tissue, was enriched in ABEVs. In contrast, negative markers for EVs, namely calnexin (CANX), APOA1, and VDAC, showed either no difference in protein amount between brainstem lysates and ABEVs (CANX and APOA1) or showed a decreased expression in ABEVs (VDAC). Both procaspase-3 (PC3) and cleaved caspase-3 (CC3) were negatively enriched in ABEVs compared to brainstem lysates. **(B)** All proteins were normalized to total protein stain as a loading control. **(C)** Quantification of normalized protein levels from A. All *p*-values are derived from two-tailed Student's *t*-tests except for procaspase-3, for which Welch's heteroscedastic *t*-test was necessary. **(D)** Proportionally accurate Venn diagram of proteins identified in each ABEV replicate. The substantial triple-overlap reflects a high degree of conservation among the proteomes of the individual ABEV replicates. **(E)** Comparison of ExoCarta dataset counts of brainstem proteins and ABEV proteins found in 1, 2, or 3 replicates. The number of EV proteomic datasets containing each protein on the EV database ExoCarta ("ExoCarta dataset counts") was used to estimate the frequency that proteins are found in EVs. ABEV proteins had higher ExoCarta dataset counts than brainstem proteins regardless of the number of replicates containing each ABEV protein. Additionally, ABEV proteins found in all 3 ABEV replicates had higher ExoCarta dataset counts than ABEV proteins found in only 1 or 2 replicates. These data suggest that the ABEV proteome resembles published EV proteomes. Plots depict smoothed probability density. Median (black horizontal line) and quartiles (red horizontal lines) are shown. *P*-values reflect Dunn's multiple comparisons tests.

To explore the association of ABC3 substrates and EVs directly, we used size exclusion chromatography (SEC) columns ("qEVoriginal" columns; IZON Science) to enrich for EVs from dissociated auditory brainstem tissue of E10 embryos. These columns are specifically designed to separate EVs from free protein, a capacity that has been independently shown to consistently yield high-purity samples of EVs in specific SEC fractions (Vogel et al., 2016; Stranska et al., 2018; Théry et al., 2018b; Antounians et al., 2019; Brennan et al., 2020). E10 was chosen because ABC3 substrates were identified in E10 brainstems. To quantitatively assess proteomic purity of our EV samples in accordance with the Minimal Information for Studies of Extracellular Vesicles (MISEV; Lötvald et al., 2014; Théry et al., 2018), we used Western blotting to compare levels of positive and negative EV markers in 3 biological replicates of auditory brainstem EV (ABEV) samples and crude brainstem lysates (Figure 1.5A-B). Neural Cell Adhesion Molecule, a positive marker for EVs released from neural tissue, was enriched more than 20-fold in ABEVs compared to crude brainstem lysates (Student's *t*-test, *p* = 0.019). We also probed for several negative markers of EV purity, namely the mitochondrial outer membrane protein

VDAC, the lipoprotein ApoA1, and the endoplasmic reticulum protein Calnexin (CANX). VDAC was present at lower levels in ABEVs than in brainstem lysates ( $p = 0.001$ ). ApoA1 and CANX were present at the same levels in ABEVs and brainstem lysates ( $p = 0.46$  and  $0.89$ , respectively). It should be noted that EV-specific proteomes contain far fewer distinct proteins than tissue-specific proteomes, so any protein found in EVs is expected to comprise a larger portion of the EV proteome than of the tissue proteome (and thus to be enriched in EVs). Equivalent amounts of a protein in ABEVs and brainstem lysates (such as that observed for ApoA1 and CANX) therefore represent a relative depletion of that protein in ABEVs compared to the protein's expected increased share of the ABEV proteome.

We next used tandem mass spectrometry to characterize the ABEV proteome. In the same three biological replicates of ABEVs, we identified a total of 284 characterized proteins (Figure 1.5C), 244 of which were previously detected in the proteomic screen used to identify ABC3 substrates. We detected several proteins that fulfill MISEV2018 requirements for EV proteomic characterization and purity, including heterotrimeric G proteins, annexins, cell adhesion molecules, cytoskeletal proteins, and a heat shock protein (Table 1.1). While we detected the negative EV marker APOB, it was observed at low Mascot scores in only two of three replicates, consistent with minor lipoprotein contamination often seen when purifying EVs by SEC (Stranska et al., 2018; Brennan et al., 2020). Taken together with our findings from immunoblotting, these results show that ABEVs are enriched for positive markers of EVs and largely devoid of negative markers of EVs, consistent with a relatively pure EV preparation with no major co-isolating contaminants.

<b>MISEV Category</b>	<b>Subtype</b>	<b>Proteins found (number of samples)</b>
Positive EV markers 1- Transmembrane or GPI-anchored proteins associated with plasma membrane and/or endosomes	1a: non-tissue specific.	<i>Heterotrimeric G proteins</i> : GNAO1 (3), GNAQ (2), GNA11 (2) <i>Integrins</i> : ITGA6 (2) EMMPRIN / BSG (1)
	1b: cell/tissue specific.	Neural cell adhesion molecule / NCAM (3) Neuronal-glia cell adhesion molecule / NgCAM (3)
Positive EV markers 2- Cytosolic proteins recovered in EVs	2a: with lipid or membrane protein-binding ability.	<i>Annexins</i> : ANXA2 (3), ANXA5 (3), ANXA6 (3) Heat shock proteins: HSC70 / HSPA8 (3) Syntenin / SDCBP (2)
	2b: promiscuous incorporation in EVs (and possibly exomeres).	<i>Cytoskeleton</i> : actin (3), tubulin (3) <i>Enzymes</i> : L-lactate dehydrogenase (2), alpha-enolase (1), pyruvate kinase (1), transketolase (1)
Negative EV markers 3- Major components of non-EV co-isolated structures	3a: lipoproteins (produced by liver, abundant in plasma, serum).	Apolipoprotein-B / APOB (2)
	3b: protein and protein/nucleic acid aggregates.	N/A

**Table 1.1 - Identification of positive and negative EV markers in ABEV proteome**

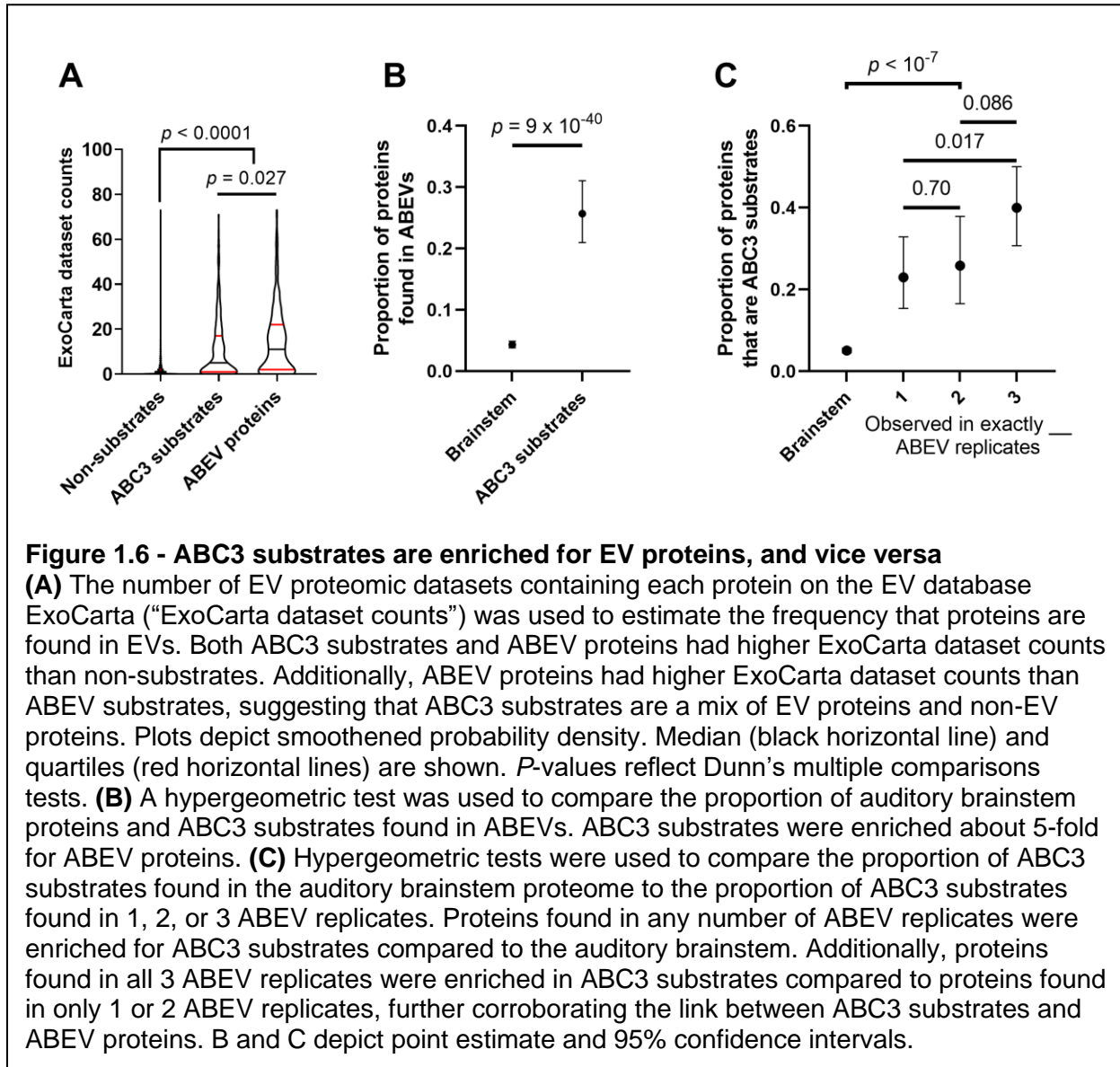
Several protein markers of EVs, both cytosolic and membrane-bound, were detected by mass spectrometry of ABEV samples. MISEV2018 requires that proteomic studies of EVs demonstrate the presence of at least one protein each in categories 1 and 2, along with the absence or depletion of proteins in category 3. We showed that all 3 ABEV replicates contain multiple proteins in categories 1 and 2. The only contaminant (category 3) protein detected by mass spectrometry, APOB, was detected at low Mascot scores in only 2 of 3 ABEV replicates, suggesting minor apolipoprotein contamination.

To obtain further evidence on the extent to which our ABEV proteome resembles published EV proteomes, we next turned to ExoCarta, a database that compiles transcriptomic, proteomic, and lipidomic datasets from studies of extracellular vesicles (Mathivanan and

Simpson, 2009; Mathivanan et al., 2012; Simpson et al., 2012; Keerthikumar et al., 2016). We used the number of EV mass spectrometry datasets represented in ExoCarta that contain each protein, designated “Dataset counts,” as an estimate of the relative frequency that EV proteomic studies have identified each protein. We compared the ExoCarta dataset counts of the brainstem proteome ( $n = 5653$ ) to those of ABEV proteins found in 1 ( $n = 106$ ), 2 ( $n = 77$ ) or all 3 ( $n = 103$ ) ABEV replicates (Figure 1.5D). A Kruskal-Wallis test found that ExoCarta dataset counts significantly differed among these four groups ( $p < 0.0001$ ). ABEV proteins were found in substantially more ExoCarta datasets than brainstem proteins (median = 0, 95% CI: 0 to 0), regardless of replicate count (Dunn’s multiple comparisons tests,  $p < 0.0001$ ). Additionally, ABEV proteins found in 1 and 2 replicates had the same ExoCarta dataset count ( $p = 0.93$ ), while ABEV proteins found in all 3 replicates had more than double the median dataset count (median = 17, 95% CI: 14 to 20) both of proteins found in 2 ABEV replicates (median = 7, 95% CI: 4 to 15;  $p = 0.0156$ ) and of proteins found in 1 ABEV replicate (median = 8, 95% CI: 4 to 12;  $p = 0.0064$ ). These results show that the ABEV proteome is highly similar to published EV proteomic datasets, and with the strongest resemblance to published EV proteomes among proteins associated most strongly with the ABEV proteome (i.e. proteins found in all 3 ABEV replicates).

We also sought to compare ExoCarta dataset counts of ABC3 substrates ( $n = 288$ ) and non-substrates ( $n = 5365$ ) to those of ABEV proteins ( $n = 286$ ) in order to determine the extent to which ABC3 substrates resemble ABEVs and published EV proteomic datasets (Figure 1.6A). A Kruskal-Wallis test showed that the three protein sets had different median ExoCarta dataset counts ( $p < 0.0001$ ). ABC3 substrates (median = 5, 95% CI: 4 to 8) had higher ExoCarta dataset counts than non-substrates (median = 0, 95% CI: 0 to 0; Dunn’s multiple comparisons test,  $p < 0.0001$ ), suggesting that ABC3 substrates resemble published EV proteomes more strongly than non-substrates. Additionally, ABEV proteins (median = 11, 95% CI: 8 to 14) had higher

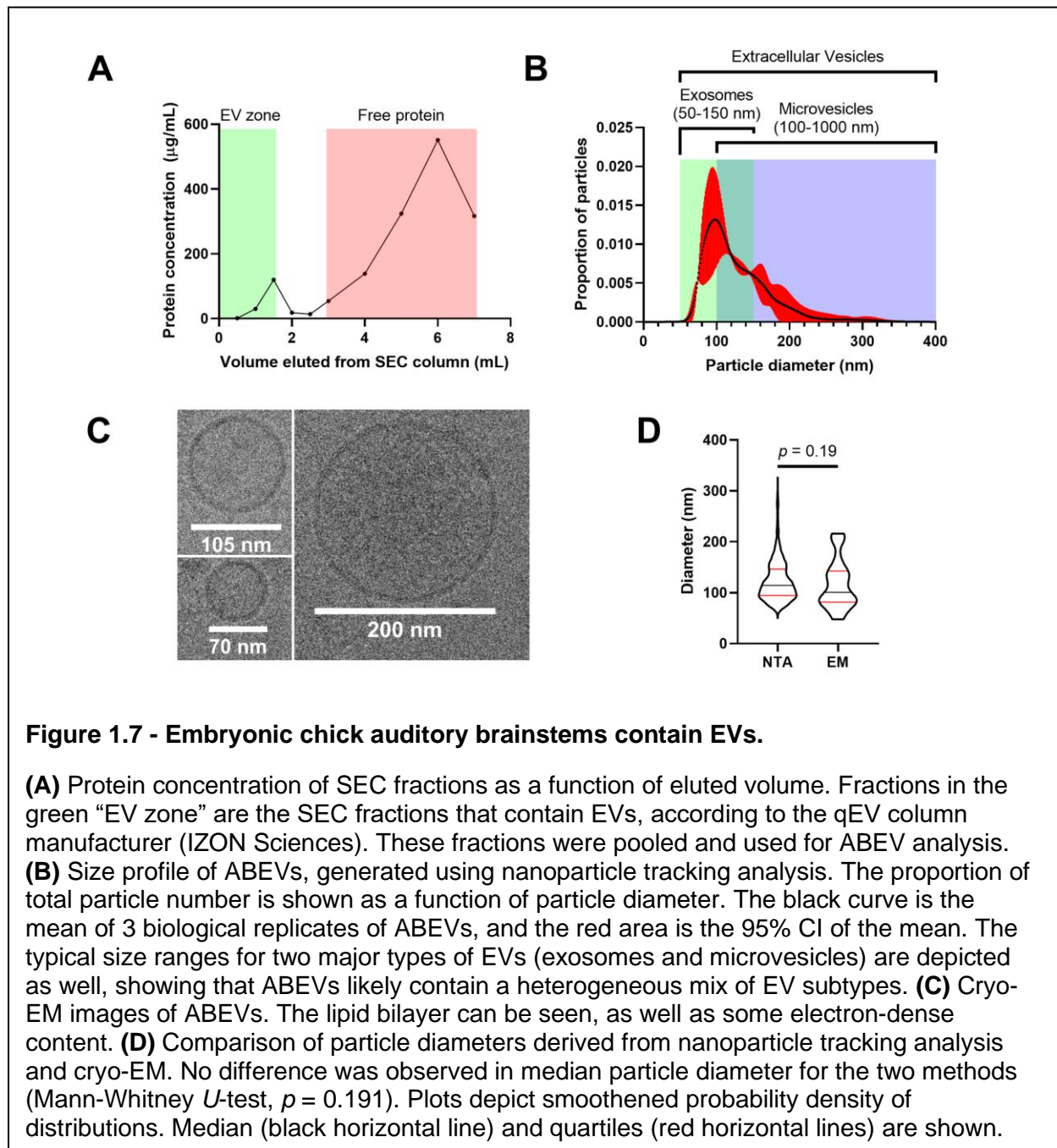
ExoCarta dataset counts than ABC3 substrates ( $p = 0.027$ ), consistent with ABC3 substrates being a heterogeneous mix of EV and non-EV proteins.



We then directly compared the ABEV proteome to our ABC3 substrates to ascertain whether ABC3 substrates are enriched in ABEVs. Given a total brainstem proteome of 5653 characterized proteins, a random overlap between the 244 previously observed EV proteins and the 288 ABC3 substrates would be expected to contain approximately 12 proteins ( $244 \times 288 / 5653 = 12.4$ ). By contrast, we observed 74 proteins that were both ABEV proteins and ABC3

substrates, which represented a nearly six-fold enrichment (Figure 1.6B, hypergeometric test,  $p = 8.71 \times 10^{-40}$ ). Thus, a large fraction (26%) of ABC3 substrates is detectable in the brainstem EV proteome, of which it composes a large proportion (30%). To test whether a protein's strength of association with the ABEV proteome is related to its probability of being an ABC3 substrate, we also looked at enrichment of ABC3 substrates among the individual sets of proteins found in 1, 2, or all 3 ABEV replicates. Each set showed heavy enrichment for ABC3 substrates (Figure 1.6C). However, the degree of enrichment differed among the 3 sets (Fisher-Freeman-Halton Exact Test,  $p = 0.032$ ). This difference was primarily driven by greater enrichment of ABC3 substrates among proteins found in all 3 ABEV replicates (Fold enrichment = 7.85) compared to proteins found in only 2 ABEV replicates (Fold enrichment = 5.07; two-tailed Fisher's Exact Test:  $p = 0.086$ ) and to proteins found in only one ABEV replicate (Fold enrichment = 4.51;  $p = 0.017$ ), not to the difference between proteins found in 2 and 1 replicates ( $p = 0.702$ ). Thus, proteins found in all 3 ABEV replicates were more likely to be ABC3 substrates than proteins found in only 1 or 2 replicates, corroborating our model that caspase-3 cleaves EV proteins in the chick auditory brainstem.

Despite this evidence that ABEV proteins are ABC3 substrates, we found that both procaspase-3 and active, cleaved caspase-3 were depleted in ABEVs compared to crude brainstem lysates (Figure 1.5A-C; Dunn's multiple comparisons tests,  $p = 0.056$  and  $p = 0.033$ , respectively), suggesting that proteolysis of ABEV proteins does not occur in ABEVs, but rather that caspase-3 cleaves ABEV proteins either before their loading into EVs or after EV uptake by recipient cells.

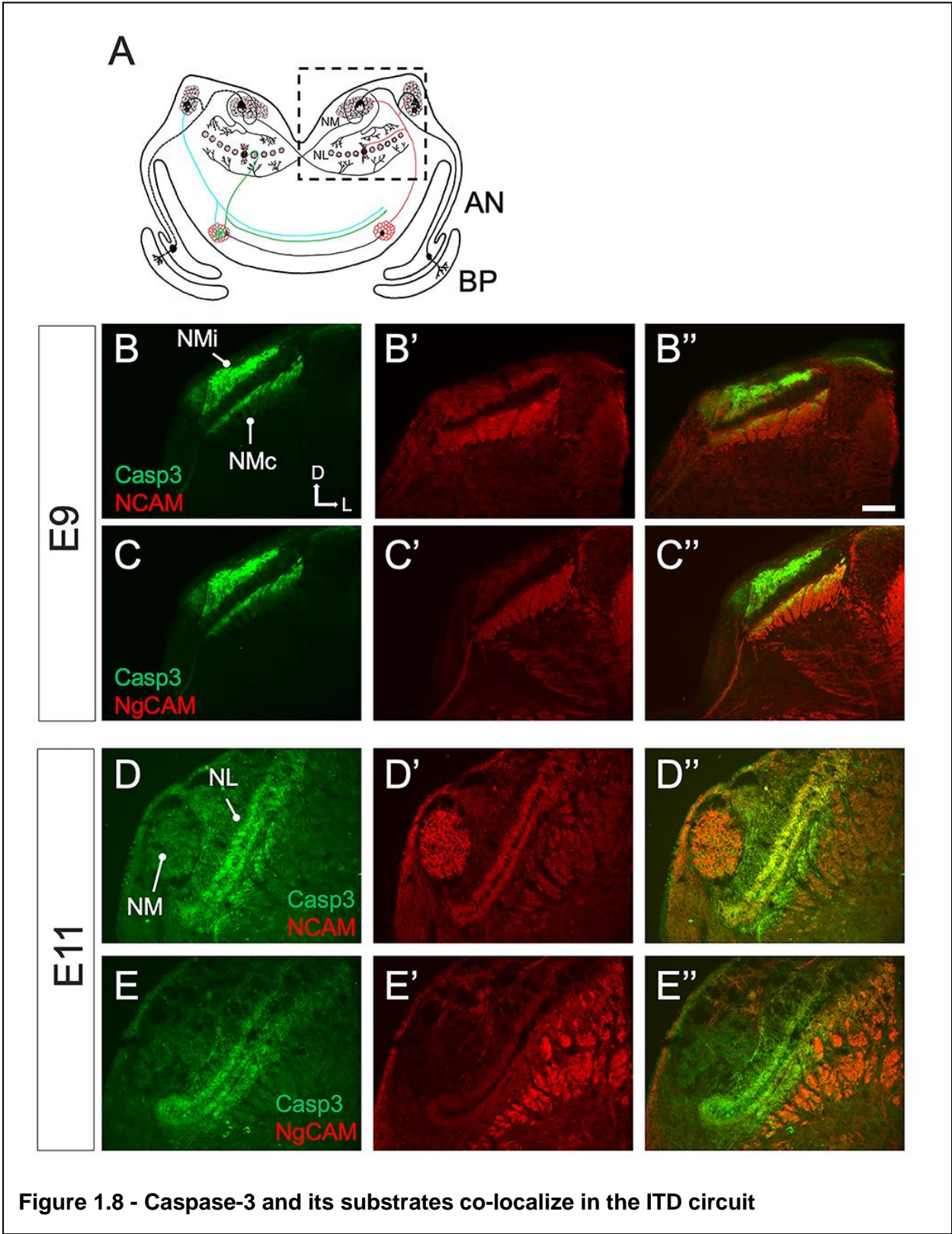


**EV characterization.** We used several additional approaches to characterize particles enriched from the auditory brainstem according to MISEV guidelines (Lötvald et al., 2014; Théry et al., 2018b). ABEVs used for proteomic characterization were derived from SEC fractions within the “EV zone” based on the recommendation of the column manufacturer (IZON Science) and independent studies verifying this claim (Böing et al., 2014; Vogel et al., 2016; Stranska et

al., 2018; Antounians et al., 2019; Brennan et al., 2020). Consistent with this expectation, a Lowry assay showed a peak in protein concentration that coincided with the EV zone fractions, as well as a peak that coincided with the “Free protein zone,” with relatively little protein in the fractions separating these two peaks (Figure 1.7A). The EV zone fractions were pooled and analyzed with nanoparticle tracking analysis (NTA), which measures the Brownian motion of particles in a sample to determine their size and concentration (Vestad *et al.* 2017) and cryogenic electron microscopy (cryo-EM) imaging (Figure 1.7B-C). NTA revealed that the pooled EV fractions contained particles with diameters ranging from 67 nm to 286 nm (1<sup>st</sup> to 99<sup>th</sup> percentile), with a peak in diameter at 99 nm (Figure 1.7B). Similarly, particles with a lipid bilayer, electron-dense content, and diameters ranging from 48 nm to 216 nm were observed by cryo-EM (Figure 1.7C). Particle diameters from NTA data corresponded to those from cryo-EM images, providing a calibration for NTA analysis (Figure 1.7D; Mann-Whitney *U*-test,  $p = 0.191$ ). Thus, particle sizes suggested that ABEVs consist of a heterogeneous mix of vesicles, including classically-defined exosomes (50-150 nm) and classically-defined microvesicles (100-1000 nm; Gould and Raposo 2013, Raposo and Stoorvogel 2013, Colombo *et al.* 2014).

**Caspase-3 substrates are co-expressed with cleaved caspase-3 in auditory brainstem structures during development.** Finally, we aimed to examine the expression patterns of ABC3 substrates during auditory brainstem development. Our screen for ABC3 substrates was conducted on chick brainstems in which caspase-3 activity had been inhibited on E9 and E10, when we observe strong cleaved caspase-3 expression exclusively in NM axons. We therefore predicted that ABC3 substrates would also be present in NM axons at this time. We focused on Neural Cell Adhesion Molecule (NCAM) and Neuronal-Glial Cell Adhesion Molecule (Ng-CAM, the chick homolog of mammalian L1CAM) because these two proteins were identified as both ABC3 substrates and ABEV proteins and because they have important roles in axon growth and guidance (Culver and Galileo, 2008; Westphal et al., 2010;

Enriquez-Barreto et al., 2012). As expected, these ABC3 substrates were expressed in NM axons on E9 (Figure 1.8A, B-B'', C-C''). In contrast, expression of NCAM and Ng-CAM in NM axons was absent at E11. Remarkably, it was instead observed in NL dendrites (Figure 1.8D-D'', E-E''), a dramatic change in expression that parallels the previously demonstrated developmental shift in cleaved caspase-3 expression through the ascending chick auditory brainstem pathway (Rotschafer et al., 2016). This result suggests that caspase-3 may facilitate proper circuit formation at multiple auditory brainstem synapses through proteolysis of a similar set of substrates that may directly influence both axonal and dendritic morphology.



**(A)** Schematic overview of a coronal section of the chick brainstem at the level of the auditory nuclei. Sound information flows from the auditory nerve (AN) to *Nucleus magnocellularis* (NM), which projects bilaterally to *Nucleus laminaris* (NL). The dashed-border rectangle shows the inset view in immunofluorescence images. **(B)** Double immunofluorescence shows that cleaved caspase-3 and the ABC3 substrates Neural Cell Adhesion Molecule (NCAM) are both expressed in NM axons on E9. **(C)** Double immunofluorescence also shows that cleaved caspase-3 and Neuronal-glia Cell Adhesion Molecule (NgCAM) are co-expressed in NM axons. **(D-E)** Cleaved caspase-3 and its substrates are expressed in NL dendrites on E11. Immunolabel of NCAM and Ng-CAM is seen both in NL dendrites and in non-auditory longitudinal axons seen in cross-section ventro-lateral of NL. NMi: NM ipsilateral axons. NMc: NM contralateral axons. Scale bar: 100 microns. Anatomical compass shows direction of Dorsal, Ventral, Lateral, and Medial.

## **DISCUSSION**

We previously showed that caspase-3 regulates normal axon targeting in the chick auditory brainstem (Rotschafer et al., 2016). Here, we used a proteomics approach to identify likely caspase-3 substrates that mediate this developmental role. We thus present, to our knowledge, the first non-apoptotic neurodevelopmental caspase degradome. Our DAVID and ExoCarta analyses revealed a heavy enrichment of extracellular vesicle proteins among ABC3 substrates. Many of our candidate substrates were proteins identified as caspase-3 substrates in other contexts, particularly in non-apoptotic proteomic analyses. We also showed that the number of ABEV replicates containing a protein was positively associated with both that protein's frequency of appearance in EV proteomic datasets on ExoCarta and with the protein's probability of being an ABC3 substrate, strongly suggesting that EV proteins and caspase-3 activity are related in the auditory brainstem. Finally, two ABC3 substrates present in ABEVs and involved in axon growth and guidance (NCAM and Ng-CAM) followed the same unusual developmental expression pattern as cleaved caspase-3, sequentially ascending the auditory pathway, corroborating the possibility that caspase-3 regulates an EV-mediated developmental process.

**Many ABC3 substrates are involved in proteostasis of cytoskeletal elements.**

Our findings suggest a novel neurodevelopmental mechanism by which caspase-3 activity in association with EVs is important for axon guidance and maturation of auditory nuclei. However, the function of caspase-3 activity in this context is still undefined. A common theme among the enriched functional categories of ABC3 substrates is that they represent several stages of the life cycle of cytoskeletal proteins, including amino acid biosynthesis, translation, protein folding, and filament polymerization and depolymerization. A key component of this model is the chaperonin-containing T (CCT) complex, an 8-subunit chaperone required for the folding of actin and tubulin monomers (Willison, 2018). We detected all 8 CCT subunits in the auditory brainstem and in ABEVs, and all subunits except CCT3 were ABC3 substrates. The CCT complex thus represents a potential node of control of cytoskeletal protein production that can be rapidly regulated by proteolysis, putting several other enriched categories of ABC3 substrates into proper perspective.

Disassembly of the cytoskeleton is a major cellular event during apoptosis. Actin was one of the first *in vivo* caspase-3 substrates identified (Mashima et al., 1997), and many caspase-3 substrates that regulate actin and microtubule dynamics have since been discovered (Lüthi and Martin, 2007; Crawford et al., 2013). Cytoskeletal degradation is known to be important for caspase-dependent axon guidance as well (Kellermeyer et al., 2018). For instance, degradation of spectrin by caspase-3 is required for NCAM-mediated neurite projection in cultured neurons (Westphal et al., 2010). In addition to cytoskeletal disassembly, caspases can stabilize the cytoskeleton by cleaving proteins responsible for cytoskeletal degradation and depolymerization, such as the proteasome and Actin-interacting protein 1 (Campbell and Holt, 2003; Li et al., 2007). The dual abilities of caspases to shape the assembly and disassembly of the cytoskeleton are especially useful in enabling integration of attraction and repulsion (Gu et al., 2017; Kellermeyer et al., 2018), which lends greater sensitivity,

complexity and temporal precision to growth cones' response to guidance cues (Buck and Zheng, 2002; Ming et al., 2002; Kaplan et al., 2014). Non-apoptotic caspase activity may therefore be a major way of achieving spatial precision in specialized synapses, such as those in the auditory brainstem.

**Functions of caspase-3 in EVs.** Caspase-3 cleavage of EV contents is known to influence intercellular communication by altering EV properties. For instance, caspase-3 must cleave the anti-apoptotic protein Bcl-xL in bone marrow stromal cell exosomes before they can be uptaken by myeloma and lymphoma cells, where the exosomes' pro-apoptotic content paradoxically contributes to cell growth and proliferation (Vardaki et al., 2016). It is also possible that caspase-3 proteolysis regulates the properties of ABEVs by determining which proteins are loaded into EVs and therefore what properties the EVs possess with respect to recipient cells (Sirois et al., 2011; Kim et al., 2017b). For example, cleavage of translationally controlled tumor protein (TCTP) by caspase-3 is required for sorting of TCTP into exosomes of apoptotic endothelial cells. These exosomes then exhibit a TCTP-dependent anti-apoptotic effect on neighboring cells, showing that caspase proteolysis of EV proteins has functional consequences even during apoptosis, when EVs are thought to function largely as a means to avoid death by removing active caspase-3 from cells (Trokovic et al., 2012; Böing et al., 2013).

The signaling roles of ABEVs may resemble those in other neural contexts (Sharma et al., 2013; Rajendran et al., 2014; Basso and Bonetto, 2016; Zappulli et al., 2016). Numerous studies have documented the ability of EVs to induce neural regeneration after injury (Ching et al., 2018; Bucan et al., 2019; Chen et al., 2019; Madison and Robinson, 2019; Ma et al., 2019; Xia et al., 2019). Recent work has shown that EVs likely function in every major aspect of neurodevelopment. Several neurodevelopmental deficits in a mouse model of Rett's disease are rescued by treatment with EVs from non-Rett's mice, which restore functions as diverse as neurogenesis, cell fate specification, synapse formation, and the establishment of normal firing

patterns (Sharma et al., 2019). Additionally, EVs carrying the receptor tyrosine kinase EphB can direct contact-independent axon repulsion by canonical receptor-ligand (EphB-ephrinB) reverse signaling (Gong et al., 2016; Zhao et al., 2018). This finding is particularly relevant to the present study because our lab has shown that ephrins and Eph receptors are expressed throughout development by NM and NL projections, where they play major roles in midline crossing, axon guidance and segregation, and establishment of tonotopic gradients (Cramer et al., 2000b, 2002, 2004; Person et al., 2004; Huffman and Cramer, 2007; Cramer and Gabriele, 2014). EphA5 is found in ABEVs, suggesting that ABEVs may have an important function in Eph-ephrin signaling in the chick auditory brainstem.

**Functional transfer of RNA in EVs.** Another major way that EVs influence neural development is by the transfer of genetic material between cells, including both mRNA and a wide variety of non-coding RNAs (ncRNAs) that can influence translation in recipient cells (Kim et al., 2017a; Mateescu et al., 2017; Fowler, 2019; Luz and Cooks, 2019; Zhou and Chen, 2019). RNAs are selectively loaded into EVs by RNA-binding proteins (RBPs), which make up about 25% of EV protein content (Santangelo et al., 2016; Di Liegro et al., 2017; Hobor et al., 2018; Sork et al., 2018; Statello et al., 2018; Groot and Lee, 2020; Leidal et al., 2020). Our ABC3 substrates showed substantial enrichment for RBPs, including RBPs with known roles in loading RNAs into EVs, such as YBX1 (Shurtleff et al., 2016; Kossinova et al., 2017; Yanshina et al., 2018), SYNCRIP (Santangelo et al., 2016; Hobor et al., 2018), and HNRNP-A2B1 and -K (Villarroya-Beltri et al., 2013; Leidal et al., 2020). The most widely studied EV RNAs are miRNAs, which have diverse roles in regulating tumor growth, synaptic plasticity, recovery from stroke, and progression of neurological disease (van Balkom et al., 2013; Xin et al., 2013; Cheng et al., 2014; Lafourcade et al., 2016; Yang et al., 2016; Xiao et al., 2019). However, a recent transcriptomic study of EVs showed that miRNAs represent a minority of the ncRNAs in most EV populations, suggesting that we have barely scratched the surface of functional

transfer of RNA in EVs (Turchinovich et al., 2019). Little is known about the functional roles of other ncRNA subtypes in EVs (Dragomir et al., 2018; Driedonks and Nolte-'t Hoen, 2019; Kolat et al., 2019; Zhou and Chen, 2019). The importance of ncRNAs for many neurodevelopmental functions and the dysregulation of ncRNAs in neurodevelopmental conditions such as autism and schizophrenia suggest that EV-mediated functional transfer of ncRNAs may contribute to translational regulation in neurodevelopment (Sun and Shi, 2015; Gillet et al., 2016; Rajman and Schratt, 2017; Wang and Bao, 2017; Cho et al., 2019).

However, the mechanism by which EV-associated RNA can influence neurodevelopment remains unclear. A likely candidate is the localized regulation of axonal translation, which is necessary for growth cone navigation and has been implicated in a variety of neurological disorders (Holt and Schuman, 2013; Hornberg and Holt, 2013; Cioni et al., 2018; Koppers et al., 2019). Interestingly, the compartmentalization of translation in growth cones in response to guidance signals is also regulated by RBPs, which comprise 1% of all growth cone protein content (Estrada-Bernal et al., 2012; Holt and Schuman, 2013; Hornberg and Holt, 2013; Cioni et al., 2018). Caspase-3 proteolysis of RBPs, like other mechanisms that regulate RBPs (Hornberg and Holt, 2013; Cioni et al., 2018; Leidal and Debnath, 2020; O'Brien et al., 2020), may therefore serve two parallel functions in auditory brainstem development: Cleavage of RBPs that protect and compartmentalize RNA in growth cones, and cleavage of RBPs that load and transport RNA in EVs. RBPs such as the HNRNP family, six of which are ABC3 substrates, are known to be involved in both processes, so the two functions are not mutually exclusive (Liu et al., 2008; Glinka et al., 2010; Hentze et al., 2018; Lee et al., 2018; Statello et al., 2018; Thelen and Kye, 2020). Caspase-3 may thus influence translation in the growth cone and in neighboring cells simultaneously by cleaving a single RBP.

**EV-mediated regulation of the apoptotic pathway.** Finally, another means by which EVs interact with caspases is the regulation of caspase activation in recipient cells. EVs,

secreted both by apoptotic and non-apoptotic cells, are capable of suppressing caspase activity in their recipient cells, often with exosomal miRNAs that alter the expression of apoptotic regulatory proteins (Yang et al., 2013; Zhao et al., 2017; Li et al., 2019; Xiao et al., 2019; Wen et al., 2020). Instances of EVs activating caspases are less common, and the examples that exist occur through an unknown mechanism (Liu et al., 2018). In the simplest scenario, EV-associated caspase-3 may induce its own activation in recipient cells of EVs. During apoptosis, caspase activation occurs through trigger waves, in which a positive feedback loop composed of caspase-3, caspase-9, and the X-linked inhibitor of apoptotic proteins (XIAP) allows for rapid dispersion of the apoptotic impulse throughout the whole cell (Cheng and Ferrell, 2018). Therefore, an additional benefit of caspase-dependent non-apoptotic processes is their potential for self-regeneration, which may be a mechanism by which caspase activity is transmitted between cells of the auditory brainstem (Rotschafer et al., 2016).

In summary, we have identified several hundred caspase-3 substrates that represent candidate mechanisms of auditory brainstem development, several of which involve communication between cells through EVs. Further work will be necessary to determine whether caspase-3-containing EVs from NM are responsible for the appearance of active caspase-3 in NL, and how EVs and their caspase-cleaved contents contribute to circuit assembly.

## **MATERIALS AND METHODS**

**Chick embryos.** Chicken (*Gallus gallus domesticus*) eggs were obtained from a flock of White Leghorn roosters and Rhode Island Red hens (AA Laboratory Eggs). Eggs were incubated at 38°C on a tilting shelf cabinet incubator for 3 days before transfer to *ex ovo* cultures.

**Ex ovo cultures.** Eggs were cleaned with 70% ethanol, and their contents were transferred to a square weigh boat (Fisher). The weigh boat was covered with a plastic culture plate (Fisher) to prevent dehydration. *Ex ovo* cultures were returned to the incubator on a stationary shelf.

**Embryo injection and brainstem dissection.** After 6 days *in vitro* (DIV), embryos were staged at Hamburger-Hamilton stage 34 (corresponding to E9; Hamburger and Hamilton 1951). The chorioallantoic and amniotic membranes were dissected and pulled aside, and the IV<sup>th</sup> ventricle of each embryo was injected with a 50  $\mu$ M solution of the caspase-3 inhibitor z-DEVD-fmk (R&D Systems, IC<sup>50</sup> = 18  $\mu$ M) or with vehicle solution (0.5% DMSO and 0.1% Fast Green in artificial cerebrospinal fluid). The injection was administered through a pulled glass capillary with a Picospritzer until the injection solution was seen in the tectum, about 5  $\mu$ L. This injection procedure was repeated the following day (7 DIV; E10). Four hours after the second injection, the cultured embryos were harvested and brainstems were removed. The portion of the brainstem containing the auditory nuclei was dissected and snap-frozen at -80°C.

**EV enrichment.** EVs were isolated using a modified version of a previously described method (Vella et al., 2017). Briefly, embryos were incubated to E10, when auditory brainstems were dissected and snap-frozen as described above. Frozen brainstems were weighed in sterile microfuge tubes, then thawed and washed with Hibernate-E medium (Fisher) to eliminate any cell debris remaining from dissection or thawing. After medium was discarded, the tissue was suspended in dissociation solution (7  $\mu$ L/mg of tissue), consisting of Hibernate-E with 150 units/mL of collagenase-3 (Worthington Biochemical). Samples were placed in a 37°C water bath on a shaking platform for 5 minutes. Tubes were gently inverted several times to resuspend tissue then incubated in the shaking water bath for an additional 10 minutes. To release EVs embedded in the extracellular space of the brainstem tissue while avoiding cell

damage or lysis, brainstem tissue was triturated gently by pipetting up and down several times with a sterile polypropylene P1000 filter tip (Corning). The dissociated tissue was returned to the shaking water bath for 5 minutes. To quench the collagenase digestion, PhosSTOP and Complete Protease Inhibitor Cocktail (Sigma) in Hibernate-E were added to the dissociate, for final concentrations of ~1X each. This quenching was followed by three serial centrifugation steps at 4°C (300xg for 5 minutes, 1500xg for 10 minutes, and 10,000xg for 30 minutes). The supernatant was transferred to a new tube for each subsequent centrifugation. The supernatant from the 10,000xg step was pipetted into a 220-nm cellulose acetate centrifugal filter tube (Corning), which was spun for 30 minutes at 10,000xg. The filtrate was used for size exclusion chromatography.

EVs were enriched using a 35-nm qEVoriginal column (IZON Science) according to the manufacturer's instructions. The column was brought to room temperature then flushed with at least 15 mL of sterile, degassed PBS. The EV-containing filtrate (above) was pipetted onto the column. After the filtrate had entered the resin, sterile degassed PBS was added to begin elution. Once the void volume (3 mL) had eluted, six 0.5-mL fractions were collected, then four 1-mL fractions were collected, all according to the manufacturer's instructions for a high-purity, low-yield EV sample. Protein in each fraction was quantitated using a Pierce modified Lowry assay (Thermo Fisher). The EV-containing fractions eluting 0 to 1.5 mL post-void were pooled and concentrated using an Amicon Ultra-2 mL centrifugal concentrator with 5 kDa MWCO (Millipore Sigma).

**NanoLC-MS/MS.** Brainstem and EV samples were prepared as described above. Equivalent microgram amounts of these samples were incubated in 70% formic acid for 72 hours at room temperature with constant shaking and occasional cuphorn ultrasonication. One crystal of cyanogen bromide (CNBr) was added to each sample. After overnight incubation at room temperature in the dark, samples were evaporated to dryness in a Speedvac vacuum

concentrator and re-dissolved in 8 M urea, 0.1 M triethylammonium bicarbonate (TEAB), and 10 mM tris(2-carboxyethyl)phosphine, pH 8.0, then incubated for 30 minutes at 37°C with occasional cuphorn ultrasonication. Samples were then diluted to 6 M urea with 0.1 M TEAB, pH 8.0 followed by addition of LysC at 1:100 (w/w) enzyme:protein ratio and incubation at 37°C. Samples were then diluted to 1 M urea with 0.1 M TEAB, pH 8.0 followed by addition of Trypsin at 1:100 (w/w) enzyme:protein ratio. After overnight incubation at 37°C, samples were supplemented with formic acid to 2% final concentration. Peptides were desalted using C18/SCX as described (Rappsilber et al., 2007), eluting with 160, 205, 255, 325, 540, and 800 mM ammonium acetate in 20% acetonitrile, 0.5% formic acid, followed by a final elution with 5% NH<sub>4</sub>OH/80% CH<sub>3</sub>CN. Elutions were dried under vacuum and re-dissolved in 0.1% formic acid in water.

Using an Easy-nLC 1000 liquid chromatograph, a portion of each sample was injected to a 250 x 0.075 mm (ID) nanocapillary column packed in-house with ReproSil-Pur C18-AQ beads (1.9 µm diameter; Dr. Maisch GmbH). The column was eluted with a gradient of CH<sub>3</sub>CN in 0.1% formic acid (0 – 5% over 5 min extending to 25% over 205 min and to 35% CH<sub>3</sub>CN over a further 30 min) at a flow rate of 250 nanoliters/min. Column eluate was sprayed into an LTQ Orbitrap Velos Pro mass spectrometer, collecting precursor spectra in the range 380 – 1600 m/z. Up to 15 of the most intense ions in each precursor spectrum with a charge of +2 to +4 and a minimum signal intensity of 5000 were fragmented by HCD with normalized collision energy of 30%. Ions were dynamically excluded for 40 s after two fragmentations within 30 sec, via a 500-entry list, with early expiration from the list after a detection within the exclusion period falling below S/N = 2.0.

Raw file data were processed to peaklists using Mascot Distiller 2.7.1. Using Mascot 2.6.1, each resulting mass list was subjected to target-decoy searching against the whole proteome of *Gallus gallus* (UniProt) plus a library of common contaminants, with semi-

CNBr+Trypsin enzyme specificity, a maximum of 2 missed cleavages, parent and product mass tolerances of 20 ppm, and variable modifications of Oxidation (M), Deamidated (NQ), Carbamyl (N-term) and Met->Hse (C-term M). Results were calculated using a threshold of  $p = 0.05$  yielding an experimental false discovery rate (FDR) of  $< 3\%$ . Matrices of peptides (rows) vs. samples (columns) were generated using in-house software.

**Identification of caspase-3 substrates.** Mascot data were thresholded at an FDR of  $< 0.03$ , and the resulting peptides were placed in a sample vs. accession matrix. The matrix was then filtered for peptides with a terminus of the form  $D\downarrow X$  or  $E\downarrow X$  (where D and E are aspartate and glutamate, the arrow represents the cleavage site, and X is any amino acid except proline) that were detected in at least one vehicle replicate but no z-DEVD-fmk (caspase-3-inhibited) replicates.  $D\downarrow P$  was excluded because the sample was treated with formic acid, which has substantial  $D\downarrow P$  specificity. Peptides meeting these criteria were considered to represent true caspase-3 cleavage sites.

**Functional annotation overrepresentation analysis.** Caspase-3 substrates were submitted for functional annotation term analysis with the Database for Annotation, Visualization, and Integrated Discovery (DAVID) Bioinformatics Resource 6.8 against a background of all proteins detected in the chick brainstem (Huang et al., 2009b, 2009a). The default database settings on DAVID were used to identify enriched functional annotation terms, defined as any term with a Benjamini-adjusted  $p$ -value of less than 0.05 (Benjamini and Hochberg, 1995).

**ExoCarta Analysis.** The relative probability of a protein appearing in an extracellular vesicle proteomic dataset was estimated using the total number of published EV datasets containing each protein on ExoCarta (Mathivanan and Simpson, 2009; Mathivanan et al., 2012; Simpson et al., 2012; Keerthikumar et al., 2016). Dataset counts included all proteins detected by mass

spectrometry. Other protein evidence was excluded from this analysis to avoid artificial inflation of dataset counts for proteins commonly used as exosome markers on Western blots. Similarly, mass spectrometry datasets within the same study and with identical protein repertoires (due to a targeted proteomics approach) were counted only once. A Kruskal-Wallis test was used to compare EV dataset counts, and Dunn's test was used for multiple comparisons.

**Nanoparticle Tracking Analysis.** EVs were purified from three biological replicates of 25-30 brainstems each, prepared on three different days as described above. Nanoparticle tracking analysis was performed as previously described (Breglio et al., 2020). Briefly, 150  $\mu$ L (approximately 1/10<sup>th</sup> of each sample) of each EV sample was diluted to 1.5 mL with PBS and filtered through a 0.2  $\mu$ m PES syringe filter (Millex 33mm, Sigma Millipore). A NanoSight NS300 controlled by NTA software version 3.1 (Malvern Panalytical) was used to measure the concentration and size distribution of EVs. Samples were pushed through a fluidics flow chamber at a constant flow rate using a syringe pump (Harvard Apparatus). The scattered light from vesicles illuminated with a 488 nm laser was recorded five times for 30 seconds at 30 frames/second using an sCMOS camera, keeping the camera sensitivity setting (13) identical between captures. Particle analysis was performed with a detection threshold of 3.

**Cryo-EM.** EVs from approximately 30 brainstems were isolated as described above. Three  $\mu$ L of sample solution was applied to a glow-discharged Quantifoil grid (Quantifoil, R2/2) then loaded on a Leica EMGP plunger (Leica Biosystems). After blotting away excess liquid, the grid was quickly plunged into liquid propane. The cryo-grid was then transferred to a JEM-2100F electron microscope using a Gatan cryo-transfer holder (Gatan, Inc.). The electron microscope was operated at 200 KV with a field emission gun, and the sample was examined under minimum dose. The images were recorded with a OneView camera (Gatan, Inc.) at 50,000x magnification, corresponding to 2.16  $\text{\AA}$ /pixel resolution of specimen space. The "draw ellipse" function in ImageJ was used to measure vesicle diameters. The ellipse was fitted to the

perimeter of each vesicle, whose diameter was taken as the average of the major and minor axes of the ellipse. A Mann-Whitney U-test was used to compare particle diameters from NTA and cryo-EM.

**Immunofluorescence.** Eggs were incubated to E9 and E11 at 38°C in a tilting cabinet incubator. Embryos were removed and brainstems were dissected and fixed in 4% paraformaldehyde in PBS at 4°C for at least 1 hour and up to overnight. Brainstems were incubated in 30% sucrose in PBS at 4°C overnight, then in a 1:1 mixture of (30% sucrose in PBS):(OCT Media) at 4°C until sectioning. Brainstems were then embedded in OCT media in a cryomold and were frozen at -20°C. Brainstems were sectioned coronally at the level of the auditory brainstem nuclei. Sections were cut at 12 µm and were flash-melted on subbed glass slides in a 1-in-4 series.

Slides with sectioned brainstems were rehydrated for 5 minutes in wash buffer (0.025% Triton X-100 in TBS), then solubilized for 10 minutes in 0.3% Tween-20 in TBS and washed with wash buffer for 3 x 10 minutes. Tissue was blocked for 1 hour at room temperature in 10% normal goat serum and 1% BSA in TBS, then incubated overnight in primary antibody (Table 1.2) diluted in 1% BSA in TBS at 4°C. Slides were immersed in wash buffer for 3 x 10 minutes, then incubated for 1 hour in secondary antibody diluted in 1% BSA in TBS. Slides were washed in wash buffer for 3 x 10 minutes, then mounted with Glycergel (Dako-Agilent) and stored at 4°C until imaging. Multichannel fluorescent images were taken at 20x magnification with an AxioCam camera mounted on an Axioskop-2 epifluorescent microscope (Zeiss) using Axiovision software.

**Western Blotting.** Three biological replicates of ABEV samples were prepared from 10-12 brainstems (30 mg of brainstem tissue) each as described above. The 300xg brainstem pellets were resuspended and dissolved by vortexing in RIPA buffer with Complete Protease Inhibitor and PhosSTOP (Roche). A Detergent-Compatible Bradford Assay was used to determine

protein concentration of crude brainstem lysates and ABEV samples. Brainstem lysates were diluted to concentrations approximately equal to those of the ABEV samples. Ten  $\mu\text{g}$  of protein from each sample were mixed with 4X Laemmli buffer (Bio-Rad) and 2-mercaptoethanol to a final concentration of 1X and 10%, respectively. Samples were loaded into an 8-20% Mini-PROTEAN TGX polyacrylamide gel (Bio-Rad). Together with a Chameleon Duo molecular weight ladder (LI-COR), samples were run in Tris/Glycine/SDS running buffer (Sigma Aldrich) for 1.5 hours at 100 V and 20 mA. Gels were removed and equilibrated for 15 minutes in Towbin buffer (Towbin et al., 1979). A PVDF membrane (Immobilon) was cut to size, activated in 100% methanol for 1 minute, then equilibrated in Towbin buffer for at least 5 minutes. The gel and membrane were sandwiched between filter paper (Bio-Rad) and transferred in Towbin buffer at 100 V and 250 mA for 1 hour. The membrane was removed, rinsed in nanopure water, and dried overnight. After reactivation in 100% methanol, the membrane was rinsed in nanopure water and incubated in REVERT Total Protein Stain for 5 minutes with gentle shaking. It was then washed twice for 30 seconds each in REVERT wash buffer (6.7% glacial acetic acid and 30% methanol in nanopure water) and imaged. Staining was reversed in REVERT reversal buffer (0.1 M NaOH and 30% methanol in nanopure water) for 15 minutes with gentle shaking. The membrane was rinsed briefly in nanopure water then blocked for 1 hour at room temperature in Odyssey Intercept Blocking Buffer (Li-Cor). The membrane was incubated overnight at 4°C in primary antibody (Table 1.2) in Odyssey antibody dilution buffer with gentle rocking. The membrane was washed 3 times for 5 minutes each in TBST (0.1% Tween-20 in Tris-buffered saline) then incubated in goat anti-rabbit IRDye 680RD antibodies diluted 1:20,000 in Odyssey antibody dilution buffer for 1 hour at room temperature. The membrane was washed 3 times for 5 minutes each in TBST, then rinsed in TBS and stored in TBS until imaging. The membrane was imaged wet at 169  $\mu\text{m}$  resolution using ImageStudio on an Odyssey CLx blot scanner (Li-Cor). NewBlot IR Stripping buffer (Li-Cor) was used to strip the blot. The membrane

was then rinsed 2 times for 5 minutes each in TBST, then rinsed 3 times for 5 minutes each in TBS before blocking and restaining in primary, as described above. Protein bands were normalized to total protein stain.

Target	Source	Antibody Name	Immunofluorescence concentration	Western blot concentration
NCAM	DSHB	4d	3.5 µg/mL	0.35 µg/mL
NgCAM	DSHB	8D9	3.5 µg/mL	N/A
Cleaved caspase-3	Cell Signaling Technologies	9664	1:100	N/A
Caspase-3 (p12 subunit)	Abcam	ab179517	N/A	1:1000
Calnexin	Abcam	ab13505	N/A	1:1000
VDAC1	Abcam	ab154856	N/A	1:1000
ApoA1	Invitrogen	PA5-21166	N/A	1:1000

**Table 1.2 - Antibody concentrations**

**Figure Design.** BioRender was used to create Figure 1.1. Microsoft PowerPoint was used to draw proportionally accurate Venn diagrams, and “Draw Venn Diagram” was used to draw the 4-way Venn Diagrams in Figure 1.4 (Bioinformatics & Evolutionary Genomics, Ghent University, <http://bioinformatics.psb.ugent.be/webtools/Venn/>). Graphpad Prism 8 was used for all other graphs not otherwise mentioned.

**Availability of Data.** The mass spectrometry proteomics data have been deposited to the ProteomeXchange Consortium (<http://proteomecentral.proteomexchange.org>) via the PRIDE partner repository (Vizcaino et al., 2013) with the dataset identifier PXD021728.

## **Chapter 2 : Non-apoptotic caspase activity preferentially targets a novel consensus sequence associated with cytoskeletal proteins in the developing auditory brainstem**

The auditory system has two main tasks: identifying sounds and determining sound source location. The first task involves encoding features of the sound itself, such as frequency, intensity, and timbre (Agus et al., 2019). However, the second task is more complex because sounds do not come with explicit information regarding their source's location. Instead, the auditory brainstem models the sound landscape by integrating differences in sound intensity and arrival time between the ears, known as interaural level differences (ILDs) and interaural time differences (ITDs), respectively (Carr and Konishi, 1990; Overholt et al., 1992; Schroger, 1996; Hyson, 2005). Highly specialized circuitry is necessary to detect microsecond-level ITDs, which are spatially represented in the auditory brainstem according to both ITD magnitude and sound frequency (Köppl and Carr, 2008; Ohmori, 2014). This dual specificity presents a unique neurodevelopmental challenge to the processes that regulate axon guidance and synapse formation in the ITD pathway. It is unsurprising, therefore, that neurodevelopmental disorders that alter circuit development are commonly accompanied by anatomical and functional deficits in the auditory brainstem (Talge et al., 2018, 2021; Smith et al., 2019; McCullagh et al., 2020; Chen et al., 2021; Miron et al., 2021). The auditory brainstem is thus an ideal model system for studying the development of ultra-precise neural circuitry.

We have addressed the molecular mechanisms behind formation of the embryonic chick auditory brainstem, specifically in the role of non-apoptotic caspase activity in the assembly of the chick ITD circuit. While caspases are classically associated with programmed cell death (Hengartner, 2000; Elmore, 2007; Fuchs and Steller, 2011), their non-lethal roles in cell

differentiation pathways and morphological change are now receiving overdue recognition (Schwerk and Schulze-Osthoff, 2003; Galluzzi et al., 2012; Unsain and Barker, 2015; Nakajima and Kuranaga, 2017). The nervous system is particularly well-equipped to use non-apoptotic caspase activity with little risk of accidental death (Campbell and Holt, 2003; Campbell and Okamoto, 2013; Wang and Luo, 2014; Gu et al., 2017; Hollville and Deshmukh, 2017; Mukherjee and Williams, 2017; Kellermeyer et al., 2018; Espinosa-Oliva et al., 2019; Nguyen et al., 2021). Neurons are remarkably resistant to injury, and the primary sites of morphological change in neurons (axons and dendrites) are often far removed from critical targets of apoptosis in and around the nucleus. We previously reported (Rotschafer et al., 2016) that expression of cleaved caspase-3 ascends the ITD pathway, appearing first in axons of the auditory nerve (AN) on embryonic days (E) 6-7; followed by expression in axons of the AN's target, Nucleus Magnocellularis (NM) on E8-10; and finally in dendrites of NM's target, Nucleus Laminaris (NL) on E10-12. Inhibition of caspase-3 activity with z-DEVD-fmk in cultures mimicking E6-9 elicited major defects in NM axon targeting and NL nucleus morphology on E10, prior to the appearance of TUNEL labeling in NM and NL cell bodies (Rotschafer et al., 2016) and to the onset of developmental cell loss in the auditory brainstem (Rubel et al., 1976). Caspase-3 thus mediates development of the auditory brainstem in the absence of cell death, suggesting a non-apoptotic function of caspase activity in circuit assembly.

To understand these developmental roles, it is important to consider how non-apoptotic caspase-3 activity facilitates neurodevelopment without causing cell death. In a recent study (Weghorst et al., 2020), we identified several hundred non-apoptotic caspase-3 substrates, which differed from apoptotic caspase substrates in both protein content and gene ontology (GO) term annotation. This distinction suggested that caspase-3 activity is actively redirected toward a novel, non-lethal substrate repertoire in the chick auditory brainstem, but the mechanism for this change remained unclear. Multiple substrate features enable caspase

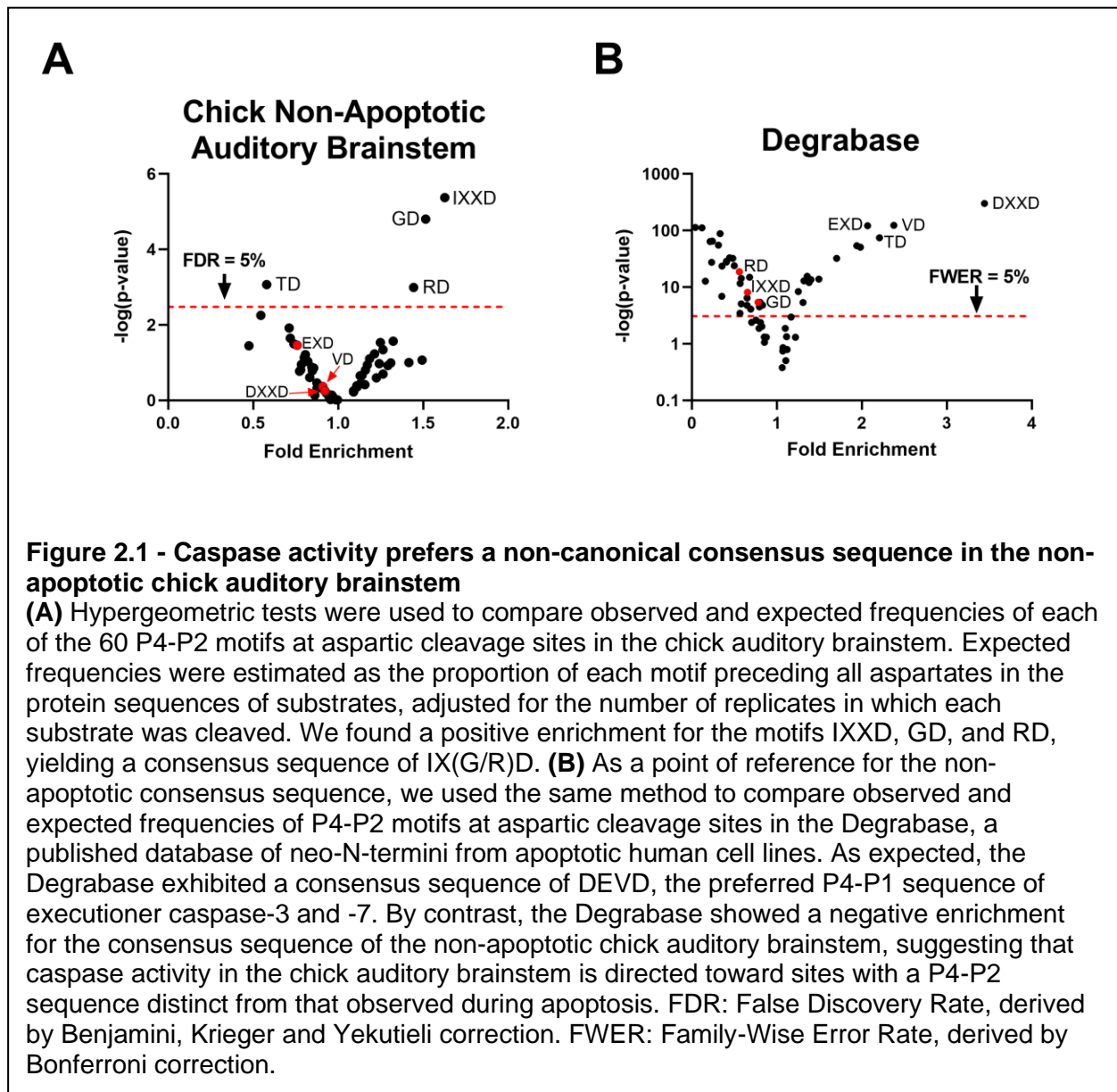
recognition, including the amino acid sequence surrounding the potential cleavage site as well as substrate-caspase interactions at allosteric protein regions, or exosites, that favorably place cleavage sites near the caspase active site (Talanian et al., 1997; Fischer et al., 2003; Timmer and Salvesen, 2007; Julien and Wells, 2017). The former category was seemingly refuted by the discovery that many *in vivo* caspase cleavage sites are cleaved with high efficiency despite their substantial deviation from the preferred cleavage site sequence, as identified via positional scanning substrate combinatorial libraries of synthetic peptides (Thornberry et al., 1997; Stennicke et al., 2000; Fischer et al., 2003; Timmer and Salvesen, 2007; Crawford et al., 2013; Julien and Wells, 2017). Exosite interactions provided a more parsimonious explanation for the cleavage of suboptimal sites, with a subsidiary role for cleavage site sequence in specific substrate recognition, binding, and proteolysis (Dagbay et al., 2014). However, a dominant role for exosites in facilitating diverse cleavages *within the context of apoptosis* does not preclude a role for cleavage site sequences in enabling a switch in substrate preference *for non-apoptotic functions*.

In the present study, we hypothesized that the preferred amino acid sequence N-terminal of the caspase cleavage site is shifted from the apoptotic consensus sequence (typically DEVD↓, where ↓ represents the cleavage site) to an alternative consensus sequence that is found in non-apoptotic substrates in the auditory brainstem. We showed that the non-apoptotic auditory brainstem caspase degradome involves a non-canonical consensus sequence, IX(G/R)D. Proteins cleaved at this consensus sequence were enriched for the GO term “Structural Constituent of Cytoskeleton” (SCoC), suggesting that the non-apoptotic consensus sequence allows caspases to preferentially target cytoskeletal proteins. We characterized the proteome of the apoptotic chick auditory brainstem and discovered the apoptotic consensus sequence (K/M)VD, suggesting that the non-apoptotic consensus sequence truly represents a switch in preference. Finally, we used the Degradbase (Crawford et

al., 2013) to predict likely candidates for an SCoC-directed non-apoptotic consensus sequence in humans.

## **RESULTS**

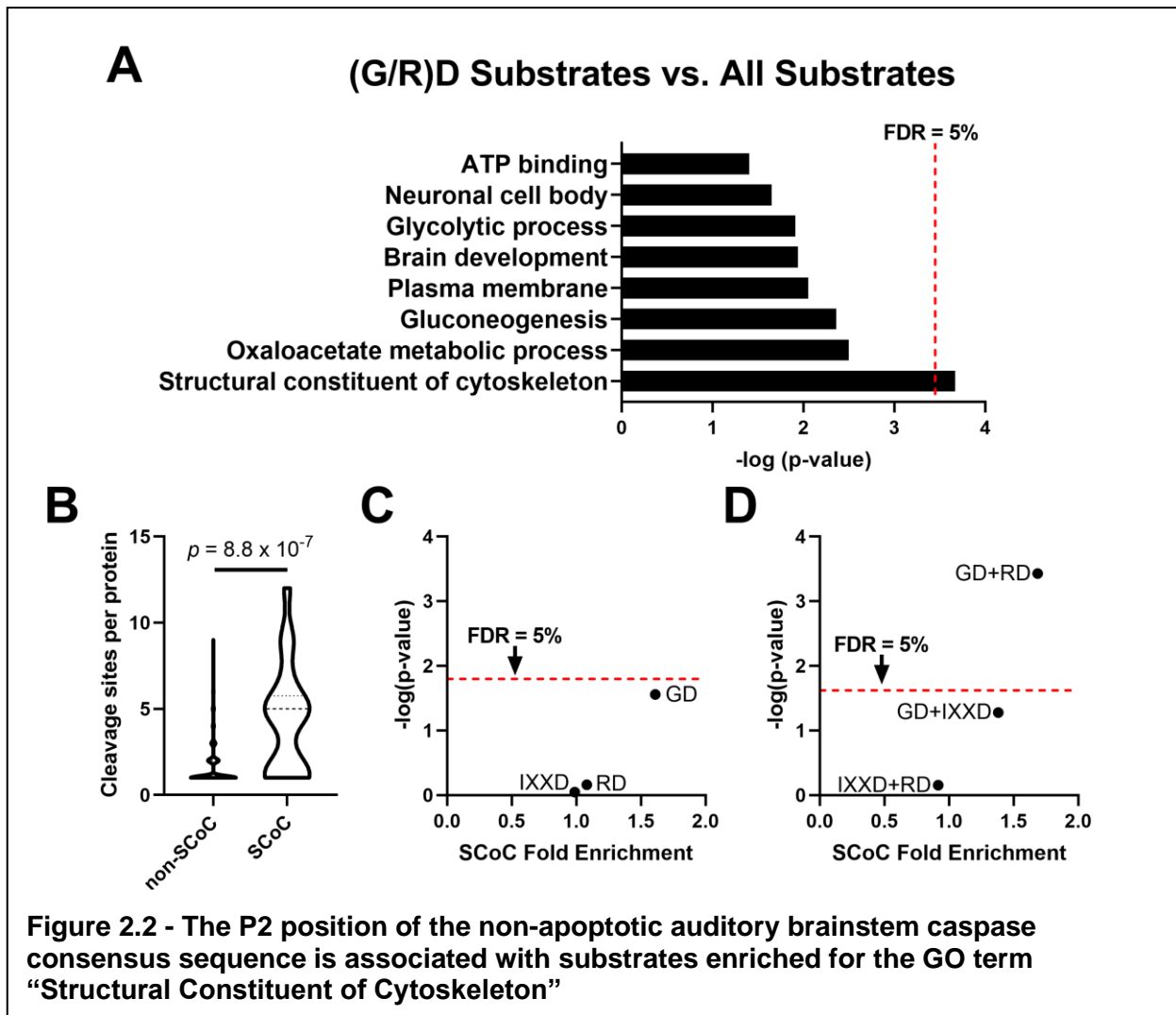
**Non-apoptotic caspase cleavage sites in the chick auditory brainstem are enriched for the motifs IXXD, RD and GD.** Using label-free peptidomic data from our prior study (Weghorst et al., 2020), we constructed a cleavage site consensus sequence for non-apoptotic caspase activity in the embryonic chick auditory brainstem. We filtered for peptides with an N-terminal D↓X terminus, where D represents the P1 aspartate, ↓ represents a cleavage site, and X represents the N-terminus of the peptide. This criterion yielded peptides corresponding to 655 distinct cleavage sites from 365 proteins. We used hypergeometric tests to compare the frequency of each single-residue motif in the P2-P4 subsites of these cleavage sites (Schechter and Berger, 1967) to the motif's frequency relative to all aspartate residues in the sequences of cleaved proteins. After correction for multiple comparisons, we found that three motifs were enriched above chance: IXXD (Fold enrichment: 1.63;  $p = 4.3 \times 10^{-6}$ ;  $q = 2.5 \times 10^{-4}$ ), GD (Fold enrichment: 1.52;  $p = 1.6 \times 10^{-5}$ ;  $q = 4.6 \times 10^{-4}$ ), and RD (Fold enrichment: 1.44;  $p = 1.0 \times 10^{-3}$ ;  $q = 0.015$ ), corresponding to the consensus sequence IX(G/R)D (Figure 2.1A). We applied the same method to a human apoptotic peptidome, Degradase (Crawford et al., 2013), both as a proof of concept for this technique of identifying caspase consensus sequences and as a point of comparison for the chick non-apoptotic consensus sequence. The Degradase consensus sequence showed the expected enrichment for the executioner caspase cleavage site preference (DEVD↓), while also exhibiting significant de-enrichment for the motifs enriched in the non-apoptotic auditory brainstem (Figure 2.1B). Conversely, the apoptotic consensus sequence was non-significantly de-enriched in the non-apoptotic auditory brainstem (Figure 2.1A).



**Non-apoptotic caspase substrates with consensus-like cleavage sites are enriched for the GO term “Structural Constituent of Cytoskeleton.”** We previously showed that caspase-3 is the most abundant caspase in the non-apoptotic auditory brainstem and is therefore likely responsible for most of the caspase cleavage sites we detected (Weghorst et al., 2020). This finding parallels the role of caspase-3 as the primary executioner caspase during apoptosis (Slee et al., 2001). However, caspase-3 has a conserved preference

for DEVD (Thornberry et al., 1997; Stennicke et al., 2000; Grinshpon et al., 2019), so the discovery of the IX(G/R)D consensus sequence is surprising. One possible explanation for this novel caspase-3 preference is a difference in the S4 and S2 active site pockets (Fuentes-Prior and Salvesen, 2004), which receive the P4 and P2 substrate residues, respectively. We performed an additional analysis to identify characteristics of substrates with cleavage sites containing these novel consensus motifs at P2 and P4. We used DAVID Bioinformatics Resource 6.8 (Huang et al., 2009a, 2009b) to identify GO terms enriched among auditory brainstem caspase substrates containing cleavage sites with enriched motifs, compared to the background of all 365 caspase substrates. Because the different active site pockets play distinct roles in substrate selection, any difference in a caspase active site pocket will affect the preference for all substrate motifs in that pocket but not necessarily of the other pockets. Consequently, changes to the S2 pocket would likely mediate preference for both RD and GD, while separate changes to the S4 pocket would shift its preference to IXXD. In this functional annotation analysis, we therefore pooled the P2 motifs (RD and GD), which we investigated separately from the enriched P4 motif (IXXD). The 57 substrates with IXXD sites showed no significant GO term enrichment after correction for multiple comparisons. By contrast, the 101 substrates with RD or GD sites were enriched for a single GO term, “Structural constituent of cytoskeleton” (“SCoC”; Figure 2.2A). According to DAVID, all 6 SCoC substrates in our dataset had at least one RD or GD cleavage site (Fold enrichment: 3.55;  $p = 2.2 \times 10^{-4}$ ;  $q = 0.032$ ), suggesting that non-apoptotic caspase activity in the auditory brainstem prefers cleavage site motifs that are found in cytoskeletal proteins.

**SCoC proteins are more likely to be cleaved at the GD motif and the combined (G/R)D motifs than expected by chance.** Two limitations in using DAVID to identify functional commonalities of consensus-like sites led us to refine our analysis. First, the chicken proteome is not as well-annotated as the proteomes of humans and more common model organisms, so chicken proteins often lack relevant GO terms. To correct this limitation, we manually searched the list of auditory brainstem caspase substrates for proteins with a human homolog that had the SCoC GO term. We identified three additional SCoC substrates, two of



**(A)** The DAVID Bioinformatics Resource 6.8 was used to examine GO terms of non-apoptotic chick auditory brainstem substrates with at least one GD or RD site. These substrates with consensus-like sites were significantly more likely to have the GO term “Structural Constituent of Cytoskeleton” (SCoC) than were auditory brainstem caspase substrates as a whole. **(B)** “Structural Constituent of Cytoskeleton” substrates had a greater number of caspase cleavage sites per protein per replicate than other substrates (Mann Whitney U-test). This result suggests that an alternative method is needed to ensure that the enrichment of SCoC proteins among caspase substrates with consensus-like sites is not due to SCoC proteins having a large number of cleavage sites, any of which could be consensus-like. **(C)** For each motif in the non-apoptotic auditory brainstem consensus sequence, Monte Carlo analysis was used to simulate the number of SCoC proteins expected to be cleaved at least once at that motif in each replicate (denoted a “protein-cleavage”) based on each replicate’s overall frequency of each motif. Total protein-cleavage counts were obtained by summing the counts for each replicate. The distribution of expected protein-cleavage totals was compared to that of observed protein-cleavage counts to obtain the SCoC Fold Enrichment and  $p$ -value. Only the GD motif was enriched among SCoC substrates ( $q = 0.086$ ), while RD and IXXD were cleaved at chance. **(D)** The three double-motif combinations of the non-apoptotic auditory brainstem consensus sequence were subjected to Monte Carlo analyses as in part C. The GD+RD motif combination was enriched among SCoC substrates even more than either of its constituent motifs ( $q = 7.8 \times 10^{-4}$ ). FDR: False Discovery Rate, derived by Benjamini, Krieger and Yekutieli correction.

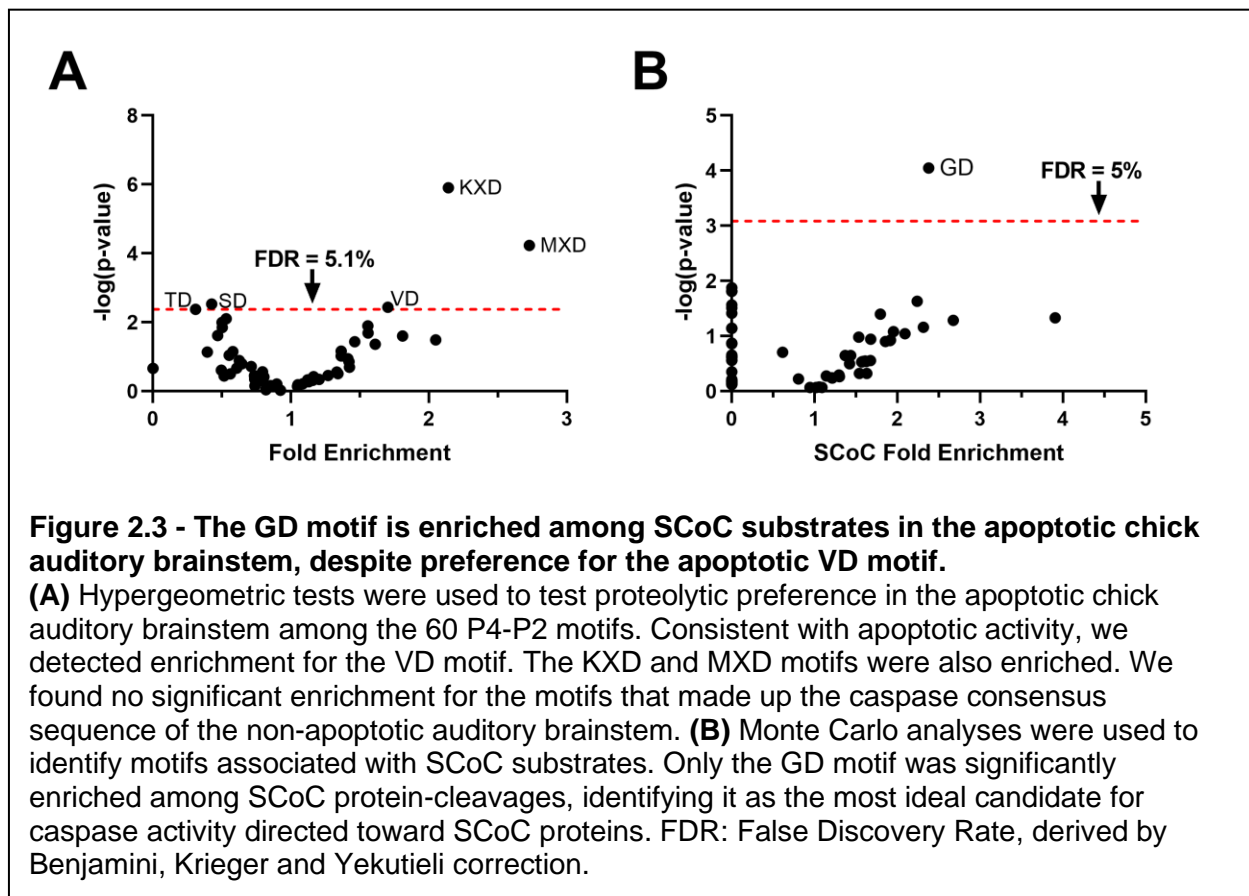
which had a GD cleavage site, bringing the fold enrichment of SCoC proteins among proteins with (G/R)D sites to 3.15 ( $p = 1.1 \times 10^{-4}$ ,  $q = 0.016$ ). Second, functional annotation analysis of proteins with consensus-like cleavage sites is biased toward substrates with greater numbers of cleavage sites. A single (G/R)D site qualifies a protein as having a consensus-like cleavage event, regardless of how many non-consensus-like sites the protein also has. Auditory brainstem SCoC proteins had substantially more cleavage sites per protein than non-SCoC proteins (Figure 2.2B; Mann-Whitney U-test,  $p = 8.8 \times 10^{-7}$ ), so SCoC proteins are inherently more likely to be cleaved at *any* site.

We therefore used Monte Carlo analyses to determine whether SCoC proteins are cleaved at consensus-like sites at a frequency greater than chance. In each biological replicate, each distinct SCoC protein was randomly “cleaved” at each of its observed sites, assuming the probability of cleavage at a specific motif was equal to the observed frequency of that motif among all cleavage sites in the same replicate. The total number of SCoC protein-cleavages attributable to each motif was obtained by summing the protein-cleavages for all SCoC proteins

in all replicates. The simulated distribution of SCoC protein-cleavages for each motif was then compared to the observed number of SCoC protein-cleavages for that motif to obtain a fold enrichment and  $p$ -value for the observation. We conducted this analysis for the 3 consensus motifs, as well as for the 3 double-motif combinations, and found that while SCoC proteins are cleaved at IXXD and RD sites at chance (Fold enrichment: 0.99 and 1.08;  $p = 0.90$  and  $0.69$ , respectively;  $q = 0.94$  for each), proteolysis of SCoC proteins occurs at GD sites at a frequency greater than chance (Figure 2.2C; Fold enrichment: 1.61;  $p = 0.028$ ;  $q = 0.087$ ). For the double-motif analyses, GD+RD was enriched among SCoC proteins even more than GD or RD alone (Figure 2.2D; Fold enrichment: 1.69;  $p = 3.7 \times 10^{-4}$ ,  $q = 7.8 \times 10^{-4}$ ), suggesting complementarity of the two motifs in cleaving SCoC proteins. Indeed, 17 of the 20 observed SCoC protein-cleavages had at least one GD or RD site, a greater proportion than any other pair of motifs. GD+IXXD was enriched among SCoC cleavage sites to a lesser extent (fold enrichment: 1.38;  $p = 0.053$ ;  $q = 0.055$ ), while IXXD+RD cleavage events of SCoC proteins were not enriched (Fold enrichment: 0.92;  $p = 0.70$ ;  $q = 0.49$ ). These data indicate that the P2 subsite preference of non-apoptotic caspase activity in the chick auditory brainstem is directed toward a specific motif (GD) and a motif combination (GD+RD) that are overrepresented among cytoskeletal protein-cleavages. These data suggest that the preferred cleavage site sequence of non-apoptotic caspase activity causes preferential proteolysis of cytoskeletal substrates during auditory brainstem development.

**SCoC cleavage events in the apoptotic chick auditory brainstem are disproportionately associated with the GD motif, despite its absence from the apoptotic consensus sequence.** We next sought to test whether the enrichment for specific motifs among cytoskeletal substrates is unique to non-apoptotic caspase activity, or whether such enrichment might be observed in apoptotic sites as well. The chick auditory brainstem undergoes apoptotic cell death starting on embryonic day (E) 12 or 13 (Rotschafer et

al., 2016), with a loss of many cells in auditory nuclei including NM and NL (Rubel et al., 1976). These are the same cells in which we observed non-apoptotic caspase activity just a few days earlier on E10 and from which our set of non-apoptotic caspase substrates was derived. We therefore conducted tandem mass spectrometry on E13 brainstems as an apoptotic counterpart to the E10 non-apoptotic auditory brainstem. As with the non-apoptotic brainstem proteome, we filtered for peptides C-terminal to a D↓X terminus, which yielded 199 distinct caspase cleavage sites from 126 distinct proteins. We used hypergeometric tests to reveal proteolytic preference for the 60 P4-P2 motifs (Figure 2.3A) and found significant enrichment for three motifs: KXD (Fold enrichment: 2.14;  $p = 1.3 \times 10^{-6}$ ;  $q = 7.6 \times 10^{-5}$ ), MXD (Fold enrichment: 2.73;  $p = 5.9 \times 10^{-5}$ ;  $q = 1.8 \times 10^{-3}$ ), and VD (Fold enrichment: 1.70;  $p = 3.7 \times 10^{-3}$ ;  $q = 0.051$ ), corresponding to a consensus sequence of (K/M)VD. After correction for multiple comparisons, we detected no significant enrichment in the motifs that comprised the chick non-apoptotic consensus



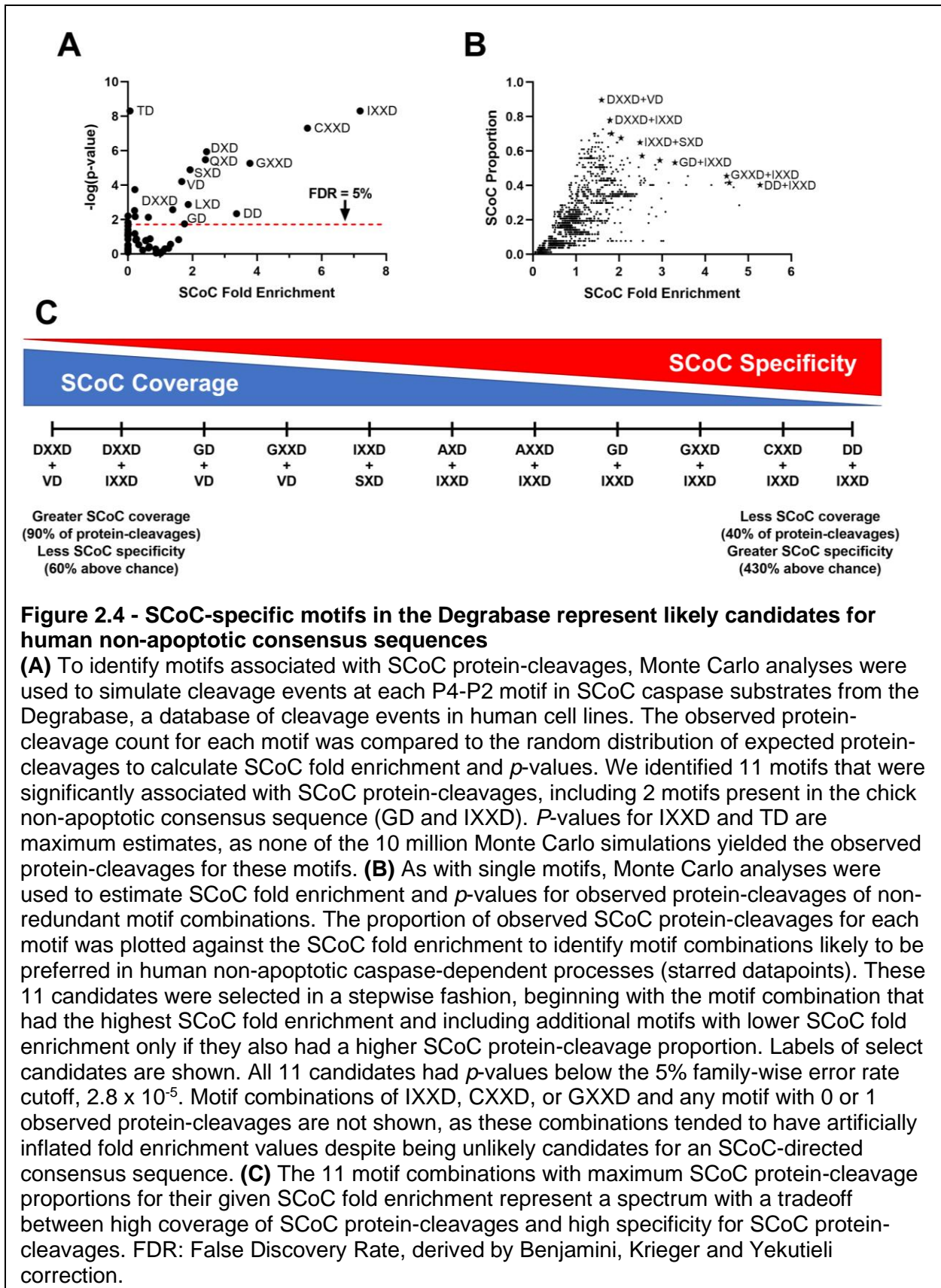
sequence: IXXD (Fold enrichment: 1.13;  $p = 0.53$ ;  $q = 0.66$ ), GD (Fold enrichment: 1.46;  $p = 0.036$ ;  $q = 0.16$ ), and RD (Fold enrichment: 0.76;  $p = 0.39$ ;  $q = 0.59$ ). Since we were primarily concerned with the role of the P2 subsite in determining cleavage site preference, we interpreted the heightened preference for the apoptotic motif VD in the E13 auditory brainstem as evidence for activity resembling the canonical apoptotic consensus sequence at the P2 subsite.

We next aimed to identify motifs associated with SCoC protein-cleavages in the chick apoptotic degradome. We subjected all 60 P2-P4 motifs to Monte Carlo analyses in which cleavage events were simulated at their observed frequencies for each motif in each replicate. Fold enrichment of SCoC protein-cleavages and  $p$ -values were obtained for each motif by comparing the observed SCoC protein-cleavages at the motif to the expected distribution of SCoC protein-cleavages at the motif (Figure 2.3B). We found that SCoC protein-cleavages were significantly enriched for one motif: GD (Fold Enrichment: 2.38;  $p = 8.9 \times 10^{-5}$ ,  $q = 5.4 \times 10^{-3}$ ). GD was part of the consensus sequence in the E10 non-apoptotic auditory brainstem, suggesting that the non-apoptotic consensus sequence represents a departure from the apoptotic consensus sequence toward a motif associated with SCoC proteins ( $p = 0.025$ ; hypergeometric test for the SCoC-enriched motif being from the non-apoptotic consensus sequence). All three SCoC proteins (actin, alpha tubulin, and beta tubulin) observed in the three replicate samples of the E13 brainstem were found to be cleaved at a GD site, so a double-motif analysis was not warranted for this dataset. Additionally, all 17 distinct SCoC cleavage sites in the E13 apoptotic brainstem were also observed in the E10 non-apoptotic brainstem, but 23 distinct SCoC cleavage sites were only found in the E10 brainstem, indicating that non-apoptotic caspase activity cleaves a mix of apoptotic and novel SCoC cleavage sites. These findings corroborate the function of the GD motif in facilitating specific caspase-dependent proteolysis of SCoC proteins in non-apoptotic contexts.

**Prediction of the neurodevelopmental non-apoptotic consensus sequence in humans.** Caspases exhibit remarkable conservation between species, so we next explored the possibility that human caspases are also capable of shifting to an SCoC-specific consensus sequence in non-apoptotic contexts. No proteome for a non-apoptotic caspase-dependent process in humans has yet been published, but the Degrabase (Crawford et al., 2013) offers a large sample of apoptotic cleavage sites that might be interrogated via the same method we used to show that the GD motif is associated with SCoC protein-cleavages both in the E10 and E13 chick auditory brainstem. Degrabase contains 1684 distinct D↓X sites, observed a total of 5713 times in 32 biological replicates and belonging to 1267 distinct Uniprot accessions. To identify which motifs are disproportionately associated with SCoC protein-cleavages, we conducted Monte Carlo analyses on the 60 P2-P4 motifs. As before, we built an expected distribution of the number of SCoC protein-cleavages for each motif by modeling proteolysis of each SCoC protein at the observed frequency of the motif in that replicate. We summed the results of all replicates and compared this distribution to the observed protein-cleavages for each motif, obtaining fold enrichment and  $p$ -values as before (Figure 2.4A). We found that 11 motifs were significantly associated with SCoC protein-cleavages in the Degrabase at a 5% false discovery rate. Notably, two motifs found in the chick non-apoptotic consensus sequence (IXXD and GD) were among these 11 ( $p = 0.044$ ; hypergeometric test for 2 or more of the 11 motifs being from the chick non-apoptotic consensus sequence).

Despite several motifs conveying substantial preference for SCoC proteins (more than 7-fold in the case of IXXD), no single motif accounted for the majority of SCoC protein-cleavages in Degrabase. We therefore sought to identify double-motif combinations that provide better coverage of SCoC protein-cleavages while maintaining specificity of proteolysis. As with the single motifs, we ran Monte Carlo simulations on the 1770 double-motif combinations. To find likely candidates for an SCoC-directed non-apoptotic consensus sequence, we plotted the

proportion of SCoC protein-cleavages attributable to each motif combination against the fold enrichment of SCoC protein-cleavages at each motif combination (Figure 2.4B). We first selected the motif combination with the highest SCoC fold enrichment (DD+IXXD) as a non-apoptotic consensus candidate. All other candidates were permitted to have a lower SCoC fold enrichment only if they also had a higher SCoC proportion than the previous candidate. This stepwise method yielded 11 motif combinations that represented a spectrum of consensus sequence candidates ranging from high specificity of SCoC proteolysis to high coverage of SCoC protein-cleavages (Figure 2.4C). All 11 of these candidates had  $p$ -values consistent with a family-wise error rate of less than 5% ( $p < 2.8 \times 10^{-5}$ ). Remarkably, one of the candidates, GD+IXXD, resembled the consensus sequence of the non-apoptotic chick auditory brainstem, indicating that the cleavage site preference in non-apoptotic caspase-dependent processes may be conserved among vertebrates ( $p = 9.3 \times 10^{-3}$ ; hypergeometric test for 1 or more of the 11 candidates containing 2 motifs from the chick non-apoptotic consensus sequence).



## **DISCUSSION**

How caspases select their substrates is key to understanding how non-apoptotic caspase-dependent processes can shape cell fate non-lethally. Here we showed that non-apoptotic caspase activity prior to programmed cell death in the chick auditory brainstem targets a non-canonical consensus sequence, IX(G/R)D↓. Portions of this consensus sequence (especially the GD motif) were associated with the GO term “Structural Constituent of Cytoskeleton” in the E10 non-apoptotic chick brainstem, as well as the E13 apoptotic chick brainstem and the human apoptotic degradome, suggesting a conserved function of the cleavage site sequence in guiding caspase activity toward cytoskeletal substrates.

**Cytoskeleton-directed caspase activity provides a mechanism by which caspases can alter cell morphology.** Our findings thus elucidate a mechanism by which caspases can specifically cleave cytoskeletal subunits, a function needed for many of their non-lethal neurodevelopmental roles. Studies on non-apoptotic neurodevelopmental roles of caspases in *Drosophila* have provided abundant evidence that axonal growth cones use local changes in caspase activity as a mechanism linking external guidance cues to internal cytoskeletal changes (reviewed in Kellermeyer et al., 2018). A variety of non-apoptotic functions for caspases in vertebrate neural circuit formation have been enumerated as well, including growth cone chemotaxis (Campbell and Holt, 2003), axon outgrowth (Westphal et al., 2010), axon branching (Campbell and Okamoto, 2013), dendritic pruning (Ertürk et al., 2014), dendritic branching (Khatri et al., 2018), and long-term depression (Li et al., 2010; Han et al., 2013). However, few studies (Westphal et al., 2010; Sokolowski et al., 2014; Khatri et al., 2018) have demonstrated that caspases directly cleave cytoskeletal proteins to carry out their neurodevelopmental roles, let alone explained how caspases avoid cleaving pro-apoptotic substrates in the process. Our study is the first to provide evidence not only that cytoskeletal proteins are cleaved in non-apoptotic caspase-dependent processes, but also that the cleavage

site preference of caspases is shifted toward sites that favor degradation of cytoskeletal proteins during neural circuit formation.

**Limitations.** Our method for determining caspase consensus sequences assumes that all aspartates within caspase substrates are equally susceptible to caspase-mediated proteolysis. However, since caspases most readily cleave residues with cytosolic topology and with high solvent accessibility (Soni and Hardy, 2021), this assumption could be improved in future studies by only considering aspartates that meet these criteria. Transmembrane proteins would be most affected by this change, since caspases do not usually operate in the luminal or extracellular space, albeit some exceptions have been observed (Hentze et al., 2001; Shamaa et al., 2015; Wang et al., 2016). Despite this drawback, the frequency of P2-P4 motifs in the entire set of substrates is likely to be a good approximation for the frequency of motifs accessible to caspase activity.

Our analysis is also constrained by the progression of caspase activity in the developing auditory brainstem. Non-apoptotic caspase activity assists in auditory brainstem circuit formation from E6 to E12, while apoptotic cell death predominates from E12 to E17 (Rubel et al., 1976; Rotschafer et al., 2016). However, it is unknown whether non-apoptotic caspase activity continues to refine auditory brainstem synapses during the period of cell death. If it does, our E13 caspase degradome may be derived from simultaneous caspase-dependent processes instead of apoptosis alone. Nevertheless, our analysis benefits from the use of a system in which apoptosis is not artificially induced but rather reflects normal developmental cell death. The different caspase consensus sequences in the E10 and E13 auditory brainstems also suggest that a distinct set of substrates is being targeted at the two ages, especially because the apoptotic VD motif was part of the E13 consensus sequence.

**Preference for IXXD during non-apoptotic processes may prevent proteins from being cleaved at pro-apoptotic sites.** Although we identified IXXD in the human caspase degradome by searching for motifs more likely to be cleaved in SCoC proteins, IXXD was not enriched among SCoC protein-cleavages in the non-apoptotic chick auditory brainstem. Indeed, we found no GO terms enriched among substrates cleaved at IXXD compared to all auditory brainstem substrates. This discrepancy may reflect inter-species differences in SCoC-associated motifs. However, if IXXD is not involved in directing caspase activity toward any functional category of substrates in the non-apoptotic chick auditory brainstem, what is the significance of this motif? One possibility is that preference for IXXD protects cells from potentially lethal cleavage events. Negatively-charged P4 residues (i.e. DXXD or EXXD motifs) are very common in the cleavage sites of major pro-apoptotic substrates (Thornberry et al., 1997; Fischer et al., 2003; Crawford et al., 2013; Rawlings et al., 2018). Even SCoC proteins, which are not canonical apoptotic signaling molecules, can promote apoptosis when cleaved at sites with negatively charged P4 residues. Caspase-mediated proteolysis of actin at ELPD<sup>244</sup> or vimentin at DSVD<sup>85</sup> yields pro-apoptotic cleavage fragments, the overexpression of which is sufficient to cause morphological changes consistent with cell death (Mashima et al., 1999; Byun et al., 2001). The preference for hydrophobic isoleucine at the P4 position in the IXXD motif may thus serve to prevent proteolysis at sites likely to lead to the cell's demise. This anti-apoptotic cleavage site preference joins the ranks of other such mechanisms that prevent cell death during non-apoptotic caspase-dependent processes, including binding by Inhibitors of Apoptotic Proteins (IAPs), which act as muzzles for the caspase active site (Scott et al., 2005; Silke and Meier, 2013); localization to cellular compartments far from the cell body and nucleus, such as growth cones and dendrites (Campbell and Holt, 2003; Li et al., 2010); low expression levels of pro-apoptotic molecules besides caspases (Wright et al., 2004; Hollville and

Deshmukh, 2017; Mukherjee and Williams, 2017); and rapid degradation of active caspases, a coordinated effort of IAPs and the proteasome (Galbán and Duckett, 2010; Ertürk et al., 2014).

**The non-apoptotic auditory brainstem likely has a greater range of caspase activity than the apoptotic auditory brainstem.** Our data show that the E10 auditory brainstem has more distinct caspase cleavage sites and substrates (655 and 365, respectively) compared to the E13 auditory brainstem (191 and 126, respectively), suggesting that there is more caspase activity in the non-apoptotic auditory brainstem than during apoptosis. However, this observation does not imply a greater density of caspase activity (per cell or per unit volume) on E10 than on E13. Many NM axons contain cleaved caspase-3 on E10 (Rotschafer et al., 2016), while relatively few NM and NL cells undergo apoptosis on E13 (Rubel et al., 1976). The greater number of non-apoptotic cleavage sites might therefore reflect the greater number of cells with active caspases, protected by the usual mechanisms of preventing non-apoptotic caspase activity from turning lethal, described above. It is also possible that developing neurites contain a greater variety of potential caspase substrates than do cell bodies and nuclei, resulting in greater diversity in caspase cleavage sites and substrates during non-apoptotic caspase activity than during apoptosis.

**Caspase-3 probably produces most of the observed cleavage sites in both the non-apoptotic and apoptotic auditory brainstem.** Though the caspase family exhibits a range of cleavage site preferences, (Thornberry et al., 1997; Stennicke et al., 2000; Julien et al., 2016; Rawlings et al., 2018) it is unlikely that the different consensus sequences we observed in apoptotic and non-apoptotic contexts are attributable to the activity of distinct caspases. Indeed, there is evidence that caspase-3 activity predominates in the Degrabase and in the chick brainstem at E10 and E13. The creators of Degrabase note that the apoptotic consensus sequence, DEVD↓, is identical to the individual preferences of caspase-3 and caspase-7 in positional scanning peptide libraries, consistent with these caspases' roles as

apoptotic executioners (Crawford et al., 2013). Caspase-3 has been shown to have a broader substrate repertoire than caspase-7 *in vitro* (Walsh et al., 2008), and caspase-3 is the only apoptotic executioner required for major apoptotic outcomes (Slee et al., 2001), suggesting that Degradase predominately reflects caspase-3 activity. Besides caspase-3, we detected three additional caspases (-6, -8 and -9) in the non-apoptotic chick auditory brainstem (Weghorst et al., 2020) and two additional caspases (-1 and -2) in the apoptotic auditory brainstem. None of these caspases exhibits substantial preference for the GD or RD motifs in synthetic peptides, so the P2 position in the non-apoptotic consensus sequence cannot be easily explained with reference to a specific caspase's known activity. Additionally, only caspase-3 was detected in every single biological replicate, and at much higher Mascot scores than every other caspase, suggesting that caspase-3 is the most abundant caspase in both the apoptotic and non-apoptotic chick auditory brainstem (Weghorst et al., 2020). Caspases, like all enzymes, are catalytic, so we cannot rule out the possibility that another less-abundant caspase contributes some of the observed caspase cleavage sites. However, caspase-3 is the most active caspase even at equal abundances (Julien et al., 2016), so it is likely responsible for most of the observed caspase cleavage sites in the auditory brainstem, as in Degradase. While we cannot rule out the possibility that another less-abundant caspase contributes some of the observed caspase cleavage sites, the plurality (if not the majority) are probably caused by caspase-3.

**Post-translational modifications to caspase-3 are likely to underlie the non-canonical caspase consensus sequence of the non-apoptotic auditory**

**brainstem.** If caspase-3 is the primary aspartate-directed protease in all contexts examined here, how is it capable of such distinct cleavage site sequence preferences? One possibility is that the optimal cleavage site sequence is altered by allosteric or post-translational modifications (PTMs) to caspase-3 itself (Agniswamy et al., 2007; Hardy and Wells, 2009; Häcker et al., 2011; Cade et al., 2014; Dagbay et al., 2014; Kavanagh et al., 2014; Maciag et

al., 2016; Eron et al., 2017; Zamaraev et al., 2017; Herr, 2018). Relatively few amino acid substitutions are required to change the P4 subsite preference of caspase-3 and -7 from the negatively-charged aspartate (i.e. DXXD) to a preference for hydrophobic residues such as isoleucine and valine (Hill et al., 2016; Bingöl et al., 2019; Grinshpon et al., 2019; Yao et al., 2021). Similar PTM-mediated changes to the caspase-3 active site may play a role in shifting the P4 consensus motif to IXXD, which we observed in the non-apoptotic chick auditory brainstem and which we predict is the most likely non-apoptotic consensus motif in humans. Modulatory PTMs of caspase substrates are common as well, but these are unlikely to produce systematic changes in cleavage site preference (Tözsér et al., 2003; Dix et al., 2012; Turowec et al., 2014; Kumar and Cieplak, 2018; Thomas et al., 2018; Maluch et al., 2021). The specific PTMs responsible for the novel caspase consensus sequence observed in the non-apoptotic chick auditory brainstem remain to be determined.

## **METHODS**

**Data Sources.** Non-apoptotic chick auditory brainstem peptidomic data were sourced from our previous publication (Weghorst et al., 2020). Briefly, eggs from a hybrid flock of White Leghorn males and Rhode Island Red females (AA Lab Eggs) were incubated in a rotating shelf incubator at 37.5°C for 72 hours. Contents were removed from the shell, transferred to *ex ovo* cultures on embryonic day (E) 3, and the cultures were incubated until 7 days *in vitro* (DIV), corresponding to approximately E10. Brainstems were dissected, snap-frozen and stored at -80°C in 3 biological replicates of 2 brainstems each. Nano-LC-MS/MS was used to characterize the peptidome of the samples. Mass spectrometry proteomics data are available under dataset identifier PXD021728 at the ProteomeXchange Consortium through the PRIDE repository (Perez-Riverol et al., 2019). Only data from control samples (not caspase-3-inhibited samples) were used for the present study. Human apoptotic substrate data were sourced from Degradase (Crawford et al., 2013). Chick apoptotic peptidomic data were generated from E13 auditory

brainstem tissue. Eggs from a hybrid flock of White Leghorn males and Rhode Island Red females (AA Lab Eggs) were incubated in a rotating shelf incubator at 37.5°C for 13 days. The auditory portion of the brainstem was dissected, snap-frozen and stored at -80°C in three biological replicates, each containing two pooled brainstems.

The three E13 samples were each disaggregated in 70% formic acid for 72 hours at room temperature with constant shaking and occasional ultrasonication in a cuphorn sonicator. One crystal of cyanogen bromide (CNBr) was added to each sample, followed by overnight incubation in the dark. Samples were evaporated to dryness in a Speedvac vacuum concentrator, then redissolved in 8 M urea, 100 mM triethyl ammonium bicarbonate (TEAB; pH 8.0), 10 mM tris(2-carboxyethyl)phosphine, diluted to 6 M urea using 100 mM TEAB, and digested overnight at 37°C with LysC (Promega - R-LysC; enzyme:substrate mass ratio =1:100). Samples were diluted to 1 M urea with 0.1 M TEAB, then trypsinized (Promega - Trypsin Gold; enzyme:substrate mass ratio = 1:100). The resulting peptides were isolated using a stacked C18/SCX STAGE tip (Rappsilber et al., 2007) eluting with 54 mM, 73 mM, 100 mM, 130 mM, 176 mM, and 395 mM ammonium acetate in 20% acetonitrile, 0.5% formic acid (FA), with a final elution in 5% ammonium hydroxide, 80% acetonitrile. Dried elutions were redissolved in 0.1% FA in water. The resulting samples were injected sequentially to an LTQ Orbitrap Velos Pro via an Easy-nLC 1200, developing a gradient from 5 – 23% B (93% CH<sub>3</sub>CN in water) over 115 min then to 35% B over 20 min, 0.25 microL/min. In each precursor scan (FTMS; 60000 resolution) up to the 15 most intense ions with intensity value of > 2000, excluded +1 charge state and dynamic exclusion (repeat count = 1, repeat duration = 30 sec, exclusion list size = 500, exclusion duration = 40 sec) were selected for MS2 (FTMS; 7500 resolution) via HCD fragmentation. Data from groups of seven elutions were combined and searched using Mascot 2.7 against the *Gallus gallus* (taxon ID 9031) UniProt reference proteome plus a database of common contaminants, with allowable charge states of +2 to +4

and allowing CNBr-trypsin cleavage specificity, as an error-tolerant search (which allows semiCNBr-trypsin specificity), and with precursor and product mass tolerances of  $\pm 20$  ppm and  $\pm 20$  mmu respectively. Data were thresholded at significance ( $p$ )  $< 0.05$ . The mass spectrometry proteomics data have been deposited to the ProteomeXchange Consortium via the PRIDE partner repository with the dataset identifier PXD030697 (Perez-Riverol et al., 2019).

**Consensus Sequence Analysis.** We previously used IceLogo (Maddelein et al., 2015) to generate a cleavage site consensus sequence for non-apoptotic caspase-3 substrates in the chick auditory brainstem (Weghorst et al., 2020). This consensus sequence (DHRD↓) was created using peptides both N- and C-terminal to the cleavage site, but some shortcomings with this method led us to consider an alternative approach for the present study. First, IceLogo assumes a normal distribution for amino acid frequencies to avoid assumptions about any subsite in the input sequences. A methodology more tailored to caspases would account for the fact that they primarily cleave C-terminal to aspartate residues (Seaman et al., 2016). This preference suggests a hypergeometric distribution. Second, the inclusion of peptides N-terminal to the cleavage site while creating an N-terminal consensus sequence is problematic because motif enrichment due to preferential proteolysis cannot be distinguished from enrichment due to greater MS detectability of peptides with specific amino acids. We therefore aimed to explore the consensus sequence for non-apoptotic caspase activity in the auditory brainstem using a more appropriate statistical method to analyze only peptides C-terminal to the caspase cleavage site.

The cleavage site consensus sequence for non-apoptotic auditory brainstem caspase activity was derived by subsite enrichment analysis of the 20 amino acids at the P4-P2 positions of caspase cleavage sites (Schechter and Berger, 1967). Caspase cleavage sites were identified by detection of peptides with a D↓X terminus (where ↓ represents a cleavage site and X represents the first amino acid of the C-terminal peptide) that appeared in at least one control

sample of our prior study (Weghorst et al., 2020). Cleavage sites from proteins in the same family with identical P4-P4' sequences were treated as a single cleavage event. For each P4-P2 motif, a two-tailed hypergeometric test (Table 2.1) was used to compare the frequency of the motif in observed caspase cleavage sites ( $k_{\text{Total}}/n_{\text{Total}}$ ) with the frequency of the motif relative to all aspartate residues in substrate sequences ( $K_{\text{Total}}/N_{\text{Total}}$ ). The mid- $p$ -value variant of the hypergeometric test was used to compute  $p$ -values (Lancaster, 1961), and a two-stage linear step-up procedure (Benjamini et al., 2006) was used to control the false discovery rate (FDR) of the 60 hypergeometric tests. This method was also used to generate a consensus sequence for Degradase.

Variable	Definition	Derivation
k	Count of sites cleaved at the motif	$k_{\text{Total}} = \sum_{i=1}^R \left( \sum_{j=1}^P k_j \right)_i$
n	Count of sites cleaved	$n_{\text{Total}} = \sum_{i=1}^R \left( \sum_{j=1}^P n_j \right)_i$
K	Count of the motif in substrate sequence	$K_{\text{Total}} = \sum_{i=1}^R \left( \sum_{j=1}^P K_j \right)_i$
N	Count of aspartates in substrate sequence	$N_{\text{Total}} = \sum_{i=1}^R \left( \sum_{j=1}^P N_j \right)_i$

**Table 2.1 - Definition and derivation of variables used in hypergeometric tests for each P4-P2 motif in caspase consensus sequences**

R: Count of replicates. P: Count of cleaved proteins.

**Functional Annotation Analysis.** The Database for Annotation, Visualization, and Integrated Discovery (DAVID) Bioinformatics Resource 6.8 (Huang et al., 2009a, 2009b) was used to compare the frequency of GO terms among caspase substrates with P2 subsites that resemble the cleavage site consensus sequence to the frequency of GO terms among all caspase substrates in the auditory brainstem. Hypergeometric mid- $p$ -values were calculated for

each GO term (Lancaster, 1961), and a two-stage linear step-up procedure (Benjamini et al., 2006) was used to control the false discovery rate (FDR) for each of the three categories of GO terms (Cellular Component, Biological Process, and Molecular Function).

**“Structural Constituent of Cytoskeleton” Subsite Analysis.** R (v. 3.6.1) was used to conduct Monte Carlo simulations to compare the observed number of SCoC cleavage events attributable to each P2-P4 motif with the expected distribution of SCoC cleavage events attributable to that motif, based on random proteolysis at the overall frequency of each motif in each biological replicate. Within each replicate, the probability that each SCoC substrate was cleaved at each motif was calculated as follows:

$$Pr(\text{Substrate cleaved at motif}) = 1 - \prod_{i=0}^{S-1} \left( 1 - \frac{\sum_{j=1}^P k_j}{(\sum_{j=1}^P n_j) - i} \right)_i$$

where P denotes the count of proteins cleaved in the replicate; S denotes the count of sites cleaved in the SCoC protein in the replicate; and definitions for k and n are shown in Table 2.1. Protein-cleavages were simulated at the observed frequency of each motif by comparing each SCoC protein’s  $Pr(\text{Substrate cleaved at motif})$  to a randomly generated variable  $x$ , where  $x \in R$  and  $x \in [0,1)$ .

$$\text{If } x < Pr(\text{Substrate cleaved at motif}): C_j = 1$$

$$\text{If } x \geq Pr(\text{Substrate cleaved at motif}): C_j = 0$$

Expected count of total protein-cleavages at each motif was then calculated in the same way as the observed count of protein cleavages:

$$C_{\text{Total}} = \sum_{i=1}^R \left( \sum_{j=1}^{\text{SCoC}} C_j \right)_i$$

Here,  $C$  denotes the count of protein-cleavages; SCoC denotes the count of cleaved SCoC proteins; and  $R$  denotes the count of replicates.

A  $p$ -value for each motif was computed by the mid- $p$ -value method for discrete distributions (Lancaster, 1961). Fold enrichment for each motif was computed as observed  $C_{\text{Total}}$  divided by the mean of the expected distribution of  $C_{\text{Total}}$ . The same method was used to assess combinations of motifs in the human apoptotic proteome.

### **Chapter 3 : Caspase activity regulates abundance of the long non-coding RNA CREVASSE in extracellular vesicles of the developing auditory brainstem**

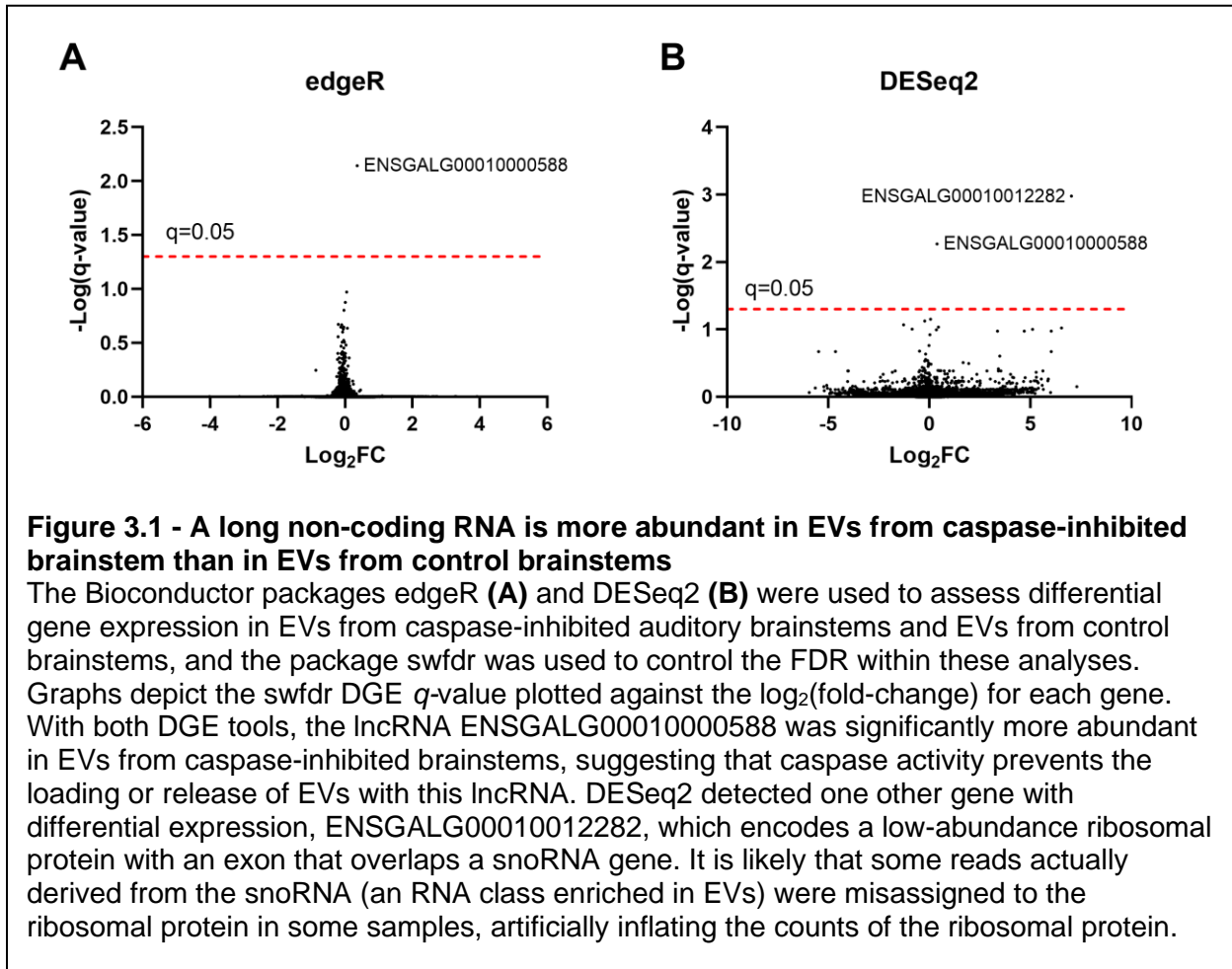
In our previous study (Chapter 1), we showed that non-apoptotic caspase activity in the chick auditory brainstem disproportionately targets extracellular vesicle (EV) proteins (Weghorst et al., 2020). Auditory brainstem caspase substrates were also enriched for RNA-binding proteins (RBPs), which are known to be enriched in extracellular vesicles (Villarroya-Beltri et al., 2013; Hentze et al., 2018; Hobor et al., 2018; Statello et al., 2018; Leidal and Debnath, 2020; Leidal et al., 2020; O'Brien et al., 2020). This dual enrichment suggests the possibility that caspase activity regulates loading of RBPs (and therefore RNAs) in the chick auditory brainstem. Here we tested this hypothesis by sequencing the RNA of extracellular vesicles purified from brainstems treated with the caspase-3 inhibitor z-DEVD-fmk or with vehicle solution. We identified a highly abundant long intergenic non-coding RNA (CREVASSE: Caspase-Regulated, Extracellular-Vesicle-Associated, Single-Stranded Effector) that was more abundant in EVs from caspase-inhibited brainstems than EVs from control brainstems. We demonstrated differences between the Ensembl annotation for this lncRNA and the transcripts observed in chick auditory brainstem EVs based on coverage and splice junction data observed in our experiment, and we predicted protein and RNA binding partners of the lncRNA. Finally, we used Gene Set Enrichment Analysis to show that the RNA binding partners of the lncRNA are enriched for proteins involved in auditory brainstem development, supporting the caspase-mediated loading of the lncRNA into EVs as a mechanism by which caspase activity may influence development and differentiation of neighboring cells in the auditory brainstem.

## **RESULTS**

To identify effects of caspase activity on the transcriptome of chick auditory brainstem EVs, we enriched for EVs from auditory brainstems treated with the caspase-3 inhibitor z-DEVD-fmk or vehicle solution, with 5 biological replicates for each condition. We purified total RNA from these EV samples, created cDNA libraries, and conducted paired-end Illumina sequencing to a depth of about 100 million reads per library. We conducted an initial FastQC run on raw reads and identified substantial sequence duplication and many over-represented sequences, with minor adapter contamination near the 3' end of reads. BLAST of overrepresented sequences suggested the presence of ribosomal RNA (rRNA). We therefore used BBduk to trim adapter sequences and filter reads arising from known contaminants. The majority of reads were removed in all samples because they mapped to genomic rRNA, indicating that the mammalian rRNA depletion technique employed by the library preparation kit was inefficient against chicken rRNA. However, FastQC of the filtered reads still showed a high degree of read duplication, suggesting that the remaining sequencing depth (5 to 10 million reads per library) provided sufficient coverage of the EV transcriptome, so we chose to proceed with downstream analysis.

**Differential Gene Expression.** We used Salmon to align reads to the chicken transcriptome, followed by differential gene expression analysis using the DESeq2 and edgeR Bioconductor packages, with the swfdr package used for weighted FDR control. Only one gene was differentially expressed in both analyses (Figure 3.1): the two-exon long intergenic non-coding RNA (lincRNA) *ENSGALG00010000588*, which was about 30% more abundant in EVs from caspase-inhibited brainstems than control brainstems (edgeR  $p = 4.0 \times 10^{-5}$ ,  $q = 7.2 \times 10^{-3}$ ; DESeq2  $p = 5.1 \times 10^{-3}$ ,  $q = 5.4 \times 10^{-3}$ ). This long non-coding RNA (lincRNA) hails from the newly-characterized chicken microchromosome 39 (NC\_052570.1), and it appeared to be among the most abundant transcripts in auditory brainstem EVs. However, transcript abundance estimation depends on accurate transcript annotation, and lincRNAs tend to have incomplete annotation

because they are usually too sparsely expressed to obtain full gene coverage, because they often appear as different isoforms in different biological contexts, and because they lack features that aid in the annotation of protein-coding RNAs such as open reading frames and poly-A signals (Lagarde et al., 2017; Melé et al., 2017; Statello et al., 2021). We therefore aimed to determine whether the annotation of *ENSGALG00010000588* was consistent with our data.



**LncRNA Annotation Differences.** We used the splice-aware genome aligner STAR and the deduplicated per-base coverage calculator Samtools Depth to align reads pooled from all samples to the genome and to determine depth of coverage in the genomic region containing *ENSGALG00010000588* (which is on the forward strand) and extending to the two neighboring

genes. We found that while the transcription start site for *ENSGALG00010000588* was consistent with the start site in our data (chromosome 39, position 37680), the transcription termination site was not (Figure 3.2A). On the contrary, there was a drop in per-base coverage near position 39500, nearly 500 bp after the annotated termination site, but coverage did not reach background levels until after position 43100, suggesting the presence of at least two classes of transcript with differing transcription termination sites. The STAR splice junction database also showed evidence that unannotated splice junctions were far more abundant in the true set of transcripts for this locus than the single annotated intron for *ENSGALG00010000588*. To determine the splice events most prevalent in the EV transcriptome, we counted the number of reads spliced out at each genomic position by summing the number of reads from all deduplicated, uniquely mapping reads that bridged splice junctions containing each position (Figure 3.2B). This approach allows the identification of positions that are frequently spliced out of the mature transcript without relying on individual splice junctions (and thus allowing for positions spliced out by alternative splice junctions to be counted as spliced out regardless of which junction is used). We also calculated the proportion of reads spliced out at each position by the formula:

$$S = \frac{J}{J + C}$$

where S is the proportion of reads spliced out at each genomic position; J is the number of uniquely-mapping, deduplicated reads that bridge a splice junction containing the position; and C is the number of uniquely-mapping, deduplicated reads that contain each position (Figure 3.2C). A single 7-bp intron was identified as the most abundant event, with some additional splice complexity present at low levels. While another intron was spliced out at the same rate per transcript as the 7-bp intron, the other intron is present only in the less-abundant long isoform class, so it was present at the same overall abundance as the additional introns present in all isoforms. For simplicity and due to the limitations of short-read sequencing on accurate

isoform characterization, we chose to represent this locus as four transcripts: long and short isoforms with and without the 7-bp intron (Figure 3.3). The proportion of reads spliced out did not exceed 0.3 at any position, suggesting that no position is spliced out in the majority of transcripts that potentially contain that position (Figure 3.2C), so these four transcripts probably account for the vast majority of transcripts present in auditory brainstem EVs. At the very least, this annotation is likely sufficient for accurate Salmon re-quantification, which we conducted next.

We used Salmon to align the reads to a transcriptome in which the original *ENSGALG00010000588* transcript was replaced by the four lncRNA transcripts. As before, we used DESeq2 and edgeR to conduct differential gene expression analysis, and we found that the lncRNA was still more abundant in caspase-inhibited samples than in control samples (edgeR  $p = 1.1 \times 10^{-3}$ ,  $q = 5.7 \times 10^{-4}$ ; DESeq2  $p = 1.9 \times 10^{-4}$ ,  $q = 0.027$ ). Additionally, the lncRNA was highly abundant overall, comprising 10% of all reads and more than 3% of all transcripts in auditory brainstem EVs (31781 Transcripts Per Million). Only one gene (7-SL, the EV-enriched Signal Recognition Particle RNA) was more abundant than the differentially expressed lncRNA, suggesting the importance of the lncRNA in EV-mediated processes of auditory brainstem development. We propose the name CREVASSE (Caspase-Regulated, Extracellular-Vesicle-Associated, Single-Stranded Effector) for this lncRNA.

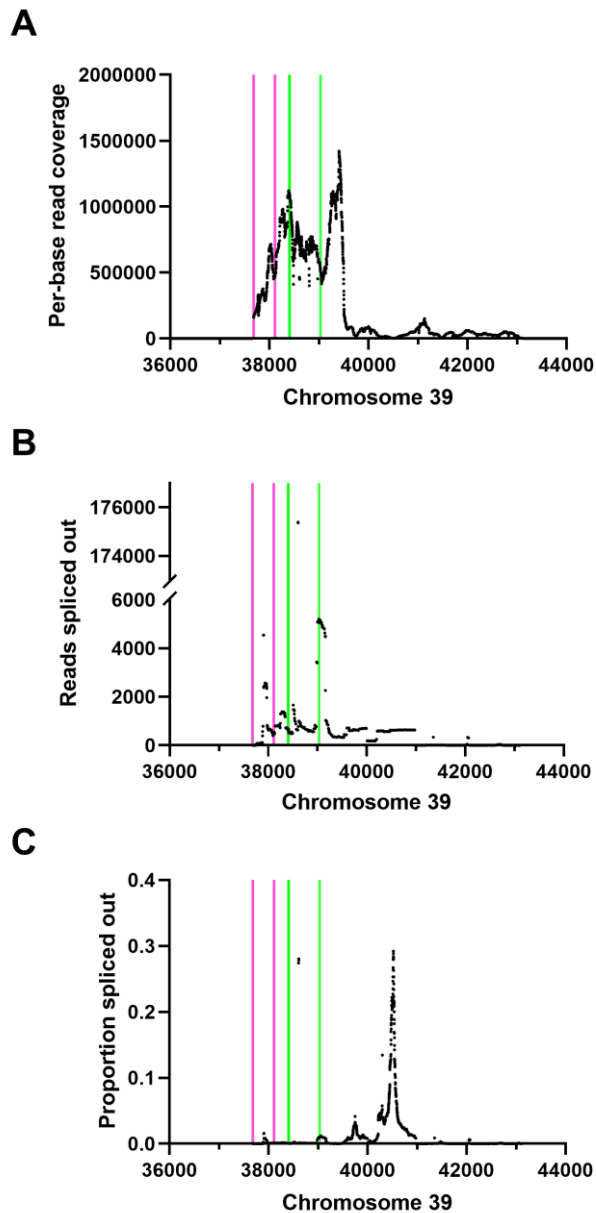


**Figure 3.2 - The transcripts of the caspase-regulated lncRNA do not match its Ensembl annotation**

**(A)** We used STAR to align pooled reads to the genome, and Samtools Depth to quantify deduplicated per-base coverage of the region containing ENSGALG00010000588. We found substantial read coverage outside the two annotated exons for the gene (bordered by pink and green lines). The lower coverage from 39500 to 43100 constitutes evidence for alternate transcription termination sites. **(B)** We used the STAR splice junction database to plot the number of uniquely mapping reads that bridge splice junctions containing each position. A single unannotated 7-bp intron predominates. **(C)** We divided the values in B by the total coverage (spliced and unspliced) at each position to obtain the proportion spliced out at each position. While a second intron is spliced out at the same proportion as the 7-bp intron, the overall abundance of this splice event is on par with the minor introns in the short transcript because the splice event is only present in the less-abundant long isoform.

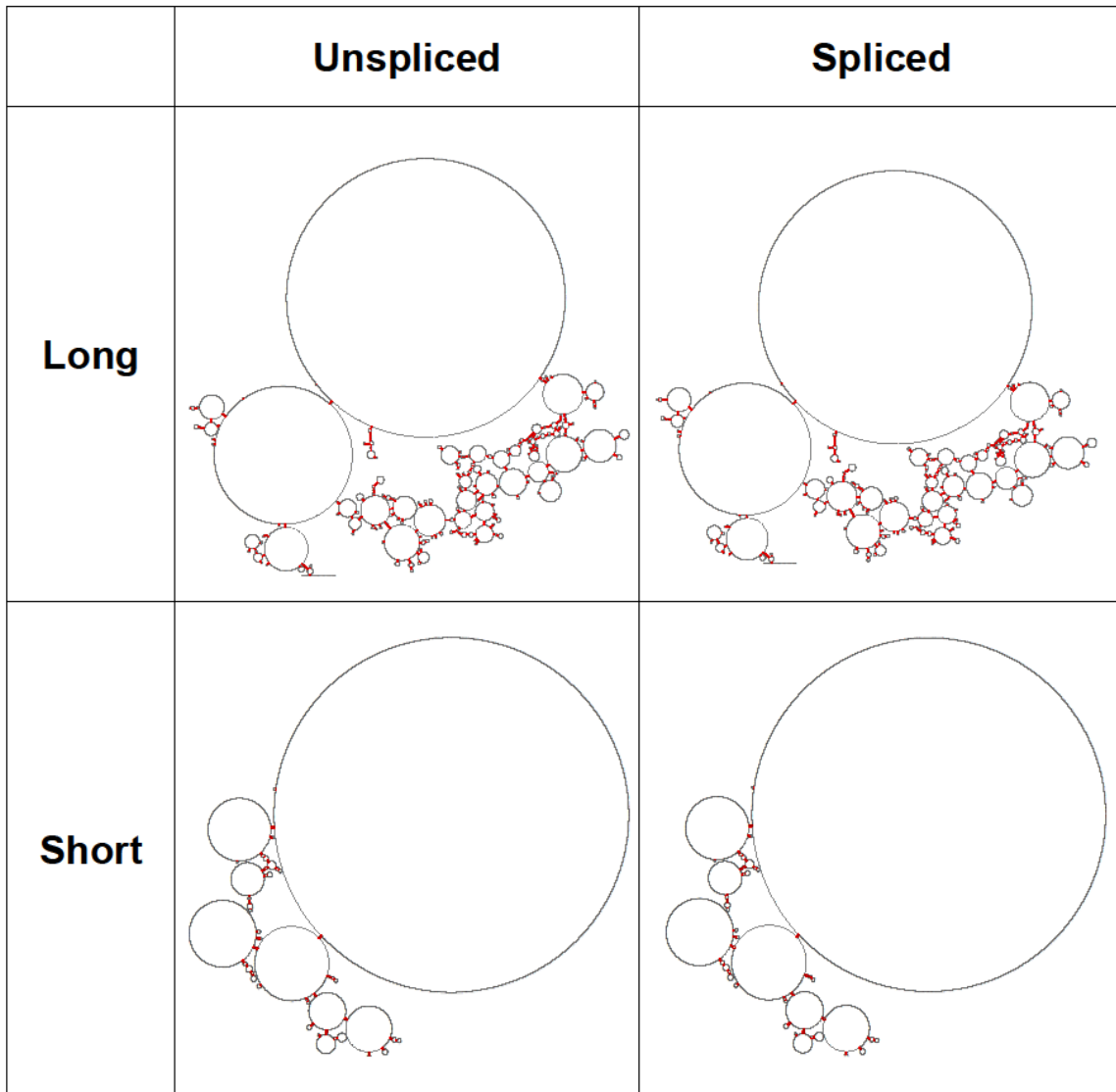


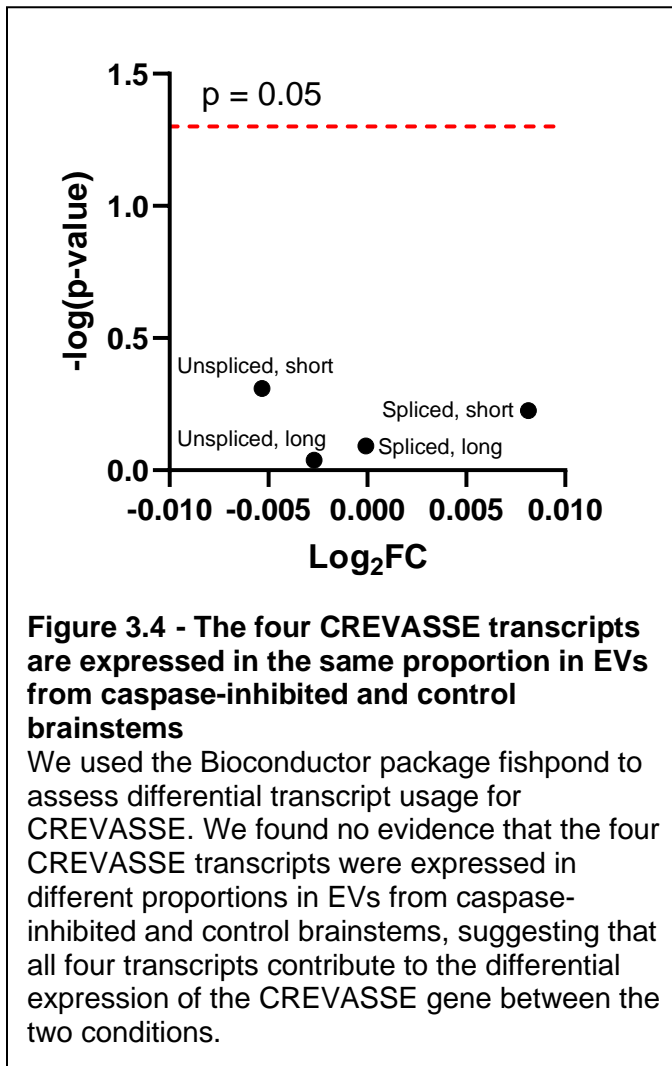
**Figure 3.3 - Secondary structures of the isoforms of CREVASSE**

We used the deep-learning tool MXfold2 to predict secondary structures of the four isoforms of CREVASSE, which were plotted with RNApuzzler. Notably, the loss of the 7-bp intron does not significantly affect the structure of the transcripts. All four isoforms contain a large unpaired region, which may be used for binding to RNA or proteins.

**Coding Potential Prediction of CREVASSE.** We next aimed to test whether the CREVASSE isoforms are predicted to be non-coding transcripts under our new annotation. We used the programs CPPred (Tong and Liu, 2019) and CPPred-sORF (Tong et al., 2020) to analyze the four CREVASSE transcript sequences for protein coding potential using either large open reading frames with canonical start codons or small open reading frames with non-canonical start codons respectively. All 4 transcripts were predicted to be non-coding RNAs by both programs, with no transcript receiving greater than 10% chance of coding potential by either algorithm. These results suggest that the new annotation did not alter the prediction that CREVASSE is a lncRNA.

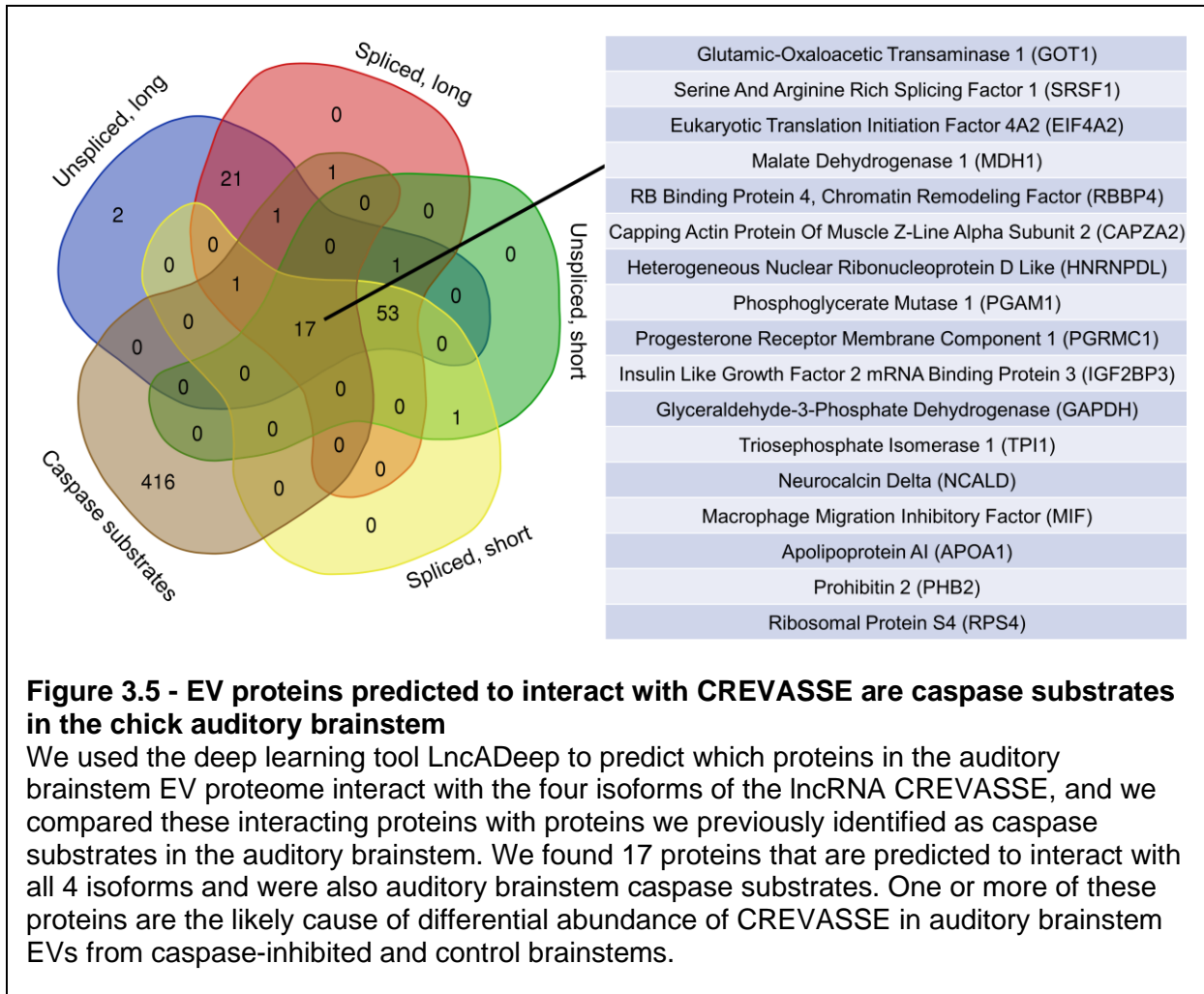
**Differential Transcript Usage.** We sought to determine which transcript(s) contributed to the differential abundance of CREVASSE in EVs from caspase-inhibited and control brainstems. We used the fishpond Bioconductor package, which tests for changes in the proportions of read counts assigned to each transcript across experimental conditions. We found no evidence of differential transcript usage for CREVASSE (Figure 3.4), suggesting that the four transcripts all contribute to the differential expression of CREVASSE in EVs from caspase-inhibited and control brainstems.

**Protein-RNA Interaction Prediction.** Caspases act directly on proteins, not RNA, so caspase-mediated proteolysis of an RNA-binding protein is the probable upstream cause of the differential abundance of CREVASSE in EVs from caspase-inhibited and control brainstems. We therefore wanted to identify likely binding partners of CREVASSE and compare them to known targets of caspase activity in the auditory brainstem. We submitted the RNA-sequenced EV samples to proteomic mass spectrometry and identified 631 proteins that were present in at least one of the 10 EV samples. We then used the deep learning tool LncADeep (Yang et al., 2018, 2021) to predict RNA-protein interactions among the four CREVASSE transcripts and the 631 proteins observed in the EVs. Since differential transcript usage analysis suggested that the



CREVASSE transcripts were expressed in the same proportions in caspase-inhibited and control brainstem EVs (Figure 3.4), we were specifically interested in proteins predicted to bind to all four CREVASSE isoforms, of which we identified 70. We compared these CREVASSE binding partners to caspase substrates, namely proteins with at least one caspase cleavage site in a control brainstem from the dataset used in chapters 1 and 2. We found 17 proteins that were caspase substrates and predicted binding partners of CREVASSE (Figure 3.5). Since differential proteolysis of single protein would be sufficient to

produce the differential expression of CREVASSE in caspase-inhibited and control EVs, we concluded that there are ample protein candidates by which caspase activity might influence the loading and release of EVs with CREVASSE.



**RNA-RNA Interaction Prediction.** A major avenue of lncRNA action is binding and regulating translation or degradation of other RNAs. We therefore used the RNA-RNA interaction prediction tool ASSA (Antonov et al., 2018, 2019) to identify RNAs in the chick transcriptome that interact with the four CREVASSE transcripts. For each transcript pair, ASSA returns *p*-values for the sequence-specificity of binding events between the two transcripts. We ranked the transcriptome by the negative  $\log_{10}$  of these *p*-values and used the Bioconductor package fgsea (Korotkevich et al., 2021) to conduct Gene Set Enrichment Analysis (Subramanian et al., 2005) with these ranks, keeping only the highest-ranked transcript from each gene. This analysis revealed that CREVASSE transcripts interact with RNAs involved in

embryonic development and morphogenesis, especially of the brainstem, cranial nerves, and auditory system. We found GO terms such as “Cochlea Morphogenesis,” “Autonomic Nervous System Development,” “Calyx of Held” (a synapse in the mammalian auditory brainstem), “Cranial Nerve Development,” “Regulation of Synapse Assembly,” and “(Positive) Regulation of Neuron Differentiation” were consistently in the top 20 GO terms for CREVASSE transcripts (Figure 3.6). Many of the genes in these sets were developmental transcription factors such as Hox genes, reflected in enrichment of the gene set “DNA-binding Transcription Activator Activity.” These results indicate that CREVASSE binds and regulates transcripts involved in development of the auditory brainstem, suggesting that caspase activity in the chick auditory brainstem may influence differentiation of neighboring cells by regulating the loading and release of extracellular vesicles with CREVASSE.

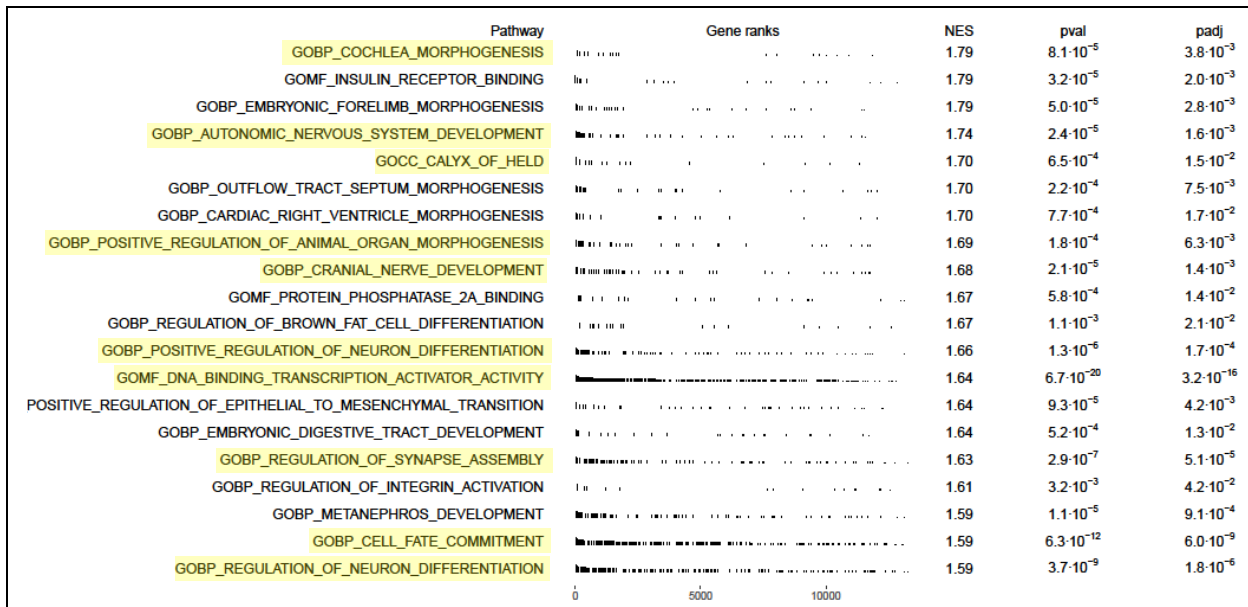


**Figure 3.6 - CREVASSE binds RNAs involved in neural, brainstem, and auditory development**

We used ASSA (an RNA-RNA interaction prediction program) to identify and rank RNAs by their likelihood of binding to each of the four CREVASSE transcripts. We then used fgsea (a parallelized R package based on the Broad Institute’s GSEA) to conduct Gene Set Enrichment Analysis using the binding probability ranks. We collapsed gene sets with redundant contents and sorted the remaining significant sets by normalized enrichment score (NES), a metric inversely correlated with the average rank of gene set members. The top 20 GO terms of the most abundant CREVASSE transcript (unspliced short) are depicted here and are representative of results for the other 3 CREVASSE transcripts. RNAs predicted to bind to CREVASSE were heavily enriched in gene sets involved in embryonic development, especially of the nervous system, auditory system, and auditory brainstem specifically. Enriched gene sets directly related to auditory brainstem development are highlighted in yellow. Most enriched gene sets not directly related to auditory brainstem development were related to development generally. Pathways were derived from the GSEA collection c5.go.v2022.1.Hs.symbols. Gene ranks reflect probability of binding to CREVASSE, where low ranks are more likely and high ranks are less likely bind to CREVASSE. Gene sets with more genes at low ranks are therefore enriched among the transcripts CREVASSE is highly likely to bind. P-values were derived from permutation tests of rank shuffling, and padj was obtained by the Benjamini-Hochberg correction. GO: Gene Ontology, BP: Biological Process, CC: Cellular Component, MF: Molecular Function.

## **DISCUSSION**

Here we have characterized CREVASSE, a novel lncRNA that is highly abundant in chick auditory brainstem extracellular vesicles, where it is differentially expressed in a caspase activity-dependent manner. We showed that while the gene for this lncRNA was already annotated in the chick genome, the annotation was incomplete and did not reflect alternative

transcription termination sites and alternative splicing present in a minority of transcripts arising from the locus. We identified RNA-binding proteins that bind to the four major CREVASSE transcripts and are also caspase substrates in the auditory brainstem. These 17 proteins are the most likely candidates by which caspase activity mediates the loading and release of extracellular vesicles with CREVASSE. Finally, we ranked the chick transcriptome by each transcript's propensity to bind to the four CREVASSE isoforms, and we conducted Gene Set Enrichment Analysis on this ranked list. Among high-binding proteins, we detected the most enrichment for GO terms that correspond to the processes occurring in the auditory brainstem at the developmental timepoint when the EVs were extracted, namely development of the nervous system, of the auditory system, of the brainstem, and of cranial nerves. Together, these data point to a role for caspase activity in modulating the intercellular regulation of chick auditory brainstem development by preventing the loading and release of EVs with CREVASSE.

**Proposed model.** The increased abundance of CREVASSE in EVs from caspase-inhibited brainstems suggests that caspase activity inhibits the loading or release of EVs with CREVASSE. The two simplest mechanisms for this function are 1) caspase activity (likely from caspase-3) cleaves an RNA-binding protein bound to CREVASSE, thus preventing that protein (and therefore CREVASSE) from being loaded into EVs; or 2) caspase activity inhibits the release of EVs constitutively loaded with CREVASSE. Abolishing caspase activity in these scenarios would result in the release of 1) more CREVASSE in the same number of EVs, or 2) a greater number of EVs with CREVASSE. Scenario 1 is more parsimonious because: (1) We have already shown that caspase activity targets RNA-binding proteins in the auditory brainstem; (2) RNAs require RBPs to be loaded into EVs (Leidal et al., 2020; Dellar et al., 2022); and (3) We do not yet know whether caspase activity directly affects the release of EVs in the auditory brainstem. However, scenario 2 cannot be ruled out at this time.

Since cleaved caspase-3 is primarily restricted to NM axons during the developmental timepoints at which the brainstems in this study were treated with caspase inhibitor (Rotschafer et al., 2016), the observed increase in CREVASSE expression upon inhibition of caspase activity was likely mediated by EVs from NM axons. The primary recipients of these EVs may be NL principal cells, glia surrounding NL (Frühbeis et al., 2013; Dinh et al., 2014; Cramer and Rubel, 2016), or other NM axons. The preponderance of transcription factors among RNA targets of CREVASSE (Figure 3.6), as well as the distance of NM axons from their nucleus (Ohmori, 2014; Seidl et al., 2014), suggest that NL principal cells and cells of the glial margin are more sensible candidate recipients than NM axons.

What might CREVASSE do once the EVs that contain it are uptaken by recipient cells? LncRNAs are involved in a wide variety of processes related to gene expression (Statello et al., 2021). LncRNAs can form triple-helices with DNA in the nucleus, regulating transcription (Li et al., 2016). They can act as miRNA sponges, binding and preventing smaller ncRNAs from encountering their targets (Paraskevopoulou and Hatzigeorgiou, 2016). Transcripts that bind lncRNAs can meet a variety of fates, including Staufen-mediated decay (Gong and Maquat, 2011), or accelerated translation via a ribosomal initiation complex assembled by the lncRNA (Carlevaro-Fita et al., 2016; Karakas and Ozpolat, 2021; Pecoraro et al., 2022). CREVASSE is predicted to bind Eukaryotic Translation Initiation Factors and ribosomal subunit proteins (Figure 3.5), so a capacity to facilitate translation of its binding partners remains an intriguing possibility. A coherent model of caspase-dependent CREVASSE action in the auditory brainstem may resemble the following (Figure 3.7). Caspase activity is necessary to guide NM axons to NL dendrites because it enables highly sensitive integration of and response to external guidance cues (Kellermeyer et al., 2018; Weghorst et al., 2022). CREVASSE is prevented from being loaded into EVs during this stage because its protein binding partner is cleaved by caspase activity. However, once NM axons form a synapse with the correct NL cells, caspase activity

subsides, and CREVASSE is loaded into EVs. These EVs are sent from NM axons to NL cell bodies. When the EVs arrive, they release CREVASSE into the cytoplasm, where it facilitates translation of transcription factor mRNA necessary for NL principal cell differentiation and synapse assembly. This mechanism ensures that NL cells do not mature until they are innervated by NM axons that have completed the caspase-mediated guidance phase. This working model suggests a number of testable hypotheses that will be the subject of future studies.

**LncRNA homology and function.** Is there a human homolog of CREVASSE? Unfortunately, lncRNAs are poorly conserved even between humans and mice, so the odds of identifying mammalian homologs of chicken lncRNAs by sequence similarity are slim. BLASTn of the CREVASSE gene sequence against refseq\_rna and nr/nt returns primarily alignments in birds and, interestingly, in *Plasmodium gallinaceum* (an avian parasite that causes malaria). If CREVASSE evolved in birds as a cellular defense against Plasmodium infection or arose directly from *Plasmodium gallinaceum* via genomic fusion in an infected individual, CREVASSE would very likely be avian-specific.

Nevertheless, CREVASSE joins the ranks of a variety of mammalian lncRNAs that regulate developmental processes, such as HOTAIR (Rinn et al., 2007), TINCR (Kretz et al., 2013), Haunt (Yin et al., 2015), Hotdog (Delpretti et al., 2013), Pnky (Andersen et al., 2019), and RNCR2 (Rapicavoli et al., 2010), and the mechanisms of these lncRNAs and of CREVASSE may be mutually informative. For instance, the human lncRNA HOXA-AS2 has been shown to suppress caspase activation (Zhao et al., 2013), suggesting a route by which CREVASSE may regulate the trans-synaptic movement of cleaved caspase-3 observed in the chick auditory brainstem (Rotschafer et al., 2016), or in preventing apoptosis of properly innervated NL cells.

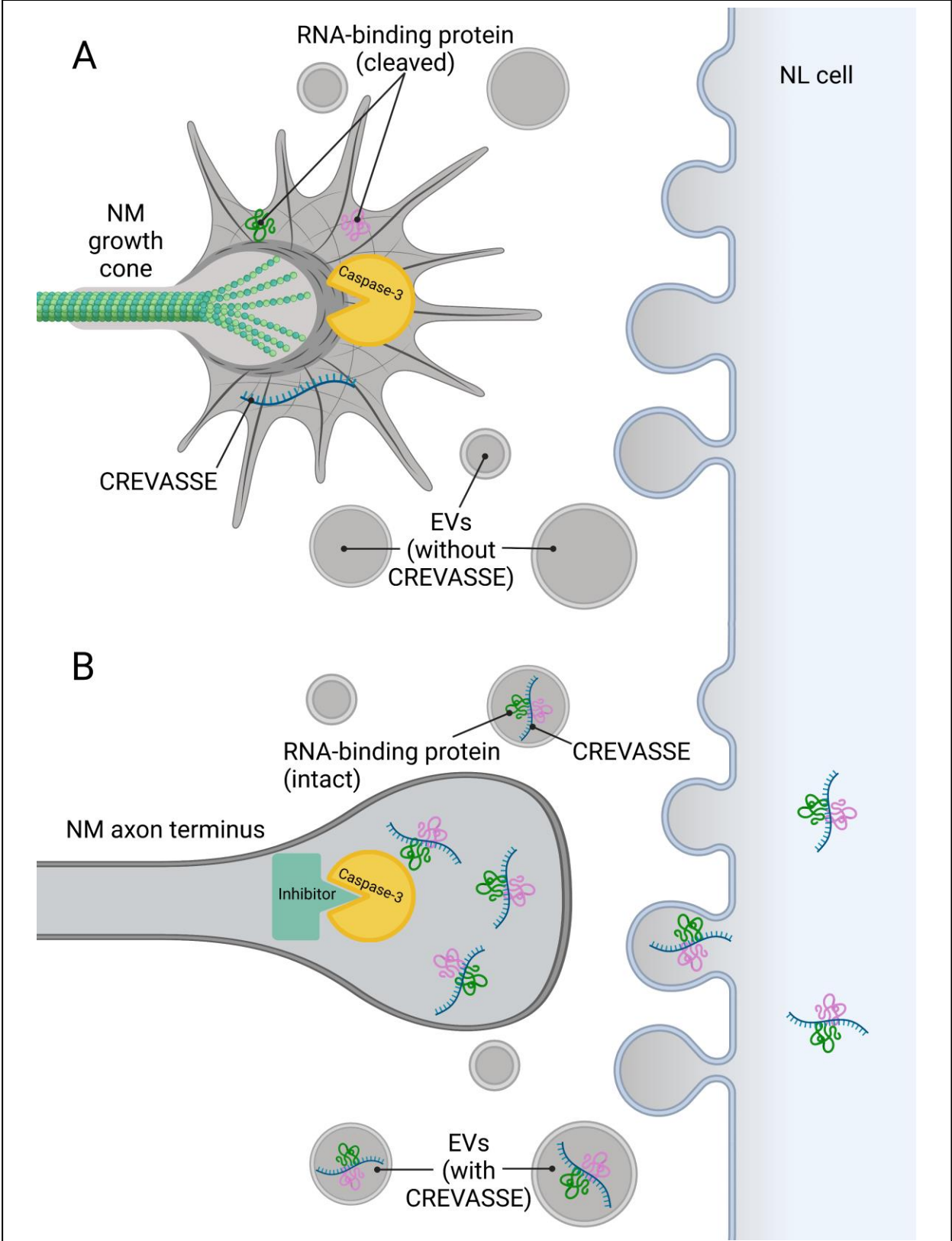


**Figure 3.7 - Model by which caspase activity regulates loading of EVs with CREVASSE**

**(A)** During the phase of active navigation of NM axons, caspase activity regulates turnover of proteins in the NM growth cone, including cytoskeletal proteins and RNA-binding proteins. Proteolysis of an RNA-binding protein that interacts with CREVASSE prevents loading of EVs with CREVASSE, so NL cells receive little CREVASSE from growth cones. **(B)** Once the NM growth cone has found its target in NL and has begun to mature into an axon terminal, caspase activity is reduced (either by endogenous inhibitors or by decreased activation of executioner caspases). CREVASSE is loaded into EVs with its RNA-binding protein, and the cargo is delivered to NL, where CREVASSE regulates differentiation of the recipient NL cell by interacting with transcripts that mediate this process. Figure created with BioRender.

Unlike most characterized mammalian lncRNAs, which spend the entirety of their lifetime in the nucleus (Schmitz et al., 2016), EV-derived lncRNAs such as CREVASSE hail from outside the recipient cell and are therefore inherently more likely to act in the cytoplasm. A cytoplasmic point of entry is consistent with CREVASSE primarily regulating mature RNAs, and our analysis of predicted RNA binding partners of CREVASSE (Figure 3.6) certainly seems to suggest that CREVASSE is capable of regulating the precise processes known to occur in the developing auditory brainstem. However, a nucleus-centered function is not out of the question for EV-derived lncRNAs, which could be transported across the nuclear membrane, so we do not rule out additional functions for CREVASSE in this context.

**CREVASSE Effects on miRNAs and other ncRNAs.** The Gene Set Enrichment Analysis of predicted CREVASSE binding partners almost exclusively considers target transcripts that are protein-coding, as these are encoded by genes whose HGNC names are identical between chicken and human gene annotations. Nevertheless, miRNAs and other ncRNAs are known targets of lncRNAs, which can act as competing endogenous RNAs (ceRNAs), i.e. decoys for the true targets of the ncRNAs, which are subsequently “sponged” by the lncRNA (Paraskevopoulou and Hatzigeorgiou, 2016; Li et al., 2021). While MSigDB (Liberzon et al., 2011) offers annotated gene sets of human and mouse miRNAs that can be included in GSEA, the relationship between miRNAs and any predicted avian homologs is more tenuous than for coding RNAs. Moreover, Gene Ontology annotation of miRNAs is sparse in

chicken, so the functional characterization of miRNAs must be approached by identifying their coding targets and using the GO annotation of the targets as a proxy annotation for the miRNAs. A principled approach to identification of miRNA targets of CREVASSE (and of targets of those miRNAs) should therefore include weighted gene co-expression network analysis (WGCNA) to identify networks of miRNAs, mRNAs, and proteins whose expression correlates with that of CREVASSE and of each other (Sheybani et al., 2021; Chen et al., 2022, 2).

**Annotation of CREVASSE.** It is unclear why the current Ensembl annotation of ENSGALG00010000588 differs from the likely set of transcripts we have observed here. Especially puzzling is the different transcription termination site, which does not match our coverage data. Perhaps the low overall coverage for lncRNAs in most RNA seq studies combined with the drop in coverage near the 3' end of exon 2 in ENSGALG00010000588 (likely due both to the presence of a region with more than 70% adenine content and to the beginning of a minor splice site) prevented curators from identifying the transcription stop site we observed and from finding an alternate transcription termination site several kilobases downstream of the first site. While we observed the annotated splice site at a low level, the major splice site we observe here was not part of the Ensembl annotation. One possibility is that the curators were not aware that birds have smaller introns than mammals (Anderson et al., 1985; Gotoh, 2018), so a 7-bp intron escaped their notice. Another possibility (which applies equally to alternate transcription termination sites) is that there may be tissue-specific forms of CREVASSE with different capacities to regulate different processes. Since our annotation is probably incomplete as well, long-read sequencing of CREVASSE in various tissues will be necessary to overcome the limitations of short-read sequencing in characterizing the full diversity of this lncRNA.

**Differential Transcript Usage.** We did not detect evidence for an effect of caspase inhibition on differential transcript usage among the four isoforms of CREVASSE. However, short-read sequencing of fragmented libraries is not particularly well-suited to the problem of

assigning reads to isoforms when the sequence differences between isoforms are separated by several kilobases because read pairs will rarely include all differentiating features of the various isoforms. Only a few dozen read pairs per sample contained both the 7-bp intron and the region unique to the long CREVASSE isoforms (data not shown), providing Salmon and fishpond very limited material for estimating the proportion of long CREVASSE isoforms that had spliced or retained the intron. As with other limitations of this study, long-read sequencing would eliminate much of the uncertainty surrounding the major isoforms of CREVASSE expressed in auditory brainstem EVs (Kuo et al., 2017; Wright et al., 2022).

**Differential Expression of CREVASSE.** One point of concern for those familiar with studies of differential gene expression via RNA sequencing may be the relatively modest increase in CREVASSE expression in EVs due to caspase inhibition. A few responses to this concern follow. First, CREVASSE is so abundant that it is relatively limited in the degree to which its expression can be increased. For a gene with a starting TPM of about 30000, the upper bound for  $\text{Log}_2\text{FC}$  is about 5, assuming that the experimental perturbation causes a new TPM of 1000000 (i.e. all transcripts in the sample are from the same gene). Smaller positive  $\text{Log}_2\text{FC}$  values are therefore to be expected for highly abundant genes. Second, RNA-seq of tissue-derived EVs is not directly comparable to RNA-seq of other sources. All cell types release EVs, and many cells release multiple subpopulations of EVs, leading to a highly heterogeneous sample (Raposo and Stoorvogel, 2013; Willms et al., 2016; Sork et al., 2018; Zhang et al., 2018; Turchinovich et al., 2019; Luo et al., 2022). It is likely that any caspase-dependent loading of RNAs into EVs in the auditory brainstem occurs with only one or a few subpopulations of EVs out of the total sample. If other EV subpopulations in the brainstem contain CREVASSE that is loaded in a non-caspase-dependent manner, a large change in CREVASSE abundance in a caspase-dependent population would be diluted and would appear small. Single-vesicle RNA-

seq (Luo et al., 2022) will be necessary to obtain finer resolution of transcriptomic changes in distinct subpopulations of EVs.

To add to this signal detection problem, it is likely that only a subset of cells is affected by caspase inhibition in a way that affects CREVASSE abundance in auditory brainstem EVs. For instance, if successful loading of CREVASSE into EVs in developing NM axon termini represents the signal that caspase activity has finished in that terminus, then termini that have already completed caspase-dependent guidance processes will constitutively contribute CREVASSE to the auditory brainstem EV pool. Only unfinished termini will be vulnerable to premature release of CREVASSE due to exogenous caspase inhibition. By this logic, inhibition of caspase activity at earlier developmental timepoints may produce larger fold-changes in the amount of CREVASSE in auditory brainstem EVs. A starting point for this analysis is to document the endogenous changes in CREVASSE abundance in auditory brainstem EVs across developmental time. In summary, we are not troubled by the modest increase in CREVASSE abundance due to caspase inhibition because there are good reasons to take seriously a small but significant increase in expression of a highly abundant RNA in EVs.

## **METHODS**

**Extracellular vesicle enrichment.** Caspase activity was inhibited in the developing chick auditory brainstem as described in Chapter 1. Briefly, chicken eggs (AA Laboratory Eggs) were incubated to embryonic day (E) 3, when their contents were transferred to *ex ovo* culture. Embryos were incubated in culture to 6 days in vitro (DIV) and were then injected with about 5  $\mu$ L of 50  $\mu$ M caspase-3 inhibitor z-DEVD-fmk in artificial cerebrospinal fluid or vehicle solution. This rejected was repeated the following (7 DIV). Four hours after the second injection, auditory brainstems were dissected, washed with Hibernate-E Medium (Thermo Fisher), and snap-

frozen at -80°C. Extracellular vesicles were enriched as described in Chapter 1, namely by tissue dissociation followed by light centrifugation, filtration at 0.22 microns, size exclusion chromatography of the filtrate, and concentration on a 5kDa MWCO centrifugal concentrator (Amicon). In total, 5 replicates of EVs from z-DEVD-fmk treated brainstems and 5 replicates of EVs from vehicle-treated were isolated, and each biological replicate contained EVs from 15 to 20 treated brainstems. EVs were purified on 2 consecutive days, with 3 biological replicates from each treatment group on the first day and 2 on the second day. This batch was included as a covariate in all analyses of EV contents.

**RNA purification.** Twenty percent of the total volume of purified EVs in each replicate was mixed with Trizol reagent in a 1:10 ratio (EVs:Trizol), and the aqueous layer was extracted according to the manufacturer's instructions. The aqueous layer was further purified with the Monarch Total RNA Miniprep Kit (New England Biolabs) according to manufacturer's instructions, including on-column DNase I digestion. RNA was eluted in 50 µL of nuclease-free water. RNA isolation of all samples was done in parallel.

**Library Preparation and RNA Sequencing.** RNA concentration was assessed by Bioanalyzer, and 2 ng of RNA was used to create cDNA libraries with the SMARTer Stranded Total RNA-Seq kit v2 Pico Input Mammalian (Clontech) according to the manufacturer's instructions, with 1 minute of fragmentation time and 11 PCR cycles. Sequencing was conducted using a NovaSeq 6000 S4 flow cell (Illumina) to a depth of about 100 million paired-end 101-bp reads per sample.

**Proteomic Mass Spectrometry.** Twenty percent of the total volume of EV solution in each replicate was subjected to nanoLC-MS/MS as described in Chapter 1.

**Software.** Data analysis was conducted via the High Performance Community Computing Cluster (HPC3) at UC Irvine. BBduk 38.97 (<http://sourceforge.net/projects/bbmap>) was used for

read trimming, adapter removal, and filtration for known contaminants (mitochondrial rRNA, genomic rRNA, and the wild-type SARS-CoV-2 genome). FastQC 0.11.9 (Andrews, 2010) was used to obtain quality metrics on the BBduk-filtered reads. STAR 2.7.10a (Dobin et al., 2013) was used for genomic alignment. Salmon 1.9.0 (Patro et al., 2017) was used for transcriptome alignment and quantification. R 4.1.2 was used to run edgeR 3.36.0 (Robinson et al., 2010), DESeq2 1.34.0 (Love et al., 2014, 2), fishpond 2.0.1 (Zhu et al., 2019), swfdr 1.20.0 (Boca and Leek, 2018; Korthauer et al., 2019), and fgsea 1.21.3 (Korotkevich et al., 2021). Samtools 1.15.1 (Li et al., 2009) was used to compute per-base depth of aligned reads. MXfold2 0.1.1 (Sato et al., 2021) was used to predict RNA secondary structure, and RNAplot 2.5.2 (Lorenz et al., 2011) was used to draw the results of MXfold2 with the RNApuzzler layout algorithm (Wiegrefe et al., 2019). CPPred (Tong and Liu, 2019) and CPPred-sORF (Tong et al., 2020) were used to predict coding potential of CREVASSE isoforms. LncADeep 1.0 (Yang et al., 2018, 2021) was used to predict lncRNA-protein interactions among the 4 CREVASSE isoforms and the observed EV proteome, while ASSA 1.0.1 (Antonov et al., 2018, 2019) was used to predict lncRNA-RNA interactions among the 4 CREVASSE isoforms and the entire chick transcriptome. fgsea was run on pre-ranked mode using the gene sets under c5.go.v2022.1.Hs.symbols (Liberzon et al., 2011). The chicken genome (GRCg7b) Fasta and GTF were obtained from Ensembl release 107, and protein sequences were obtained from Uniprot.

**Differential gene expression analysis.** Tximport 1.22.0 was used to compile read counts from Salmon into R, with an offset matrix used to estimate transcript counts from abundance, as described in Love et al., 2018. The glmQLF analysis pathway of edgeR was used to compare transcripts in EVs from caspase-inhibited brainstems to EVs from control brainstems, with the day of EV isolation included as a 2-level batch factor. Likewise, Tximeta 1.12.4 was used to import unscaled Salmon counts into the default analysis pipeline of DESeq2, which was used for a GLM analysis of caspase-inhibited and vehicle EVs, with EV isolation

batch as a covariate. The swfdr package was used to control the false discovery rate of the resulting p-values from each of these methods of analysis, with total per-gene read counts as a weighting factor.

**Differential transcript usage analysis.** The Swish function of the fishpond package was used to assess differential transcript usage amongst the 4 major isoforms of the CREVASSE gene. Tximeta was used to import Salmon counts and 30 Gibbs replicates, and EV isolation batch was included as a covariate in the analysis.

**Figure Design.** RApuzzler (Wiegrefte et al., 2019) was used to create Figure 3.3 via RNAplot (Lorenz et al., 2011). Draw Venn Diagram

(<http://bioinformatics.psb.ugent.be/webtools/Venn/>) was used to create Figure 3.5. Figure 3.6 was created with fgsea (Korotkevich et al., 2021). BioRender was used to create Figure 3.7. GraphPad Prism 9 was used to create all other figures.

## Chapter 4 : Conclusions and Future Directions

### CONCLUSIONS

Taken together, the data I have presented suggest a coherent narrative for the mechanisms by which caspase activity influences chick auditory brainstem development. In Chapter 1, I showed that caspase activity is directed toward a variety of proteins, including cytoskeletal proteins, extracellular vesicle proteins, and RNA-binding proteins. The proteolysis of cytoskeletal structural and regulatory proteins makes sense in the context of axon guidance and synapse formation, which are most precise when the integration of and response to extracellular cues happens rapidly and locally, such as when they are controlled by caspase activity (Kellermeyer et al., 2018). In Chapter 2, we saw that non-apoptotic caspase activity in the auditory brainstem is directed toward cleavage sites associated with cytoskeletal proteins, suggesting that caspases are biochemically modified during auditory brainstem development to suit their non-apoptotic developmental roles. Finally, in Chapter 3, I demonstrated that the three-way enrichment among caspase substrates, extracellular vesicle proteins, and RNA-binding proteins is not a coincidence. The increased expression of the lncRNA CREVASSE in EVs from caspase-inhibited brainstems, combined with the predicted role for CREVASSE in binding transcripts involved in auditory brainstem development, suggest that caspase activity influences the differentiation of neighboring cells by controlling whether CREVASSE is loaded into EVs released from NM axons.

A possible “grand unified theory” for the role of caspase activity in auditory brainstem development is as follows: As NM axons approach their targets in NL, caspase activity controls NM growth cone morphology by breaking down cytoskeletal proteins in response to external guidance cues. Caspase activity may be required at this stage of NM axon guidance and not prior stages because short-range target approach is more of a navigational challenge for growth cones than long-range target seeking, especially in circuits where precision is as essential as in

the auditory brainstem. NM growth cones contact many NL cells during this stage, but synapse formation must be delayed until the correct target is innervated. Once NM axons have reached their destination, large changes in cell morphology are no longer necessary, so caspase activity is reduced. The reduction in caspase activity applies to all caspase substrates in NM axons, including not only cytoskeletal proteins but also extracellular vesicle proteins and the RNA-binding proteins that are loaded into EVs. The reduction in caspase activity is therefore accompanied by an increase in CREVASSE being loaded into EVs from NM axons and being sent to NL cells. When CREVASSE arrives at NL, it binds and facilitates translation of transcription factors that are involved in neuronal differentiation of auditory brainstem cells, causing NL cells that receive CREVASSE to begin to mature. In this way, differentiation only occurs in NL cells that are sufficiently innervated by NM axons that have finished the guidance phase. Thus caspase activity controls both NM axon guidance and maturation of the NL target cells, which matches the dual phenotypes of NM axon mistargeting and NL morphology disruption observed upon caspase inhibition in the auditory brainstem. We believe this mechanism may be used to coordinate axon guidance and synapse formation not only in the auditory brainstem but also in a variety of contexts in which non-apoptotic activity of the apoptotic machinery is used to facilitate neural development.

### **FUTURE DIRECTIONS**

This model has several knowledge gaps that recommend next steps for understanding the role of caspase activity in auditory brainstem development.

#### **Developmental expression profile of CREVASSE in auditory brainstem EVs.**

First, the model predicts that CREVASSE expression occurs at low levels in auditory brainstem EVs when caspase activity peaks in NM axons (i.e. around E8-9), then increases as caspase activity wanes in NM axons (i.e. around E10). An expression profile of auditory brainstem EVs

would shed light on this prediction, preferably using long-read sequencing in order to identify any differential transcript usage at the splice sites and alternate transcription termination sites observed in Chapter 3. A developmental expression profile of CREVASSE would be enhanced by single-vesicle RNA-seq since CREVASSE is likely only loaded into a subset of all EVs in the auditory brainstem. However, a single-EV strategy may be less feasible with current technology if CREVASSE is primarily expressed in small EVs, since only single large EVs (>100 nm) have been transcriptionally profiled as of this writing (Luo et al., 2022).

**RNA-FISH against CREVASSE.** Our current model predicts that CREVASSE is loaded into EVs from NM axon termini, which requires that CREVASSE is present in this location. This hypothesis can be tested by RNA fluorescent *in situ* hybridization against CREVASSE. We would expect to detect CREVASSE at nearly constitutive levels in NM axons from E8 to E10, since the limiting step for CREVASSE's ability to influence NL differentiation is expected to be efficiency of loading CREVASSE into EVs, not expression levels of CREVASSE in NM axons. We would also expect a gradual increase in levels of CREVASSE in NL cells during the same time period as NM cells deposit transcripts via EVs, and NL cells with the fewest CREVASSE transcripts are expected to undergo apoptosis beginning at E12.

RNA-FISH would also permit detection of CREVASSE at other developmental timepoints in other locations in the auditory system, specifically at E6-7 in the auditory nerve (AN). Chapter 3 dealt with EVs that were collected when cleaved caspase-3 expression is highest in NM axons, but this is only one stage in cleaved caspase-3's ascension of the auditory brainstem. Just days earlier, cleaved caspase-3 is expressed in AN axons (Rotschafer et al., 2016), which innervate NM, so it seems likely that caspase activity mediates a similar process in the formation of the AN-NM synapse as it does in the formation of the NM-NL synapse, possibly including control of loading of CREVASSE into EVs. If RNA-FISH reveals CREVASSE expression on E6-7 in auditory nerve axons that resembles CREVASSE expression on E8-10 in

NM axons, then it would likely be worthwhile to sequence RNA of auditory brainstem EVs at the earlier ages to determine whether CREVASSE is also EV-associated at these timepoints too and whether this association is caspase-dependent.

**Identification of protein binding partners of CREVASSE.** Additionally, while we have predicted several candidate RNA-binding proteins (RBPs) that mediate the loading of CREVASSE into EVs, we do not have evidence suggesting which (if any) of these proteins is actually responsible for this process. We could address this question by RNA-RBP UV cross-linking of auditory brainstem EVs, followed by protein pulldown with probes against CREVASSE, and finally with protein mass spectrometry of the isolated proteins (Gerber, 2021). If EVs do not provide enough material for this experiment, auditory brainstem tissue could be used instead, though this strategy may yield less relevant results since CREVASSE may be bound to different repertoires of RBPs in cells and EVs.

**Identification of RNA binding partners of CREVASSE.** Gene Set Enrichment Analysis of predicted CREVASSE binding partners suggested that CREVASSE binds transcripts involved in auditory brainstem development and differentiation. However, this claim requires direct evidence. As with abovementioned experiments to identify protein binding partners of CREVASSE, this question would benefit from cross-linking experiments: RNA-RNA cross-linking of auditory brainstem tissue, followed by pulldown with CREVASSE probes, and finally sequencing of CREVASSE-associated transcripts would allow us to determine whether the predicted binding partners of CREVASSE were correct (Torres et al., 2018).

**Gain/loss of function for CREVASSE and its protein binding partners.** Functional studies of CREVASSE in the auditory brainstem are also needed. Overexpression of CREVASSE in either NM or NL may simulate a premature end to caspase activity in NM axons, bringing about precocious differentiation of NL cells and possibly leading to NL overpopulation

and dysmorphogenesis. A similar outcome would be expected upon NM-specific overexpression of a caspase-uncleavable form of the RBP(s) expected to ferry CREVASSE into EVs.

These gain-of-function experiments should be complemented by loss-of-function studies. Once the site(s) of CREVASSE expression in the auditory brainstem at each developmental timepoint are identified, CREVASSE knockdown in that location via RNA interference (Thijssen et al., 2021) or by CRISPR knockout (if the location is thought to be the site of CREVASSE transcription) would enable us to test the veracity of our predictions about the role of CREVASSE in auditory brainstem development. Notably, an RNA interference strategy would allow us to test the effects of CREVASSE knockdown in either donor or recipient cells, so while it would not reveal the identity of donors or recipients, it would permit a test of function without a *priori* knowledge of donors and recipients.

**Search for mammalian analog of CREVASSE.** Finally, this model would be most relevant to research on human health if it has correlates in mammalian systems. We have evidence that cleaved caspase-3 expression ascends the murine auditory brainstem during early postnatal development, analogous to events during chick embryonic development. LncRNAs have poor sequence conservation because they tend to bind to non-coding regions of their target RNAs, which also have poor sequence conservation (Johnsson et al., 2014). Therefore, while there is no obvious homolog for CREVASSE in human or mouse genomes, one or more lncRNAs with very different sequences from CREVASSE may serve as functional analogs of CREVASSE during mammalian auditory brainstem development. Transcriptional profiling of mouse auditory brainstem EVs during and after developmental timepoints with high caspase activity (i.e. postnatal day 8-9) would likely be a fruitful starting point for this search. This analysis would benefit from the creation of a mouse line in which a dominant-negative caspase-3 transgene is conditionally expressed in auditory brainstem neurons using the auditory-brainstem-specific *Egr2* promoter (Zuccotti et al., 2013), allowing us to probe the

effects of premature suspension of caspase activity in auditory brainstem circuits on the RNA content of mouse auditory brainstem EVs, as we did pharmacologically in chick embryos in Chapter 3.

## BIBLIOGRAPHY

- Agniswamy, J., Fang, B., and Weber, I. T. (2007). Plasticity of S2–S4 specificity pockets of executioner caspase-7 revealed by structural and kinetic analysis. *FEBS J.* 274, 4752–4765. doi: 10.1111/j.1742-4658.2007.05994.x.
- Agus, T. R., Suied, C., and Pressnitzer, D. (2019). “Timbre Recognition and Sound Source Identification,” in *Timbre: Acoustics, Perception, and Cognition* Springer Handbook of Auditory Research., eds. K. Siedenburg, C. Saitis, S. McAdams, A. N. Popper, and R. R. Fay (Cham: Springer International Publishing), 59–85. doi: 10.1007/978-3-030-14832-4\_3.
- Allen-Sharpley, M. R., Tjia, M., and Cramer, K. S. (2013). Differential roles for EphA and EphB signaling in segregation and patterning of central vestibulocochlear nerve projections. *PLoS One* 8, e78658. doi: 10.1371/journal.pone.0078658.
- Andersen, R. E., Hong, S. J., Lim, J. J., Cui, M., Harpur, B. A., Hwang, E., et al. (2019). The Long Noncoding RNA Pnky Is a Trans-acting Regulator of Cortical Development In Vivo. *Dev. Cell* 49, 632-642.e7. doi: 10.1016/j.devcel.2019.04.032.
- Anderson, S., Gibbs, C., Tanaka, A., Kung, H.-J., and Fujita, D. (1985). Human cellular src gene: Nucleotide sequence and derived amino acid sequence of the region coding for the carboxy-terminal two-thirds of pp60(c-src). *Mol. Cell. Biol.* 5, 1122–9. doi: 10.1128/MCB.5.5.1122.
- Andrews, S. (2010). FastQC: A Quality Control Tool for High Throughput Sequence Data [Online]. Available at: <http://www.bioinformatics.babraham.ac.uk/projects/fastqc/>.
- Antonov, I., Marakhonov, A., Zamkova, M., and Medvedeva, Y. (2018). ASSA: Fast identification of statistically significant interactions between long RNAs. *J. Bioinform. Comput. Biol.* 16, 1840001. doi: 10.1142/S0219720018400012.
- Antonov, I. V., Mazurov, E., Borodovsky, M., and Medvedeva, Y. A. (2019). Prediction of lncRNAs and their interactions with nucleic acids: benchmarking bioinformatics tools. *Brief. Bioinform.* 20, 551–564. doi: 10.1093/bib/bby032.
- Antounians, L., Tzanetakis, A., Pellerito, O., Catania, V. D., Sulisty, A., Montalva, L., et al. (2019). The Regenerative Potential of Amniotic Fluid Stem Cell Extracellular Vesicles: Lessons Learned by Comparing Different Isolation Techniques. *Sci. Rep.* 9, 1837. doi: 10.1038/s41598-018-38320-w.
- Ashida, G., and Carr, C. E. (2011). Sound localization: Jeffress and beyond. *Curr. Opin. Neurobiol.* 21, 745–751. doi: 10.1016/j.conb.2011.05.008.
- Balakrishnan, R., Harris, M. A., Huntley, R., Van Auken, K., and Cherry, J. M. (2013). A guide to best practices for Gene Ontology (GO) manual annotation. *Database J. Biol. Databases Curation* 2013. doi: 10.1093/database/bat054.
- Basso, M., and Bonetto, V. (2016). Extracellular Vesicles and a Novel Form of Communication in the Brain. *Front. Neurosci.* 10. doi: 10.3389/fnins.2016.00127.

- Benjamini, Y., and Hochberg, Y. (1995). Controlling the False Discovery Rate: A Practical and Powerful Approach to Multiple Testing. *J. R. Stat. Soc. Ser. B Methodol.* 57, 289–300.
- Benjamini, Y., Krieger, A. M., and Yekutieli, D. (2006). Adaptive linear step-up procedures that control the false discovery rate. *Biometrika* 93, 491–507. doi: 10.1093/biomet/93.3.491.
- Berger, A. B., Sexton, K. B., and Bogoyo, M. (2006). Commonly used caspase inhibitors designed based on substrate specificity profiles lack selectivity. *Cell Res.* 16, 961–963. doi: 10.1038/sj.cr.7310112.
- Bingöl, E. N., Serçinoğlu, O., and Ozbek, P. (2019). How do mutations and allosteric inhibitors modulate caspase-7 activity? A molecular dynamics study. *J. Biomol. Struct. Dyn.* 37, 3456–3466. doi: 10.1080/07391102.2018.1517611.
- Boca, S. M., and Leek, J. T. (2018). A direct approach to estimating false discovery rates conditional on covariates. *PeerJ* 6, e6035. doi: 10.7717/peerj.6035.
- Böing, A. N., Pol, E. van der, Grootemaat, A. E., Coumans, F. A. W., Sturk, A., and Nieuwland, R. (2014). Single-step isolation of extracellular vesicles by size-exclusion chromatography. *J. Extracell. Vesicles* 3, 23430. doi: 10.3402/jev.v3.23430.
- Böing, A. N., Stap, J., Hau, C. M., Afink, G. B., Ris-Stalpers, C., Reits, E. A., et al. (2013). Active caspase-3 is removed from cells by release of caspase-3-enriched vesicles. *Biochim. Biophys. Acta BBA - Mol. Cell Res.* 1833, 1844–1852. doi: 10.1016/j.bbamcr.2013.03.013.
- Book, K. J., and Morest, D. K. (1990). Migration of neuroblasts by perikaryal translocation: Role of cellular elongation and axonal outgrowth in the acoustic nuclei of the chick embryo medulla. *J. Comp. Neurol.* 297, 55–76. doi: 10.1002/cne.902970105.
- Breglio, A. M., May, L. A., Barzik, M., Welsh, N. C., Francis, S. P., Costain, T. Q., et al. (2020). Exosomes mediate sensory hair cell protection in the inner ear. *J. Clin. Invest.* 130, 2657–2672. doi: 10.1172/JCI128867.
- Brennan, K., Martin, K., FitzGerald, S. P., O’Sullivan, J., Wu, Y., Blanco, A., et al. (2020). A comparison of methods for the isolation and separation of extracellular vesicles from protein and lipid particles in human serum. *Sci. Rep.* 10, 1039. doi: 10.1038/s41598-020-57497-7.
- Brentnall, M., Rodriguez-Menocal, L., De Guevara, R. L., Cepero, E., and Boise, L. H. (2013). Caspase-9, caspase-3 and caspase-7 have distinct roles during intrinsic apoptosis. *BMC Cell Biol.* 14, 32. doi: 10.1186/1471-2121-14-32.
- Bucan, V., Vaslaitis, D., Peck, C.-T., Strauß, S., Vogt, P. M., and Radtke, C. (2019). Effect of Exosomes from Rat Adipose-Derived Mesenchymal Stem Cells on Neurite Outgrowth and Sciatic Nerve Regeneration After Crush Injury. *Mol. Neurobiol.* 56, 1812–1824. doi: 10.1007/s12035-018-1172-z.
- Buck, K. B., and Zheng, J. Q. (2002). Growth Cone Turning Induced by Direct Local Modification of Microtubule Dynamics. *J. Neurosci.* 22, 9358–9367. doi: 10.1523/JNEUROSCI.22-21-09358.2002.

- Byun, Y., Chen, F., Chang, R., Trivedi, M., Green, K. J., and Cryns, V. L. (2001). Caspase cleavage of vimentin disrupts intermediate filaments and promotes apoptosis. *Cell Death Differ.* 8, 443–450. doi: 10.1038/sj.cdd.4400840.
- Cade, C., Swartz, P., MacKenzie, S. H., and Clark, A. C. (2014). Modifying Caspase-3 Activity by Altering Allosteric Networks. *Biochemistry* 53, 7582–7595. doi: 10.1021/bi500874k.
- Campbell, D. S., and Holt, C. E. (2001). Chemotropic Responses of Retinal Growth Cones Mediated by Rapid Local Protein Synthesis and Degradation. *Neuron* 32, 1013–1026. doi: 10.1016/S0896-6273(01)00551-7.
- Campbell, D. S., and Holt, C. E. (2003). Apoptotic Pathway and MAPKs Differentially Regulate Chemotropic Responses of Retinal Growth Cones. *Neuron* 37, 939–952. doi: 10.1016/S0896-6273(03)00158-2.
- Campbell, D. S., and Okamoto, H. (2013). Local caspase activation interacts with Slit-Robo signaling to restrict axonal arborization. *J Cell Biol* 203, 657–672. doi: 10.1083/jcb.201303072.
- Carlevaro-Fita, J., Rahim, A., Guigó, R., Vardy, L. A., and Johnson, R. (2016). Cytoplasmic long noncoding RNAs are frequently bound to and degraded at ribosomes in human cells. *RNA* 22, 867–882. doi: 10.1261/rna.053561.115.
- Carr, C. E., and Konishi, M. (1990). A circuit for detection of interaural time differences in the brain stem of the barn owl. *J. Neurosci.* 10, 3227–3246. doi: 10.1523/JNEUROSCI.10-10-03227.1990.
- Caruso, S., and Poon, I. K. H. (2018). Apoptotic Cell-Derived Extracellular Vesicles: More Than Just Debris. *Front. Immunol.* 9. doi: 10.3389/fimmu.2018.01486.
- Chen, J., Ren, S., Duscher, D., Kang, Y., Liu, Y., Wang, C., et al. (2019). Exosomes from human adipose-derived stem cells promote sciatic nerve regeneration via optimizing Schwann cell function. *J. Cell. Physiol.* 234, 23097–23110. doi: 10.1002/jcp.28873.
- Chen, J., Wei, Z., Liang, C., Liu, B., Guo, J., Kong, X., et al. (2021). Dysfunction of the Auditory Brainstem as a Neurophysiology Subtype of Autism Spectrum Disorder. *Front. Neurosci.* 15, 237. doi: 10.3389/fnins.2021.637079.
- Chen, X., He, X.-Y., Dan, Q., and Li, Y. (2022). FAM201A, a long noncoding RNA potentially associated with atrial fibrillation identified by ceRNA network analyses and WGCNA. *BMC Med. Genomics* 15, 80. doi: 10.1186/s12920-022-01232-w.
- Cheng, L., Sharples, R. A., Scicluna, B. J., and Hill, A. F. (2014). Exosomes provide a protective and enriched source of miRNA for biomarker profiling compared to intracellular and cell-free blood. *J. Extracell. Vesicles* 3, 23743. doi: 10.3402/jev.v3.23743.
- Cheng, X., and Ferrell, J. E. (2018). Apoptosis propagates through the cytoplasm as trigger waves. *Science* 361, 607–612. doi: 10.1126/science.aah4065.

- Ching, R. C., Wiberg, M., and Kingham, P. J. (2018). Schwann cell-like differentiated adipose stem cells promote neurite outgrowth via secreted exosomes and RNA transfer. *Stem Cell Res. Ther.* 9, 266. doi: 10.1186/s13287-018-1017-8.
- Cho, K. H. T., Xu, B., Blenkiron, C., and Fraser, M. (2019). Emerging Roles of miRNAs in Brain Development and Perinatal Brain Injury. *Front. Physiol.* 10. doi: 10.3389/fphys.2019.00227.
- Cioni, J.-M., Koppers, M., and Holt, C. E. (2018). Molecular control of local translation in axon development and maintenance. *Curr. Opin. Neurobiol.* 51, 86–94. doi: 10.1016/j.conb.2018.02.025.
- Colombo, M., Raposo, G., and Théry, C. (2014). Biogenesis, Secretion, and Intercellular Interactions of Exosomes and Other Extracellular Vesicles. *Annu. Rev. Cell Dev. Biol.* 30, 255–289. doi: 10.1146/annurev-cellbio-101512-122326.
- Connolly, P. F., Jäger, R., and Fearnhead, H. O. (2014). New roles for old enzymes: killer caspases as the engine of cell behavior changes. *Front. Physiol.* 5. doi: 10.3389/fphys.2014.00149.
- Corso, G., Mäger, I., Lee, Y., Görgens, A., Bultema, J., Giebel, B., et al. (2017). Reproducible and scalable purification of extracellular vesicles using combined bind-elute and size exclusion chromatography. *Sci. Rep.* 7, 11561. doi: 10.1038/s41598-017-10646-x.
- Cramer, K. S., Bermingham-McDonogh, O., Krull, C. E., and Rubel, E. W. (2004). EphA4 signaling promotes axon segregation in the developing auditory system. *Dev. Biol.* 269, 26–35. doi: 10.1016/j.ydbio.2004.01.002.
- Cramer, K. S., Cerretti, D. P., and Siddiqui, S. A. (2006). EphB2 regulates axonal growth at the midline in the developing auditory brainstem. *Dev. Biol.* 295, 76–89. doi: 10.1016/j.ydbio.2006.03.010.
- Cramer, K. S., Fraser, S. E., and Rubel, E. W. (2000a). Embryonic Origins of Auditory Brainstem Nuclei in the Chick Hindbrain. *Dev. Biol.* 224, 138–151. doi: 10.1006/dbio.2000.9779.
- Cramer, K. S., and Gabriele, M. L. (2014). Axon guidance in the auditory system: Multiple functions of Eph receptors. *Neuroscience* 277, 152–162. doi: 10.1016/j.neuroscience.2014.06.068.
- Cramer, K. S., Karam, S. D., Bothwell, M., Cerretti, D. P., Pasquale, E. B., and Rubel, E. W. (2002). Expression of EphB receptors and EphrinB ligands in the developing chick auditory brainstem. *J. Comp. Neurol.* 452, 51–64. doi: 10.1002/cne.10399.
- Cramer, K. S., Rosenberger, M. H., Frost, D. M., Cochran, S. L., Pasquale, E. B., and Rubel, E. W. (2000b). Developmental regulation of ephA4 expression in the chick auditory brainstem. *J. Comp. Neurol.* 426, 270–278. doi: 10.1002/1096-9861(20001016)426:2<270::AID-CNE8>3.0.CO;2-8.
- Cramer, K. S., and Rubel, E. W. (2016). Glial Cell Contributions to Auditory Brainstem Development. 10, 83. doi: 10.3389/fncir.2016.00083.

- Crawford, E. D., Seaman, J. E., Agard, N., Hsu, G. W., Julien, O., Mahrus, S., et al. (2013). The DegraBase: a database of proteolysis in healthy and apoptotic human cells. *Mol. Cell. Proteomics MCP* 12, 813–824. doi: 10.1074/mcp.O112.024372.
- Crawford, E. D., Seaman, J. E., Barber, A. E., David, D. C., Babbitt, P. C., Burlingame, A. L., et al. (2012). Conservation of caspase substrates across metazoans suggests hierarchical importance of signaling pathways over specific targets and cleavage site motifs in apoptosis. *Cell Death Differ.* 19, 2040–2048. doi: 10.1038/cdd.2012.99.
- Crawford, E. D., and Wells, J. A. (2011). Caspase Substrates and Cellular Remodeling. *Annu. Rev. Biochem.* 80, 1055–1087. doi: 10.1146/annurev-biochem-061809-121639.
- Culver, S., and Galileo, D. S. (2008). The Effects of Cell Surface NgCAM Expression on Developing Chick Brain Axons In Vitro. *FASEB J.* 22, 823.8-823.8. doi: 10.1096/fasebj.22.1\_supplement.823.8.
- Cusack, C. L., Swahari, V., Hampton Henley, W., Michael Ramsey, J., and Deshmukh, M. (2013). Distinct pathways mediate axon degeneration during apoptosis and axon-specific pruning. *Nat. Commun.* 4, 1876. doi: 10.1038/ncomms2910.
- Dagbay, K., Eron, S. J., Serrano, B. P., Velázquez-Delgado, E. M., Zhao, Y., Lin, D., et al. (2014). A multi-pronged approach for compiling a global map of allosteric regulation in the apoptotic caspases. *Methods Enzymol.* 544, 215–249. doi: 10.1016/B978-0-12-417158-9.00009-1.
- De Maio, A., and Vazquez, D. (2013). EXTRACELLULAR HEAT SHOCK PROTEINS: A NEW LOCATION, A NEW FUNCTION. *Shock Augusta Ga* 40, 239–246. doi: 10.1097/SHK.0b013e3182a185ab.
- Dellar, E. R., Hill, C., Melling, G. E., Carter, D. R. F., and Baena-Lopez, L. A. (2022). Unpacking extracellular vesicles: RNA cargo loading and function. *J. Extracell. Biol.* 1, e40. doi: 10.1002/jex2.40.
- Delpretti, S., Montavon, T., Leleu, M., Joye, E., Tzika, A., Milinkovitch, M., et al. (2013). Multiple Enhancers Regulate Hoxd Genes and the Hotdog LncRNA during Cecum Budding. *Cell Rep.* 5, 137–150. doi: 10.1016/j.celrep.2013.09.002.
- Di Liegro, C. M., Schiera, G., and Di Liegro, I. (2017). Extracellular Vesicle-Associated RNA as a Carrier of Epigenetic Information. *Genes* 8, 240. doi: 10.3390/genes8100240.
- Dinh, M. L., Koppel, S. J., Korn, M. J., and Cramer, K. S. (2014). Distribution of glial cells in the auditory brainstem: Normal development and effects of unilateral lesion. *Neuroscience* 278, 237–252. doi: 10.1016/j.neuroscience.2014.08.016.
- Dix, M. M., Simon, G. M., Wang, C., Okerberg, E., Patricelli, M. P., and Cravatt, B. F. (2012). Functional interplay between caspase cleavage and phosphorylation sculpts the apoptotic proteome. *Cell* 150, 426–440. doi: 10.1016/j.cell.2012.05.040.
- Dobin, A., Davis, C. A., Schlesinger, F., Drenkow, J., Zaleski, C., Jha, S., et al. (2013). STAR: ultrafast universal RNA-seq aligner. *Bioinformatics* 29, 15–21. doi: 10.1093/bioinformatics/bts635.

- Dragomir, M., Chen, B., and Calin, G. A. (2018). Exosomal lncRNAs as new players in cell-to-cell communication. *Transl. Cancer Res.* 7, S243–S252. doi: 10.21037/tcr.2017.10.46.
- Driedonks, T. A. P., and Nolte-'t Hoen, E. N. M. (2019). Circulating Y-RNAs in Extracellular Vesicles and Ribonucleoprotein Complexes; Implications for the Immune System. *Front. Immunol.* 9. doi: 10.3389/fimmu.2018.03164.
- Elmore, S. (2007). Apoptosis: a review of programmed cell death. *Toxicol. Pathol.* 35, 495–516. doi: 10.1080/01926230701320337.
- Enriquez-Barreto, L., Palazzetti, C., Brennaman, L. H., Maness, P. F., and Fairén, A. (2012). Neural cell adhesion molecule, NCAM, regulates thalamocortical axon pathfinding and the organization of the cortical somatosensory representation in mouse. *Front. Mol. Neurosci.* 5. doi: 10.3389/fnmol.2012.00076.
- Eron, S. J., Raghupathi, K., and Hardy, J. A. (2017). Dual Site Phosphorylation of Caspase-7 by PAK2 Blocks Apoptotic Activity by Two Distinct Mechanisms. *Struct. Lond. Engl.* 1993 25, 27–39. doi: 10.1016/j.str.2016.11.001.
- Ertürk, A., Wang, Y., and Sheng, M. (2014). Local Pruning of Dendrites and Spines by Caspase-3-Dependent and Proteasome-Limited Mechanisms. *J. Neurosci.* 34, 1672–1688. doi: 10.1523/JNEUROSCI.3121-13.2014.
- Espinosa-Oliva, A. M., García-Revilla, J., Alonso-Bellido, I. M., and Burguillos, M. A. (2019). Brainiac Caspases: Beyond the Wall of Apoptosis. *Front. Cell. Neurosci.* 13. doi: 10.3389/fncel.2019.00500.
- Estrada-Bernal, A., Sanford, S. D., Sosa, L. J., Simon, G. C., Hansen, K. C., and Pfenninger, K. H. (2012). Functional Complexity of the Axonal Growth Cone: A Proteomic Analysis. *PLOS ONE* 7, e31858. doi: 10.1371/journal.pone.0031858.
- Fischer, B. J., and Seidl, A. H. (2014). Resolution of interaural time differences in the avian sound localization circuit—a modeling study. *Front. Comput. Neurosci.* 8. doi: 10.3389/fncom.2014.00099.
- Fischer, U., Jänicke, R. U., and Schulze-Osthoff, K. (2003). Many cuts to ruin: a comprehensive update of caspase substrates. *Cell Death Differ.* 10, 76–100. doi: 10.1038/sj.cdd.4401160.
- Fowler, C. D. (2019). NeuroEVs: Characterizing Extracellular Vesicles Generated in the Neural Domain. *J. Neurosci.* 39, 9262–9268. doi: 10.1523/JNEUROSCI.0146-18.2019.
- Friauf, E., and Lohmann, C. (1999). Development of auditory brainstem circuitry. Activity-dependent and activity-independent processes. *Cell Tissue Res.* 297, 187–195.
- Frühbeis, C., Fröhlich, D., Kuo, W. P., and Krämer-Albers, E.-M. (2013). Extracellular vesicles as mediators of neuron-glia communication. *Front. Cell. Neurosci.* 7. doi: 10.3389/fncel.2013.00182.
- Fuchs, Y., and Steller, H. (2011). Programmed Cell Death in Animal Development and Disease. *Cell* 147, 742–758. doi: 10.1016/j.cell.2011.10.033.

- Fuentes-Prior, P., and Salvesen, G. S. (2004). The protein structures that shape caspase activity, specificity, activation and inhibition. *Biochem. J.* 384, 201–232. doi: 10.1042/BJ20041142.
- Galbán, S., and Duckett, C. S. (2010). XIAP as a ubiquitin ligase in cellular signaling. *Cell Death Differ.* 17, 54–60. doi: 10.1038/cdd.2009.81.
- Galluzzi, L., Kepp, O., Trojel-Hansen, C., and Kroemer, G. (2012). Non-apoptotic functions of apoptosis-regulatory proteins. *EMBO Rep.* 13, 322–330. doi: 10.1038/embor.2012.19.
- Gerber, A. P. (2021). RNA-Centric Approaches to Profile the RNA–Protein Interaction Landscape on Selected RNAs. *Non-Coding RNA* 7, 11. doi: 10.3390/ncrna7010011.
- Gillet, V., Hunting, D., and Takser, L. (2016). Turing Revisited: Decoding the microRNA Messages in Brain Extracellular Vesicles for Early Detection of Neurodevelopmental Disorders. *Curr. Environ. Health Rep.* 3, 188–201. doi: 10.1007/s40572-016-0093-0.
- Glinka, M., Herrmann, T., Funk, N., Havlicek, S., Rossoll, W., Winkler, C., et al. (2010). The heterogeneous nuclear ribonucleoprotein-R is necessary for axonal beta-actin mRNA translocation in spinal motor neurons. *Hum. Mol. Genet.* 19, 1951–1966. doi: 10.1093/hmg/ddq073.
- Gong, C., and Maquat, L. E. (2011). lncRNAs transactivate STAU1-mediated mRNA decay by duplexing with 3' UTRs via Alu elements. *Nature* 470, 284–288. doi: 10.1038/nature09701.
- Gong, J., Körner, R., Gaitanos, L., and Klein, R. (2016). Exosomes mediate cell contact-independent ephrin-Eph signaling during axon guidance. *J. Cell Biol.* 214, 35–44. doi: 10.1083/jcb.201601085.
- Gotoh, O. (2018). Modeling one thousand intron length distributions with fitild. *Bioinformatics* 34, 3258–3264. doi: 10.1093/bioinformatics/bty353.
- Gould, S. J., and Raposo, G. (2013). As we wait: coping with an imperfect nomenclature for extracellular vesicles. *J. Extracell. Vesicles* 2, 20389. doi: 10.3402/jev.v2i0.20389.
- Grinshpon, R. D., Shrestha, S., Titus-McQuillan, J., Hamilton, P. T., Swartz, P. D., and Clark, A. C. (2019). Resurrection of ancestral effector caspases identifies novel networks for evolution of substrate specificity. *Biochem. J.* 476, 3475–3492. doi: 10.1042/BCJ20190625.
- Groot, M., and Lee, H. (2020). Sorting Mechanisms for MicroRNAs into Extracellular Vesicles and Their Associated Diseases. *Cells* 9, 1044. doi: 10.3390/cells9041044.
- Gross, A., McDonnell, J. M., and Korsmeyer, S. J. (1999). BCL-2 family members and the mitochondria in apoptosis. *Genes Dev.* 13, 1899–1911.
- Grothe, B., and Pecka, M. (2014). The natural history of sound localization in mammals – a story of neuronal inhibition. *Front. Neural Circuits* 8. doi: 10.3389/fncir.2014.00116.

- Gu, Z., Serradj, N., Ueno, M., Liang, M., Li, J., Baccei, M. L., et al. (2017). Skilled Movements Require Non-apoptotic Bax/Bak Pathway-Mediated Corticospinal Circuit Reorganization. *Neuron* 94, 626-641.e4. doi: 10.1016/j.neuron.2017.04.019.
- Gulyaeva, N. V. (2003). Non-apoptotic Functions of Caspase-3 in Nervous Tissue. *Biochem. Mosc.* 68, 1171–1180. doi: 10.1023/B:BIRY.0000009130.62944.35.
- Gutwein, P., Mechttersheimer, S., Riedle, S., Stoeck, A., Gast, D., Joumaa, S., et al. (2003). ADAM10-mediated cleavage of L1 adhesion molecule at the cell surface and in released membrane vesicles. *FASEB J. Off. Publ. Fed. Am. Soc. Exp. Biol.* 17, 292–294. doi: 10.1096/fj.02-0430fje.
- Häcker, H.-G., Sisay, M. T., and Gütschow, M. (2011). Allosteric modulation of caspases. *Pharmacol. Ther.* 132, 180–195. doi: 10.1016/j.pharmthera.2011.07.003.
- Hamburger, V., and Hamilton, H. L. (1951). A series of normal stages in the development of the chick embryo. *J. Morphol.* 88, 49–92.
- Han, M.-H., Jiao, S., Jia, J.-M., Chen, Y., Chen, C. Y., Gucek, M., et al. (2013). The Novel Caspase-3 Substrate Gap43 is Involved in AMPA Receptor Endocytosis and Long-Term Depression. *Mol. Cell. Proteomics* 12, 3719–3731. doi: 10.1074/mcp.M113.030676.
- Hardy, J. A., and Wells, J. A. (2009). Dissecting an Allosteric Switch in Caspase-7 Using Chemical and Mutational Probes \*. *J. Biol. Chem.* 284, 26063–26069. doi: 10.1074/jbc.M109.001826.
- Hendricks, S. J., Rubel, E. W., and Nishi, R. (2006). Formation of the avian nucleus magnocellularis from the auditory anlage. *J. Comp. Neurol.* 498, 433–442. doi: 10.1002/cne.21031.
- Hengartner, M. O. (2000). The biochemistry of apoptosis. *Nature* 407, 770–776. doi: 10.1038/35037710.
- Hentze, H., Schwoebel, F., Lund, S., Keel, M., Ertel, W., Wendel, A., et al. (2001). In vivo and in vitro evidence for extracellular caspase activity released from apoptotic cells. *Biochem. Biophys. Res. Commun.* 283, 1111–1117. doi: 10.1006/bbrc.2001.4918.
- Hentze, M. W., Castello, A., Schwarzl, T., and Preiss, T. (2018). A brave new world of RNA-binding proteins. *Nat. Rev. Mol. Cell Biol.* 19, 327–341. doi: 10.1038/nrm.2017.130.
- Herr, A. B. (2018). Evolution of an allosteric “off switch” in apoptotic caspases. *J. Biol. Chem.* 293, 5462–5463. doi: 10.1074/jbc.H118.002379.
- Hill, M. E., MacPherson, D. J., Wu, P., Julien, O., Wells, J. A., and Hardy, J. A. (2016). Reprogramming Caspase-7 Specificity by Regio-Specific Mutations and Selection Provides Alternate Solutions for Substrate Recognition. *ACS Chem. Biol.* 11, 1603–1612. doi: 10.1021/acscchembio.5b00971.
- Hobor, F., Dallmann, A., Ball, N. J., Cicchini, C., Battistelli, C., Ogradowicz, R. W., et al. (2018). A cryptic RNA-binding domain mediates Syncrip recognition and exosomal partitioning of miRNA targets. *Nat. Commun.* 9, 831. doi: 10.1038/s41467-018-03182-3.

- Hollville, E., and Deshmukh, M. (2017). Physiological functions of non-apoptotic caspase activity in the nervous system. *Semin. Cell Dev. Biol.* doi: 10.1016/j.semcdb.2017.11.037.
- Holt, C. E., and Schuman, E. M. (2013). The Central Dogma Decentralized: New Perspectives on RNA Function and Local Translation in Neurons. *Neuron* 80, 648–657. doi: 10.1016/j.neuron.2013.10.036.
- Hong, H., and Sanchez, J. T. (2018). Need for Speed and Precision: Structural and Functional Specialization in the Cochlear Nucleus of the Avian Auditory System. *J. Exp. Neurosci.* 12, 1179069518815628. doi: 10.1177/1179069518815628.
- Hornberg, H. K., and Holt, C. (2013). RNA-binding proteins and translational regulation in axons and growth cones. *Front. Neurosci.* 7. doi: 10.3389/fnins.2013.00081.
- Huang, D. W., Sherman, B. T., and Lempicki, R. A. (2009a). Bioinformatics enrichment tools: paths toward the comprehensive functional analysis of large gene lists. *Nucleic Acids Res.* 37, 1–13. doi: 10.1093/nar/gkn923.
- Huang, D. W., Sherman, B. T., and Lempicki, R. A. (2009b). Systematic and integrative analysis of large gene lists using DAVID bioinformatics resources. *Nat. Protoc.* 4, 44–57. doi: 10.1038/nprot.2008.211.
- Huffman, K. J., and Cramer, K. S. (2007). EphA4 misexpression alters tonotopic projections in the auditory brainstem. *Dev. Neurobiol.* 67, 1655–1668. doi: 10.1002/dneu.20535.
- Hyson, R. L. (2005). The analysis of interaural time differences in the chick brain stem. *Physiol. Behav.* 86, 297–305. doi: 10.1016/j.physbeh.2005.08.003.
- Ishihama, Y., Oda, Y., Tabata, T., Sato, T., Nagasu, T., Rappsilber, J., et al. (2005). Exponentially Modified Protein Abundance Index (emPAI) for Estimation of Absolute Protein Amount in Proteomics by the Number of Sequenced Peptides per Protein. *Mol. Cell. Proteomics* 4, 1265–1272. doi: 10.1074/mcp.M500061-MCP200.
- Jeffress, L. A. (1948). A place theory of sound localization. *J. Comp. Physiol. Psychol.* 41, 35–39. doi: 10.1037/h0061495.
- Jeppesen, D. K., Hvam, M. L., Primdahl-Bengtson, B., Boysen, A. T., Whitehead, B., Dyrskjøt, L., et al. (2014). Comparative analysis of discrete exosome fractions obtained by differential centrifugation. *J. Extracell. Vesicles* 3. doi: 10.3402/jev.v3.25011.
- Jhaveri, S., and Morest, D. K. (1982a). Neuronal architecture in nucleus magnocellularis of the chicken auditory system with observations on nucleus laminaris: a light and electron microscope study. *Neuroscience* 7, 809–836.
- Jhaveri, S., and Morest, D. K. (1982b). Sequential alterations of neuronal architecture in nucleus magnocellularis of the developing chicken: A golgi study. *Neuroscience* 7, 837–853. doi: 10.1016/0306-4522(82)90046-X.
- Jhaveri, S., and Morest, D. K. (1982c). Sequential alterations of neuronal architecture in nucleus magnocellularis of the developing chicken: An electron microscope study. *Neuroscience* 7, 855–870. doi: 10.1016/0306-4522(82)90047-1.

- Johnsson, P., Lipovich, L., Grandér, D., and Morris, K. V. (2014). Evolutionary conservation of long noncoding RNAs; sequence, structure, function. *Biochim. Biophys. Acta* 1840, 1063–1071. doi: 10.1016/j.bbagen.2013.10.035.
- Joseph, A. W., and Hyson, R. L. (1993). Coincidence detection by binaural neurons in the chick brain stem. *J. Neurophysiol.* 69, 1197–1211. doi: 10.1152/jn.1993.69.4.1197.
- Julien, O., and Wells, J. A. (2017). Caspases and their substrates. *Cell Death Differ.* 24, 1380–1389. doi: 10.1038/cdd.2017.44.
- Julien, O., Zhuang, M., Wiita, A. P., O'Donoghue, A. J., Knudsen, G. M., Craik, C. S., et al. (2016). Quantitative MS-based enzymology of caspases reveals distinct protein substrate specificities, hierarchies, and cellular roles. *Proc. Natl. Acad. Sci.* 113, E2001–E2010. doi: 10.1073/pnas.1524900113.
- Kandler, K., Clause, A., and Noh, J. (2009). Tonotopic reorganization of developing auditory brainstem circuits. *Nat. Neurosci.* 12, 711–717. doi: 10.1038/nn.2332.
- Kaplan, A., Kent, C. B., Charron, F., and Fournier, A. E. (2014). Switching Responses: Spatial and Temporal Regulators of Axon Guidance. *Mol. Neurobiol.* 49, 1077–1086. doi: 10.1007/s12035-013-8582-8.
- Karakas, D., and Ozpolat, B. (2021). The Role of LncRNAs in Translation. *Non-Coding RNA* 7, 16. doi: 10.3390/ncrna7010016.
- Karpievitch, Y. V., Dabney, A. R., and Smith, R. D. (2012). Normalization and missing value imputation for label-free LC-MS analysis. *BMC Bioinformatics* 13, S5. doi: 10.1186/1471-2105-13-S16-S5.
- Kavanagh, E., Rodhe, J., Burguillos, M. A., Venero, J. L., and Joseph, B. (2014). Regulation of caspase-3 processing by ciAP2 controls the switch between pro-inflammatory activation and cell death in microglia. *Cell Death Dis.* 5, e1565–e1565. doi: 10.1038/cddis.2014.514.
- Keerthikumar, S., Chisanga, D., Ariyaratne, D., Al Saffar, H., Anand, S., Zhao, K., et al. (2016). ExoCarta: A Web-Based Compendium of Exosomal Cargo. *J. Mol. Biol.* 428, 688–692. doi: 10.1016/j.jmb.2015.09.019.
- Kellermeyer, R., Heydman, L. M., Mastick, G. S., and Kidd, T. (2018). The Role of Apoptotic Signaling in Axon Guidance. *J. Dev. Biol.* 6, 24. doi: 10.3390/jdb6040024.
- Khatri, N., Gilbert, J. P., Huo, Y., Sharafliari, R., Nee, M., Qiao, H., et al. (2018). The Autism Protein Ube3A/E6AP Remodels Neuronal Dendritic Arborization via Caspase-Dependent Microtubule Destabilization. *J. Neurosci.* 38, 363–378. doi: 10.1523/JNEUROSCI.1511-17.2017.
- Kim, K. M., Abdelmohsen, K., Mustapic, M., Kapogiannis, D., and Gorospe, M. (2017a). RNA in extracellular vesicles. *WIREs RNA* 8, e1413. doi: 10.1002/wrna.1413.

- Kim, S. B., Kim, H. R., Park, M. C., Cho, S., Goughnour, P. C., Han, D., et al. (2017b). Caspase-8 controls the secretion of inflammatory lysyl-tRNA synthetase in exosomes from cancer cells. *J Cell Biol* 216, 2201–2216. doi: 10.1083/jcb.201605118.
- Kołat, D., Hammouz, R., Bednarek, A. K., and Płuciennik, E. (2019). Exosomes as carriers transporting long non-coding RNAs: Molecular characteristics and their function in cancer. *Mol. Med. Rep.* 20, 851–862. doi: 10.3892/mmr.2019.10340.
- Kole, A. J., Annis, R. P., and Deshmukh, M. (2013). Mature neurons: equipped for survival. *Cell Death Dis.* 4, e689–e689. doi: 10.1038/cddis.2013.220.
- Koppers, M., Cagnetta, R., Shigeoka, T., Wunderlich, L. C., Vallejo-Ramirez, P., Qiaojin Lin, J., et al. (2019). Receptor-specific interactome as a hub for rapid cue-induced selective translation in axons. *eLife* 8, e48718. doi: 10.7554/eLife.48718.
- Köppl, C. (1994). Auditory nerve terminals in the cochlear nucleus magnocellularis: Differences between low and high frequencies. *J. Comp. Neurol.* 339, 438–446. doi: 10.1002/cne.903390310.
- Köppl, C., and Carr, C. E. (2008). Maps of interaural time difference in the chicken's brainstem nucleus laminaris. *Biol. Cybern.* 98, 541–559. doi: 10.1007/s00422-008-0220-6.
- Korotkevich, G., Sukhov, V., Budin, N., Shpak, B., Artyomov, M. N., and Sergushichev, A. (2021). Fast gene set enrichment analysis. 060012. doi: 10.1101/060012.
- Korthauer, K., Kimes, P. K., Duvallet, C., Reyes, A., Subramanian, A., Teng, M., et al. (2019). A practical guide to methods controlling false discoveries in computational biology. *Genome Biol.* 20, 118. doi: 10.1186/s13059-019-1716-1.
- Kossinova, O. A., Gopanenko, A. V., Tamkovich, S. N., Krasheninina, O. A., Tupikin, A. E., Kiseleva, E., et al. (2017). Cytosolic YB-1 and NSUN2 are the only proteins recognizing specific motifs present in mRNAs enriched in exosomes. *Biochim. Biophys. Acta BBA - Proteins Proteomics* 1865, 664–673. doi: 10.1016/j.bbapap.2017.03.010.
- Kowal, J., Arras, G., Colombo, M., Jouve, M., Morath, J. P., Primdal-Bengtson, B., et al. (2016). Proteomic comparison defines novel markers to characterize heterogeneous populations of extracellular vesicle subtypes. *Proc. Natl. Acad. Sci.* 113, E968–E977. doi: 10.1073/pnas.1521230113.
- Kretz, M., Siprashvili, Z., Chu, C., Webster, D. E., Zehnder, A., Qu, K., et al. (2013). Control of somatic tissue differentiation by the long non-coding RNA TINCR. *Nature* 493, 231–235. doi: 10.1038/nature11661.
- Kubke, M. F., Gilland, E., and Baker, R. (1998). Lipophilic Dye Labeling Distinguishes Segregated Central Components of the Eighth Cranial Nerve in Embryonic Chicken. *Biol. Bull.* 195, 218–220. doi: 10.2307/1542848.
- Kumar, S., and Cieplak, P. (2018). Effect of phosphorylation and single nucleotide polymorphisms on caspase substrates processing. *Apoptosis Int. J. Program. Cell Death* 23, 194–200. doi: 10.1007/s10495-018-1442-2.

- Kuo, R. I., Tseng, E., Eory, L., Paton, I. R., Archibald, A. L., and Burt, D. W. (2017). Normalized long read RNA sequencing in chicken reveals transcriptome complexity similar to human. *BMC Genomics* 18, 323. doi: 10.1186/s12864-017-3691-9.
- Lachica, E. A., Rübtsamen, R., and Rubel, E. W. (1994). GABAergic terminals in nucleus magnocellularis and laminaris originate from the superior olivary nucleus. *J. Comp. Neurol.* 348, 403–418. doi: 10.1002/cne.903480307.
- Lafourcade, C., Ramírez, J. P., Luarte, A., Fernández, A., and Wyneken, U. (2016). MIRNAS in Astrocyte-Derived Exosomes as Possible Mediators of Neuronal Plasticity: Supplementary Issue: Brain Plasticity and Repair. *J. Exp. Neurosci.* doi: 10.4137/JEN.S39916.
- Lagarde, J., Uszczyńska-Ratajczak, B., Carbonell, S., Pérez-Lluch, S., Abad, A., Davis, C., et al. (2017). High-throughput annotation of full-length long noncoding RNAs with capture long-read sequencing. *Nat. Genet.* 49, 1731–1740. doi: 10.1038/ng.3988.
- Lancaster, H. O. (1961). Significance Tests in Discrete Distributions. *J. Am. Stat. Assoc.* 56, 223–234. doi: 10.2307/2282247.
- Lee, S. J., Osés-Prieto, J. A., Kawaguchi, R., Sahoo, P. K., Kar, A. N., Rozenbaum, M., et al. (2018). hnRNPs Interacting with mRNA Localization Motifs Define Axonal RNA Regulons. *Mol. Cell. Proteomics* 17, 2091–2106. doi: 10.1074/mcp.RA118.000603.
- Leidal, A. M., and Debnath, J. (2020). Unraveling the mechanisms that specify molecules for secretion in extracellular vesicles. *Methods* 177, 15–26. doi: 10.1016/j.ymeth.2020.01.008.
- Leidal, A. M., Huang, H. H., Marsh, T., Solvik, T., Zhang, D., Ye, J., et al. (2020). The LC3-conjugation machinery specifies the loading of RNA-binding proteins into extracellular vesicles. *Nat. Cell Biol.* 22, 187–199. doi: 10.1038/s41556-019-0450-y.
- Li, C., Jiao, G., Wu, W., Wang, H., Ren, S., Zhang, L., et al. (2019). Exosomes from Bone Marrow Mesenchymal Stem Cells Inhibit Neuronal Apoptosis and Promote Motor Function Recovery via the Wnt/ $\beta$ -catenin Signaling Pathway. *Cell Transplant.* 28, 1373–1383. doi: 10.1177/0963689719870999.
- Li, H., Handsaker, B., Wysoker, A., Fennell, T., Ruan, J., Homer, N., et al. (2009). The Sequence Alignment/Map format and SAMtools. *Bioinformatics* 25, 2078–2079. doi: 10.1093/bioinformatics/btp352.
- Li, J., Briehner, W. M., Scimone, M. L., Kang, S. J., Zhu, H., Yin, H., et al. (2007). Caspase-11 regulates cell migration by promoting Aip1–Cofilin-mediated actin depolymerization. *Nat. Cell Biol.* 9, 276. doi: 10.1038/ncb1541.
- Li, J., Han, T., Wang, X., Wang, Y., and Yang, Q. (2021). Identification of novel survival-related lncRNA-miRNA-mRNA competing endogenous RNA network associated with immune infiltration in colorectal cancer. *Am. J. Transl. Res.* 13, 5815–5834.
- Li, Y., Syed, J., and Sugiyama, H. (2016). RNA-DNA Triplex Formation by Long Noncoding RNAs. *Cell Chem. Biol.* 23, 1325–1333. doi: 10.1016/j.chembiol.2016.09.011.

- Li, Z., Jo, J., Jia, J.-M., Lo, S.-C., Whitcomb, D. J., Jiao, S., et al. (2010). Caspase-3 activation via mitochondria is required for long-term depression and AMPA receptor internalization. *Cell* 141, 859–871. doi: 10.1016/j.cell.2010.03.053.
- Li, Z., Okamoto, K.-I., Hayashi, Y., and Sheng, M. (2004). The Importance of Dendritic Mitochondria in the Morphogenesis and Plasticity of Spines and Synapses. *Cell* 119, 873–887. doi: 10.1016/j.cell.2004.11.003.
- Liberzon, A., Subramanian, A., Pinchback, R., Thorvaldsdóttir, H., Tamayo, P., and Mesirov, J. P. (2011). Molecular signatures database (MSigDB) 3.0. *Bioinformatics* 27, 1739–1740. doi: 10.1093/bioinformatics/btr260.
- Lipovsek, M., and Wingate, R. J. (2018). Conserved and divergent development of brainstem vestibular and auditory nuclei. *eLife* 7, e40232. doi: 10.7554/eLife.40232.
- Liu, Y., Gervasi, C., and Szaro, B. G. (2008). A crucial role for hnRNP K in axon development in *Xenopus laevis*. *Dev. Camb. Engl.* 135, 3125–3135. doi: 10.1242/dev.022236.
- Liu, Y., Song, B., Wei, Y., Chen, F., Chi, Y., Fan, H., et al. (2018). Exosomes from mesenchymal stromal cells enhance imatinib-induced apoptosis in human leukemia cells via activation of caspase signaling pathway. *Cytotherapy* 20, 181–188. doi: 10.1016/j.jcyt.2017.11.006.
- Loo, G. van, Saelens, X., Matthijssens, F., Schotte, P., Beyaert, R., Declercq, W., et al. (2002). Caspases are not localized in mitochondria during life or death. *Cell Death Differ.* 9, 1207. doi: 10.1038/sj.cdd.4401101.
- Lorenz, R., Bernhart, S. H., Höner zu Siederdissen, C., Tafer, H., Flamm, C., Stadler, P. F., et al. (2011). ViennaRNA Package 2.0. *Algorithms Mol. Biol.* 6, 26. doi: 10.1186/1748-7188-6-26.
- Lötvall, J., Hill, A. F., Hochberg, F., Buzás, E. I., Di Vizio, D., Gardiner, C., et al. (2014). Minimal experimental requirements for definition of extracellular vesicles and their functions: a position statement from the International Society for Extracellular Vesicles. *J. Extracell. Vesicles* 3. doi: 10.3402/jev.v3.26913.
- Love, M. I., Huber, W., and Anders, S. (2014). Moderated estimation of fold change and dispersion for RNA-seq data with DESeq2. *Genome Biol.* 15, 550. doi: 10.1186/s13059-014-0550-8.
- Love, M. I., Soneson, C., and Patro, R. (2018). Swimming downstream: statistical analysis of differential transcript usage following Salmon quantification. doi: 10.12688/f1000research.15398.3.
- Luo, T., Chen, S.-Y., Qiu, Z.-X., Miao, Y.-R., Ding, Y., Pan, X.-Y., et al. (2022). Transcriptomic Features in a Single Extracellular Vesicle via Single-Cell RNA Sequencing. *Small Methods*, e2200881. doi: 10.1002/smt.202200881.
- Lüthi, A. U., and Martin, S. J. (2007). The CASBAH: a searchable database of caspase substrates. *Cell Death Differ.* 14, 641–650. doi: 10.1038/sj.cdd.4402103.

- Luz, I., and Cooks, T. (2019). Extracellular vesicles: what secrets do they hold inside? *Cell Death Dis.* 10, 1–2. doi: 10.1038/s41419-019-1643-9.
- Ma, Y., Dong, L., Zhou, D., Li, L., Zhang, W., Zhen, Y., et al. (2019). Extracellular vesicles from human umbilical cord mesenchymal stem cells improve nerve regeneration after sciatic nerve transection in rats. *J. Cell. Mol. Med.* 23, 2822–2835. doi: 10.1111/jcmm.14190.
- Maas, S. L. N., Breakefield, X. O., and Weaver, A. M. (2017). Extracellular vesicles: unique intercellular delivery vehicles. *Trends Cell Biol.* 27, 172–188. doi: 10.1016/j.tcb.2016.11.003.
- Maciag, J. J., Mackenzie, S. H., Tucker, M. B., Schipper, J. L., Swartz, P., and Clark, A. C. (2016). Tunable allosteric library of caspase-3 identifies coupling between conserved water molecules and conformational selection. *Proc. Natl. Acad. Sci. U. S. A.* 113, E6080–E6088. doi: 10.1073/pnas.1603549113.
- Maddelein, D., Colaert, N., Buchanan, I., Hulstaert, N., Gevaert, K., and Martens, L. (2015). The iceLogo web server and SOAP service for determining protein consensus sequences. *Nucleic Acids Res.* 43, W543–W546. doi: 10.1093/nar/gkv385.
- Madison, R. D., and Robinson, G. A. (2019). Muscle-Derived Extracellular Vesicles Influence Motor Neuron Regeneration Accuracy. *Neuroscience* 419, 46–59. doi: 10.1016/j.neuroscience.2019.08.028.
- Maluch, I., Grzyska, J., Snipas, S. J., Salvesen, G. S., and Drag, M. (2021). Evaluation of the effects of phosphorylation of synthetic peptide substrates on their cleavage by caspase-3 and -7. *Biochem. J.* 478, 2233–2245. doi: 10.1042/BCJ20210255.
- Marín, F., and Puelles, L. (1995). Morphological Fate of Rhombomeres in Quail/Chick Chimeras: A Segmental Analysis of Hindbrain Nuclei. *Eur. J. Neurosci.* 7, 1714–1738. doi: 10.1111/j.1460-9568.1995.tb00693.x.
- Mashima, T., Naito, M., Noguchi, K., Miller, D. K., Nicholson, D. W., and Tsuruo, T. (1997). Actin cleavage by CPP-32/apopain during the development of apoptosis. *Oncogene* 14, 1007–1012. doi: 10.1038/sj.onc.1200919.
- Mashima, T., Naito, M., and Tsuruo, T. (1999). Caspase-mediated cleavage of cytoskeletal actin plays a positive role in the process of morphological apoptosis. *Oncogene* 18, 2423–2430. doi: 10.1038/sj.onc.1202558.
- Mateescu, B., Kowal, E. J. K., van Balkom, B. W. M., Bartel, S., Bhattacharyya, S. N., Buzás, E. I., et al. (2017). Obstacles and opportunities in the functional analysis of extracellular vesicle RNA – an ISEV position paper. *J. Extracell. Vesicles* 6, 1286095. doi: 10.1080/20013078.2017.1286095.
- Mathivanan, S., Fahner, C. J., Reid, G. E., and Simpson, R. J. (2012). ExoCarta 2012: database of exosomal proteins, RNA and lipids. *Nucleic Acids Res.* 40, D1241–D1244. doi: 10.1093/nar/gkr828.
- Mathivanan, S., and Simpson, R. J. (2009). ExoCarta: A compendium of exosomal proteins and RNA. *PROTEOMICS* 9, 4997–5000. doi: 10.1002/pmic.200900351.

- McCullagh, E. A., Rotschafer, S. E., Auerbach, B. D., Klug, A., Kaczmarek, L. K., Cramer, K. S., et al. (2020). Mechanisms underlying auditory processing deficits in Fragile X syndrome. *FASEB J.* 34, 3501–3518. doi: 10.1096/fj.201902435R.
- McGurk, K. A., Dagliati, A., Chiasserini, D., Lee, D., Plant, D., Baricevic-Jones, I., et al. (2020). The use of missing values in proteomic data-independent acquisition mass spectrometry to enable disease activity discrimination. *Bioinforma. Oxf. Engl.* 36, 2217–2223. doi: 10.1093/bioinformatics/btz898.
- McStay, G. P. (2016). “In Vitro Use of Peptide Based Substrates and Inhibitors of Apoptotic Caspases,” in *Programmed Cell Death Methods in Molecular Biology*. (Humana Press, New York, NY), 57–67. doi: 10.1007/978-1-4939-3581-9\_5.
- Melé, M., Mattioli, K., Mallard, W., Shechner, D. M., Gerhardinger, C., and Rinn, J. L. (2017). Chromatin environment, transcriptional regulation, and splicing distinguish lincRNAs and mRNAs. *Genome Res.* 27, 27–37. doi: 10.1101/gr.214205.116.
- Ming, G., Wong, S. T., Henley, J., Yuan, X., Song, H., Spitzer, N. C., et al. (2002). Adaptation in the chemotactic guidance of nerve growth cones. *Nature* 417, 411–418. doi: 10.1038/nature745.
- Miron, O., Delgado, R. E., Delgado, C. F., Simpson, E. A., Yu, K.-H., Gutierrez, A., et al. (2021). Prolonged Auditory Brainstem Response in Universal Hearing Screening of Newborns with Autism Spectrum Disorder. *Autism Res. Off. J. Int. Soc. Autism Res.* 14, 46–52. doi: 10.1002/aur.2422.
- Miura, M. (2012). Apoptotic and Nonapoptotic Caspase Functions in Animal Development. *Cold Spring Harb. Perspect. Biol.* 4, a008664. doi: 10.1101/cshperspect.a008664.
- Mukherjee, A., and Williams, D. W. (2017). More alive than dead: non-apoptotic roles for caspases in neuronal development, plasticity and disease. *Cell Death Differ.* 24, 1411–1421. doi: 10.1038/cdd.2017.64.
- Nakajima, Y., and Kuranaga, E. (2017). Caspase-dependent non-apoptotic processes in development. *Cell Death Differ.* 24, 1422–1430. doi: 10.1038/cdd.2017.36.
- Nakhaei, P., Sun, Q., Solis, M., Mesplede, T., Bonneil, E., Paz, S., et al. (2012). I $\kappa$ B Kinase  $\epsilon$ -Dependent Phosphorylation and Degradation of X-Linked Inhibitor of Apoptosis Sensitizes Cells to Virus-Induced Apoptosis. *J. Virol.* 86, 726–737. doi: 10.1128/JVI.05989-11.
- Nelken, I. (2008). Processing of complex sounds in the auditory system. *Curr. Opin. Neurobiol.* 18, 413–417. doi: 10.1016/j.conb.2008.08.014.
- Nguyen, T. T. M., Gillet, G., and Popgeorgiev, N. (2021). Caspases in the Developing Central Nervous System: Apoptosis and Beyond. *Front. Cell Dev. Biol.* 9, 1910. doi: 10.3389/fcell.2021.702404.
- O'Brien, K., Breyne, K., Ughetto, S., Laurent, L. C., and Breakefield, X. O. (2020). RNA delivery by extracellular vesicles in mammalian cells and its applications. *Nat. Rev. Mol. Cell Biol.*, 1–22. doi: 10.1038/s41580-020-0251-y.

- Ohmori, H. (2014). Neuronal specializations for the processing of interaural difference cues in the chick. *Front. Neural Circuits* 8. doi: 10.3389/fncir.2014.00047.
- Ohsawa, S., Hamada, S., Asou, H., Kuida, K., Uchiyama, Y., Yoshida, H., et al. (2009). Caspase-9 Activation Revealed by Semaphorin 7A Cleavage Is Independent of Apoptosis in the Aged Olfactory Bulb. *J. Neurosci.* 29, 11385–11392. doi: 10.1523/JNEUROSCI.4780-08.2009.
- Ohsawa, S., Hamada, S., Kuida, K., Yoshida, H., Igaki, T., and Miura, M. (2010). Maturation of the olfactory sensory neurons by Apaf-1/caspase-9-mediated caspase activity. *Proc. Natl. Acad. Sci.* 107, 13366–13371. doi: 10.1073/pnas.0910488107.
- Onódi, Z., Pelyhe, C., Terézia Nagy, C., Brenner, G. B., Almási, L., Kittel, Á., et al. (2018). Isolation of High-Purity Extracellular Vesicles by the Combination of Iodixanol Density Gradient Ultracentrifugation and Bind-Elute Chromatography From Blood Plasma. *Front. Physiol.* 9. doi: 10.3389/fphys.2018.01479.
- Overholt, E. M., Rubel, E. W., and Hyson, R. L. (1992). A circuit for coding interaural time differences in the chick brainstem. *J. Neurosci.* 12, 1698–1708. doi: 10.1523/JNEUROSCI.12-05-01698.1992.
- Paraskevopoulou, M. D., and Hatzigeorgiou, A. G. (2016). Analyzing MiRNA-LncRNA Interactions. *Methods Mol. Biol. Clifton NJ* 1402, 271–286. doi: 10.1007/978-1-4939-3378-5\_21.
- Park, S. J., Kim, J. M., Kim, J., Hur, J., Park, S., Kim, K., et al. (2018). Molecular mechanisms of biogenesis of apoptotic exosome-like vesicles and their roles as damage-associated molecular patterns. *Proc. Natl. Acad. Sci.* 115, E11721–E11730. doi: 10.1073/pnas.1811432115.
- Parks, T. N., and Jackson, H. (1984). A developmental gradient of dendritic loss in the avian cochlear nucleus occurring independently of primary afferents. *J. Comp. Neurol.* 227, 459–466. doi: 10.1002/cne.902270315.
- Parks, T. N., and Rubel, E. W. (1975). Organization and development of brain stem auditory nuclei of the chicken: Organization of projections from N. magnocellularis to N. laminaris. *J. Comp. Neurol.* 164, 435–448. doi: 10.1002/cne.901640404.
- Parks, T. N., and Rubel, E. W. (1978). Organization and development of the brain stem auditory nuclei of the chicken: Primary afferent projections. *J. Comp. Neurol.* 180, 439–448. doi: 10.1002/cne.901800303.
- Patro, R., Duggal, G., Love, M. I., Irizarry, R. A., and Kingsford, C. (2017). Salmon: fast and bias-aware quantification of transcript expression using dual-phase inference. *Nat. Methods* 14, 417–419. doi: 10.1038/nmeth.4197.
- Pecoraro, V., Rosina, A., and Polacek, N. (2022). Ribosome-Associated ncRNAs (rancRNAs) Adjust Translation and Shape Proteomes. *Non-Coding RNA* 8, 22. doi: 10.3390/ncrna8020022.

- Pereira, N. A., and Song, Z. (2008). Some commonly used caspase substrates and inhibitors lack the specificity required to monitor individual caspase activity. *Biochem. Biophys. Res. Commun.* 377, 873–877. doi: 10.1016/j.bbrc.2008.10.101.
- Perez-Riverol, Y., Csordas, A., Bai, J., Bernal-Llinares, M., Hewapathirana, S., Kundu, D. J., et al. (2019). The PRIDE database and related tools and resources in 2019: improving support for quantification data. *Nucleic Acids Res.* 47, D442–D450. doi: 10.1093/nar/gky1106.
- Person, A. L., Cerretti, D. P., Pasquale, E. B., Rubel, E. W., and Cramer, K. S. (2004). Tonotopic gradients of Eph family proteins in the chick nucleus laminaris during synaptogenesis. *J. Neurobiol.* 60, 28–39. doi: 10.1002/neu.10330.
- Poręba, M., Stróżyk, A., Salvesen, G. S., and Drąg, M. (2013). Caspase Substrates and Inhibitors. *Cold Spring Harb. Perspect. Biol.* 5. doi: 10.1101/cshperspect.a008680.
- Rajendran, L., Bali, J., Barr, M. M., Court, F. A., Krämer-Albers, E.-M., Picou, F., et al. (2014). Emerging Roles of Extracellular Vesicles in the Nervous System. *J. Neurosci.* 34, 15482–15489. doi: 10.1523/JNEUROSCI.3258-14.2014.
- Rajendran, L., Honsho, M., Zahn, T. R., Keller, P., Geiger, K. D., Verkade, P., et al. (2006). Alzheimer's disease  $\beta$ -amyloid peptides are released in association with exosomes. *Proc. Natl. Acad. Sci. U. S. A.* 103, 11172–11177. doi: 10.1073/pnas.0603838103.
- Rajman, M., and Schrott, G. (2017). MicroRNAs in neural development: from master regulators to fine-tuners. *Development* 144, 2310–2322. doi: 10.1242/dev.144337.
- Rapicavoli, N. A., Poth, E. M., and Blackshaw, S. (2010). The long noncoding RNA RNCR2 directs mouse retinal cell specification. *BMC Dev. Biol.* 10, 49. doi: 10.1186/1471-213X-10-49.
- Raposo, G., and Stoorvogel, W. (2013). Extracellular vesicles: Exosomes, microvesicles, and friends. *J Cell Biol* 200, 373–383. doi: 10.1083/jcb.201211138.
- Rappsilber, J., Mann, M., and Ishihama, Y. (2007). Protocol for micro-purification, enrichment, pre-fractionation and storage of peptides for proteomics using StageTips. *Nat. Protoc.* 2, 1896–1906. doi: 10.1038/nprot.2007.261.
- Rawlings, N. D., Barrett, A. J., and Bateman, A. (2010). MEROPS: the peptidase database. *Nucleic Acids Res.* 38, D227–D233. doi: 10.1093/nar/gkp971.
- Rawlings, N. D., Barrett, A. J., Thomas, P. D., Huang, X., Bateman, A., and Finn, R. D. (2018). The MEROPS database of proteolytic enzymes, their substrates and inhibitors in 2017 and a comparison with peptidases in the PANTHER database. *Nucleic Acids Res.* 46, D624–D632. doi: 10.1093/nar/gkx1134.
- Rinn, J. L., Kertesz, M., Wang, J. K., Squazzo, S. L., Xu, X., Brugmann, S. A., et al. (2007). Functional Demarcation of Active and Silent Chromatin Domains in Human HOX Loci by Noncoding RNAs. *Cell* 129, 1311–1323. doi: 10.1016/j.cell.2007.05.022.

- Robinson, M. D., McCarthy, D. J., and Smyth, G. K. (2010). edgeR: a Bioconductor package for differential expression analysis of digital gene expression data. *Bioinformatics* 26, 139–140. doi: 10.1093/bioinformatics/btp616.
- Rotschafer, S. E., Allen-Sharp, M. R., and Cramer, K. S. (2016). Axonal Cleaved Caspase-3 Regulates Axon Targeting and Morphogenesis in the Developing Auditory Brainstem. *Front. Neural Circuits* 10. doi: 10.3389/fncir.2016.00084.
- Rubel, E. W., and Parks, T. N. (1975). Organization and development of brain stem auditory nuclei of the chicken: Tonotopic organization of N. magnocellularis and N. laminaris. *J. Comp. Neurol.* 164, 411–433. doi: 10.1002/cne.901640403.
- Rubel, E. W., and Parks, T. N. (1988). Organization and development of the avian brainstem auditory system. in.
- Rubel, E. W., Smith, D. J., and Miller, L. C. (1976). Organization and development of brain stem auditory nuclei of the chicken: Ontogeny of N. magnocellularis and N. laminaris. *J. Comp. Neurol.* 166, 469–489. doi: 10.1002/cne.901660408.
- Rubel, E. W., Smith, D. J., and Miller, L. C. (2004). Organization and development of brain stem auditory nuclei of the chicken: Ontogeny of N. magnocellularis and N. laminaris. *J. Comp. Neurol.* 166, 469–489. doi: 10.1002/cne.901660408.
- Ryugo, D. K., and Parks, T. N. (2003). Primary innervation of the avian and mammalian cochlear nucleus. *Brain Res. Bull.* 60, 435–456. doi: 10.1016/S0361-9230(03)00049-2.
- Santangelo, L., Giurato, G., Cicchini, C., Montaldo, C., Mancone, C., Tarallo, R., et al. (2016). The RNA-Binding Protein SYNCRIP Is a Component of the Hepatocyte Exosomal Machinery Controlling MicroRNA Sorting. *Cell Rep.* 17, 799–808. doi: 10.1016/j.celrep.2016.09.031.
- Sato, K., Akiyama, M., and Sakakibara, Y. (2021). RNA secondary structure prediction using deep learning with thermodynamic integration. *Nat. Commun.* 12, 941. doi: 10.1038/s41467-021-21194-4.
- Schechter, I., and Berger, A. (1967). On the size of the active site in proteases. I. Papain. *Biochem. Biophys. Res. Commun.* 27, 157–162. doi: 10.1016/S0006-291X(67)80055-X.
- Schmitz, S. U., Grote, P., and Herrmann, B. G. (2016). Mechanisms of long noncoding RNA function in development and disease. *Cell. Mol. Life Sci.* 73, 2491–2509. doi: 10.1007/s00018-016-2174-5.
- Schroger, E. (1996). Interaural time and level differences: integrated or separated processing? *Hear. Res.* 96, 191–198. doi: 10.1016/0378-5955(96)00066-4.
- Schwerk, C., and Schulze-Osthoff, K. (2003). Non-apoptotic functions of caspases in cellular proliferation and differentiation. *Biochem. Pharmacol.* 66, 1453–1458. doi: 10.1016/S0006-2952(03)00497-0.

- Scott, F. L., Denault, J.-B., Riedl, S. J., Shin, H., Renatus, M., and Salvesen, G. S. (2005). XIAP inhibits caspase-3 and -7 using two binding sites: evolutionarily conserved mechanism of IAPs. *EMBO J.* 24, 645–655. doi: 10.1038/sj.emboj.7600544.
- Seaman, J. E., Julien, O., Lee, P. S., Rettenmaier, T. J., Thomsen, N. D., and Wells, J. A. (2016). Caspases: caspases can cleave after aspartate, glutamate and phosphoserine residues. *Cell Death Differ.* 23, 1717–1726. doi: 10.1038/cdd.2016.62.
- Seidl, A. H., Rubel, E. W., and Barría, A. (2014). Differential Conduction Velocity Regulation in Ipsilateral and Contralateral Collaterals Innervating Brainstem Coincidence Detector Neurons. *J. Neurosci.* 34, 4914–4919. doi: 10.1523/JNEUROSCI.5460-13.2014.
- Shamaa, O. R., Mitra, S., Gavrilin, M. A., and Wewers, M. D. (2015). Monocyte Caspase-1 Is Released in a Stable, Active High Molecular Weight Complex Distinct from the Unstable Cell Lysate-Activated Caspase-1. *PLOS ONE* 10, e0142203. doi: 10.1371/journal.pone.0142203.
- Sharma, P., Mesci, P., Carromeu, C., McClatchy, D. R., Schiapparelli, L., Yates, J. R., et al. (2019). Exosomes regulate neurogenesis and circuit assembly. *Proc. Natl. Acad. Sci.* 116, 16086–16094. doi: 10.1073/pnas.1902513116.
- Sharma, P., Schiapparelli, L., and Cline, H. T. (2013). Exosomes function in cell–cell communication during brain circuit development. *Curr. Opin. Neurobiol.* 23, 997–1004. doi: 10.1016/j.conb.2013.08.005.
- Sheybani, N., Bakhtiarizadeh, M. R., and Salehi, A. (2021). An integrated analysis of mRNAs, lncRNAs, and miRNAs based on weighted gene co-expression network analysis involved in bovine endometritis. *Sci. Rep.* 11, 18050. doi: 10.1038/s41598-021-97319-y.
- Shi, Y. (2004). Caspase activation, inhibition, and reactivation: A mechanistic view. *Protein Sci. Publ. Protein Soc.* 13, 1979–1987. doi: 10.1110/ps.04789804.
- Shurtleff, M. J., Temoche-Diaz, M. M., Karfilis, K. V., Ri, S., and Schekman, R. (2016). Y-box protein 1 is required to sort microRNAs into exosomes in cells and in a cell-free reaction. *eLife* 5, e19276. doi: 10.7554/eLife.19276.
- Silke, J., and Meier, P. (2013). Inhibitor of Apoptosis (IAP) Proteins—Modulators of Cell Death and Inflammation. *Cold Spring Harb. Perspect. Biol.* 5, a008730. doi: 10.1101/cshperspect.a008730.
- Simpson, R. J., Kalra, H., and Mathivanan, S. (2012). ExoCarta as a resource for exosomal research. *J. Extracell. Vesicles* 1. doi: 10.3402/jev.v1i0.18374.
- Sirois, I., Raymond, M.-A., Brassard, N., Cailhier, J.-F., Fedjaev, M., Hamelin, K., et al. (2011). Caspase-3-dependent export of TCTP: a novel pathway for antiapoptotic intercellular communication. *Cell Death Differ.* 18, 549–562. doi: 10.1038/cdd.2010.126.
- Slee, E. A., Adrain, C., and Martin, S. J. (2001). Executioner Caspase-3, -6, and -7 Perform Distinct, Non-redundant Roles during the Demolition Phase of Apoptosis. *J. Biol. Chem.* 276, 7320–7326. doi: 10.1074/jbc.M008363200.

- Smith, A., Storti, S., Lukose, R., and Jr, R. J. K. (2019). Structural and Functional Aberrations of the Auditory Brainstem in Autism Spectrum Disorder. *J. Am. Osteopath. Assoc.* 119, 41–50. doi: 10.7556/jaoa.2019.007.
- Smith, D. J., and Rubel, E. W. (1979). Organization and development of brain stem auditory nuclei of the chicken: Dendritic gradients in nucleus laminaris. *J. Comp. Neurol.* 186, 213–239. doi: 10.1002/cne.901860207.
- Smith, Z. D. J. (1981). Organization and development of brain stem auditory nuclei of the chicken: Dendritic development in N. Laminaris. *J. Comp. Neurol.* 203, 309–333. doi: 10.1002/cne.902030302.
- Sokolowski, J. D., Gamage, K. K., Heffron, D. S., LeBlanc, A. C., Deppmann, C. D., and Mandell, J. W. (2014). Caspase-mediated cleavage of actin and tubulin is a common feature and sensitive marker of axonal degeneration in neural development and injury. *Acta Neuropathol. Commun.* 2, 16. doi: 10.1186/2051-5960-2-16.
- Soni, I. V., and Hardy, J. A. (2021). Caspase-9 Activation of Procaspace-3 but Not Procaspace-6 Is Based on the Local Context of Cleavage Site Motifs and on Sequence. *Biochemistry* 60, 2824–2835. doi: 10.1021/acs.biochem.1c00459.
- Sork, H., Corso, G., Krjutskov, K., Johansson, H. J., Nordin, J. Z., Wiklander, O. P. B., et al. (2018). Heterogeneity and interplay of the extracellular vesicle small RNA transcriptome and proteome. *Sci. Rep.* 8, 10813. doi: 10.1038/s41598-018-28485-9.
- Srinivasula, S. M., and Ashwell, J. D. (2008). IAPs: What's in a Name? *Mol. Cell* 30, 123–135. doi: 10.1016/j.molcel.2008.03.008.
- Statello, L., Guo, C.-J., Chen, L.-L., and Huarte, M. (2021). Gene regulation by long non-coding RNAs and its biological functions. *Nat. Rev. Mol. Cell Biol.* 22, 96–118. doi: 10.1038/s41580-020-00315-9.
- Statello, L., Maugeri, M., Garre, E., Nawaz, M., Wahlgren, J., Papadimitriou, A., et al. (2018). Identification of RNA-binding proteins in exosomes capable of interacting with different types of RNA: RBP-facilitated transport of RNAs into exosomes. *PLOS ONE* 13, e0195969. doi: 10.1371/journal.pone.0195969.
- Stennicke, H. R., Ratus, M., Meldal, M., and Salvesen, G. S. (2000). Internally quenched fluorescent peptide substrates disclose the subsite preferences of human caspases 1, 3, 6, 7 and 8. *Biochem. J.* 350 Pt 2, 563–568.
- Stranska, R., Gysbrechts, L., Wouters, J., Vermeersch, P., Bloch, K., Dierickx, D., et al. (2018). Comparison of membrane affinity-based method with size-exclusion chromatography for isolation of exosome-like vesicles from human plasma. *J. Transl. Med.* 16, 1. doi: 10.1186/s12967-017-1374-6.
- Subramanian, A., Tamayo, P., Mootha, V. K., Mukherjee, S., Ebert, B. L., Gillette, M. A., et al. (2005). Gene set enrichment analysis: A knowledge-based approach for interpreting genome-wide expression profiles. *Proc. Natl. Acad. Sci.* 102, 15545–15550. doi: 10.1073/pnas.0506580102.

- Sun, E., and Shi, Y. (2015). MicroRNAs: Small molecules with big roles in neurodevelopment and diseases. *Exp. Neurol.* 268, 46–53. doi: 10.1016/j.expneurol.2014.08.005.
- Suzuki, Y., Nakabayashi, Y., Nakata, K., Reed, J. C., and Takahashi, R. (2001). X-linked Inhibitor of Apoptosis Protein (XIAP) Inhibits Caspase-3 and -7 in Distinct Modes. *J. Biol. Chem.* 276, 27058–27063. doi: 10.1074/jbc.M102415200.
- Talanian, R. V., Quinlan, C., Trautz, S., Hackett, M. C., Mankovich, J. A., Banach, D., et al. (1997). Substrate Specificities of Caspase Family Proteases. *J. Biol. Chem.* 272, 9677–9682. doi: 10.1074/jbc.272.15.9677.
- Talge, N. M., Adkins, M., Kileny, P. R., and Frownfelter, I. (2021). Click-evoked auditory brainstem responses and autism spectrum disorder: a meta-analytic investigation of disorder specificity. *Pediatr. Res.*, 1–7. doi: 10.1038/s41390-021-01730-0.
- Talge, N. M., Tudor, B. M., and Kileny, P. R. (2018). Click-evoked auditory brainstem responses and autism spectrum disorder: A meta-analytic review. *Autism Res. Off. J. Int. Soc. Autism Res.* 11, 916–927. doi: 10.1002/aur.1946.
- Thelen, M. P., and Kye, M. J. (2020). The Role of RNA Binding Proteins for Local mRNA Translation: Implications in Neurological Disorders. *Front. Mol. Biosci.* 6. doi: 10.3389/fmolb.2019.00161.
- Théry, C., Boussac, M., Véron, P., Ricciardi-Castagnoli, P., Raposo, G., Garin, J., et al. (2001). Proteomic Analysis of Dendritic Cell-Derived Exosomes: A Secreted Subcellular Compartment Distinct from Apoptotic Vesicles. *J. Immunol.* 166, 7309–7318. doi: 10.4049/jimmunol.166.12.7309.
- Théry, C., Witwer, K. W., Aikawa, E., Alcaraz, M. J., Anderson, J. D., Andriantsitohaina, R., et al. (2018a). Minimal information for studies of extracellular vesicles 2018 (MISEV2018): a position statement of the International Society for Extracellular Vesicles and update of the MISEV2014 guidelines. *J. Extracell. Vesicles* 7, 1535750. doi: 10.1080/20013078.2018.1535750.
- Théry, C., Witwer, K. W., Aikawa, E., Alcaraz, M. J., Anderson, J. D., Andriantsitohaina, R., et al. (2018b). Minimal information for studies of extracellular vesicles 2018 (MISEV2018): a position statement of the International Society for Extracellular Vesicles and update of the MISEV2014 guidelines. *J. Extracell. Vesicles* 7, 1535750. doi: 10.1080/20013078.2018.1535750.
- Thijssen, M. S., Bintz, J., and Arnes, L. (2021). “In Vitro Silencing of lncRNA Expression Using siRNAs,” in *Long Non-Coding RNAs in Cancer Methods in Molecular Biology.*, ed. A. Navarro (New York, NY: Springer US), 141–156. doi: 10.1007/978-1-0716-1581-2\_9.
- Thomas, M. E., Grinshpon, R., Swartz, P., and Clark, A. C. (2018). Modifications to a common phosphorylation network provide individualized control in caspases. *J. Biol. Chem.* 293, 5447–5461. doi: 10.1074/jbc.RA117.000728.
- Thornberry, N. A., Rano, T. A., Peterson, E. P., Rasper, D. M., Timkey, T., Garcia-Calvo, M., et al. (1997). A Combinatorial Approach Defines Specificities of Members of the Caspase

- Family and Granzyme B. *J. Biol. Chem.* 272, 17907–17911. doi: 10.1074/jbc.272.29.17907.
- Timmer, J. C., and Salvesen, G. S. (2007). Caspase substrates. *Cell Death Differ.* 14, 66–72. doi: 10.1038/sj.cdd.4402059.
- Tong, X., Hong, X., Xie, J., and Liu, S. (2020). CPPred-sORF: Coding Potential Prediction of sORF based on non-AUG. 2020.03.31.017525. doi: 10.1101/2020.03.31.017525.
- Tong, X., and Liu, S. (2019). CPPred: coding potential prediction based on the global description of RNA sequence. *Nucleic Acids Res.* 47, e43. doi: 10.1093/nar/gkz087.
- Torres, M., Becquet, D., Guillen, S., Boyer, B., Moreno, M., Blanchard, M.-P., et al. (2018). RNA Pull-down Procedure to Identify RNA Targets of a Long Non-coding RNA. *J. Vis. Exp. JoVE*, 57379. doi: 10.3791/57379.
- Towbin, H., Staehelin, T., and Gordon, J. (1979). Electrophoretic transfer of proteins from polyacrylamide gels to nitrocellulose sheets: procedure and some applications. *Proc. Natl. Acad. Sci. U. S. A.* 76, 4350–4354.
- Tözsér, J., Bagossi, P., Zahuczky, G., Specht, S. I., Majerova, E., and Copeland, T. D. (2003). Effect of caspase cleavage-site phosphorylation on proteolysis. *Biochem. J.* 372, 137–143. doi: 10.1042/BJ20021901.
- Trokovic, N., Pöllänen, R., Porola, P., Stegaev, V., Hetzel, U., Tivesten, Å., et al. (2012). Exosomal secretion of death bullets: a new way of apoptotic escape? *Am. J. Physiol.-Endocrinol. Metab.* 303, E1015–E1024. doi: 10.1152/ajpendo.00139.2012.
- Tsang, A. H. K., Lee, Y.-I., Ko, H. S., Savitt, J. M., Pletnikova, O., Troncoso, J. C., et al. (2009). S-nitrosylation of XIAP compromises neuronal survival in Parkinson's disease. *Proc. Natl. Acad. Sci.* 106, 4900–4905. doi: 10.1073/pnas.0810595106.
- Turchinovich, A., Drapkina, O., and Tonevitsky, A. (2019). Transcriptome of Extracellular Vesicles: State-of-the-Art. *Front. Immunol.* 10. doi: 10.3389/fimmu.2019.00202.
- Turowec, J. P., Zukowski, S. A., Knight, J. D. R., Smalley, D. M., Graves, L. M., Johnson, G. L., et al. (2014). An Unbiased Proteomic Screen Reveals Caspase Cleavage Is Positively and Negatively Regulated by Substrate Phosphorylation. *Mol. Cell. Proteomics MCP* 13, 1184–1197. doi: 10.1074/mcp.M113.037374.
- Unsain, N., and Barker, P. A. (2015). New Views on the Misconstrued: Executioner Caspases and Their Diverse Non-apoptotic Roles. *Neuron* 88, 461–474. doi: 10.1016/j.neuron.2015.08.029.
- van Balkom, B. W. M., de Jong, O. G., Smits, M., Brummelman, J., den Ouden, K., de Bree, P. M., et al. (2013). Endothelial cells require miR-214 to secrete exosomes that suppress senescence and induce angiogenesis in human and mouse endothelial cells. *Blood* 121, 3997–4006. doi: 10.1182/blood-2013-02-478925.
- van Niel, G., D'Angelo, G., and Raposo, G. (2018). Shedding light on the cell biology of extracellular vesicles. *Nat. Rev. Mol. Cell Biol.* 19, 213–228. doi: 10.1038/nrm.2017.125.

- Vardaki, I., Sanchez, C., Fonseca, P., Olsson, M., Chioureas, D., Rassidakis, G., et al. (2016). Caspase-3–dependent cleavage of Bcl-xL in the stroma exosomes is required for their uptake by hematological malignant cells. *Blood* 128, 2655–2665. doi: 10.1182/blood-2016-05-715961.
- Vella, L. J., Scicluna, B. J., Cheng, L., Bawden, E. G., Masters, C. L., Ang, C.-S., et al. (2017). A rigorous method to enrich for exosomes from brain tissue. *J. Extracell. Vesicles* 6. doi: 10.1080/20013078.2017.1348885.
- Vestad, B., Llorente, A., Neurauder, A., Phuyal, S., Kierulf, B., Kierulf, P., et al. (2017). Size and concentration analyses of extracellular vesicles by nanoparticle tracking analysis: a variation study. *J. Extracell. Vesicles* 6. doi: 10.1080/20013078.2017.1344087.
- Victor, K. G., Heffron, D. S., Sokolowski, J. D., Majumdar, U., Leblanc, A., and Mandell, J. W. (2018). Proteomic identification of synaptic caspase substrates. *Synapse* 72, e22014. doi: 10.1002/syn.22014.
- Villarroya-Beltri, C., Gutiérrez-Vázquez, C., Sánchez-Cabo, F., Pérez-Hernández, D., Vázquez, J., Martín-Cofreces, N., et al. (2013). Sumoylated hnRNPA2B1 controls the sorting of miRNAs into exosomes through binding to specific motifs. *Nat. Commun.* 4, 2980. doi: 10.1038/ncomms3980.
- Vogel, R., Coumans, F. A. W., Maltesen, R. G., Böing, A. N., Bonnington, K. E., Broekman, M. L., et al. (2016). A standardized method to determine the concentration of extracellular vesicles using tunable resistive pulse sensing. *J. Extracell. Vesicles* 5, 31242. doi: 10.3402/jev.v5.31242.
- Walsh, J. G., Cullen, S. P., Sheridan, C., Lüthi, A. U., Gerner, C., and Martin, S. J. (2008). Executioner caspase-3 and caspase-7 are functionally distinct proteases. *Proc. Natl. Acad. Sci.* 105, 12815–12819. doi: 10.1073/pnas.0707715105.
- Wang, B., and Bao, L. (2017). Axonal microRNAs: localization, function and regulatory mechanism during axon development. *J. Mol. Cell Biol.* 9, 82–90. doi: 10.1093/jmcb/mjw050.
- Wang, J.-Y., and Luo, Z.-G. (2014). Non-apoptotic role of caspase-3 in synapse refinement. *Neurosci. Bull.* 30, 667–670. doi: 10.1007/s12264-014-1454-4.
- Wang, L., Fu, H., Nanayakkara, G., Li, Y., Shao, Y., Johnson, C., et al. (2016). Novel extracellular and nuclear caspase-1 and inflammasomes propagate inflammation and regulate gene expression: a comprehensive database mining study. *J. Hematol. Oncol. J Hematol Oncol* 9, 122. doi: 10.1186/s13045-016-0351-5.
- Wang, X., Hong, H., Brown, D. H., Sanchez, J. T., and Wang, Y. (2017). Distinct Neural Properties in the Low-Frequency Region of the Chicken Cochlear Nucleus Magnocellularis. *eNeuro* 4, ENEURO.0016-17.2017. doi: 10.1523/ENEURO.0016-17.2017.
- Weghorst, F., Mirzakhanyan, Y., Hernandez, K. L., Gershon, P. D., and Cramer, K. S. (2022). Non-Apoptotic Caspase Activity Preferentially Targets a Novel Consensus Sequence Associated With Cytoskeletal Proteins in the Developing Auditory Brainstem. *Front. Cell*

*Dev. Biol.* 10. Available at: <https://www.frontiersin.org/articles/10.3389/fcell.2022.844844> [Accessed September 13, 2022].

- Weghorst, F., Mirzakhanyan, Y., Samimi, K., Dhillon, M., Barzik, M., Cunningham, L. L., et al. (2020). Caspase-3 Cleaves Extracellular Vesicle Proteins During Auditory Brainstem Development. *Front. Cell. Neurosci.* 14. doi: 10.3389/fncel.2020.573345.
- Wei, R., Wang, J., Su, M., Jia, E., Chen, S., Chen, T., et al. (2018). Missing Value Imputation Approach for Mass Spectrometry-based Metabolomics Data. *Sci. Rep.* 8, 663. doi: 10.1038/s41598-017-19120-0.
- Wen, Z., Mai, Z., Zhu, X., Wu, T., Chen, Y., Geng, D., et al. (2020). Mesenchymal stem cell-derived exosomes ameliorate cardiomyocyte apoptosis in hypoxic conditions through microRNA144 by targeting the PTEN/AKT pathway. *Stem Cell Res. Ther.* 11, 36. doi: 10.1186/s13287-020-1563-8.
- Westerberg, B. D., and Schwarz, D. W. (1995). Connections of the superior olive in the chicken. *J. Otolaryngol.* 24, 20–30.
- Westphal, D., Sytnyk, V., Schachner, M., and Leshchyns'ka, I. (2010). Clustering of the Neural Cell Adhesion Molecule (NCAM) at the Neuronal Cell Surface Induces Caspase-8- and -3-dependent Changes of the Spectrin Meshwork Required for NCAM-mediated Neurite Outgrowth. *J. Biol. Chem.* 285, 42046–42057. doi: 10.1074/jbc.M110.177147.
- Wiegrefe, D., Alexander, D., Stadler, P. F., and Zeckzer, D. (2019). RNApuzzler: efficient outerplanar drawing of RNA-secondary structures. *Bioinformatics* 35, 1342–1349. doi: 10.1093/bioinformatics/bty817.
- Willison, K. R. (2018). The substrate specificity of eukaryotic cytosolic chaperonin CCT. *Philos. Trans. R. Soc. B Biol. Sci.* 373, 20170192. doi: 10.1098/rstb.2017.0192.
- Willms, E., Johansson, H. J., Mäger, I., Lee, Y., Blomberg, K. E. M., Sadik, M., et al. (2016). Cells release subpopulations of exosomes with distinct molecular and biological properties. *Sci. Rep.* 6, 22519. doi: 10.1038/srep22519.
- Witwer, K. W., Soekmadji, C., Hill, A. F., Wauben, M. H., Buzás, E. I., Di Vizio, D., et al. (2017). Updating the MISEV minimal requirements for extracellular vesicle studies: building bridges to reproducibility. *J. Extracell. Vesicles* 6. doi: 10.1080/20013078.2017.1396823.
- Wright, D. J., Hall, N. A. L., Irish, N., Man, A. L., Glynn, W., Mould, A., et al. (2022). Long read sequencing reveals novel isoforms and insights into splicing regulation during cell state changes. *BMC Genomics* 23, 42. doi: 10.1186/s12864-021-08261-2.
- Wright, K. M., Linhoff, M. W., Potts, P. R., and Deshmukh, M. (2004). Decreased apoptosome activity with neuronal differentiation sets the threshold for strict IAP regulation of apoptosis. *J. Cell Biol.* 167, 303–313. doi: 10.1083/jcb.200406073.
- Xia, B., Gao, J., Li, S., Huang, L., Ma, T., Zhao, L., et al. (2019). Extracellular Vesicles Derived From Olfactory Ensheathing Cells Promote Peripheral Nerve Regeneration in Rats. *Front. Cell. Neurosci.* 13, 548. doi: 10.3389/fncel.2019.00548.

- Xiao, Y., Geng, F., Wang, G., Li, X., Zhu, J., and Zhu, W. (2019). Bone marrow–derived mesenchymal stem cells–derived exosomes prevent oligodendrocyte apoptosis through exosomal miR-134 by targeting caspase-8. *J. Cell. Biochem.* 120, 2109–2118. doi: 10.1002/jcb.27519.
- Xin, H., Li, Y., Liu, Z., Wang, X., Shang, X., Cui, Y., et al. (2013). MiR-133b Promotes Neural Plasticity and Functional Recovery After Treatment of Stroke with Multipotent Mesenchymal Stromal Cells in Rats Via Transfer of Exosome-Enriched Extracellular Particles. *STEM CELLS* 31, 2737–2746. doi: 10.1002/stem.1409.
- Yáñez-Mó, M., Siljander, P. R.-M., Andreu, Z., Zavec, A. B., Borràs, F. E., Buzas, E. I., et al. (2015). Biological properties of extracellular vesicles and their physiological functions. *J. Extracell. Vesicles* 4. doi: 10.3402/jev.v4.27066.
- Yang, C., Yang, L., Zhou, M., Xie, H., Zhang, C., Wang, M. D., et al. (2018). LncADeep: an ab initio lncRNA identification and functional annotation tool based on deep learning. *Bioinforma. Oxf. Engl.* 34, 3825–3834. doi: 10.1093/bioinformatics/bty428.
- Yang, C., Zhou, M., Xie, H., and Zhu, H. (2021). LncADeep performance on full-length transcripts. *Nat. Mach. Intell.* 3, 197–198. doi: 10.1038/s42256-019-0108-2.
- Yang, L., Monsivais, P., and Rubel, E. W. (1999). The superior olivary nucleus and its influence on nucleus laminaris: A source of inhibitory feedback for coincidence detection in the avian auditory brainstem. *J. Neurosci.* 19, 2313–2325.
- Yang, L., Wu, X.-H., Wang, D., Luo, C.-L., and Chen, L.-X. (2013). Bladder cancer cell-derived exosomes inhibit tumor cell apoptosis and induce cell proliferation in vitro. *Mol. Med. Rep.* 8, 1272–1278. doi: 10.3892/mmr.2013.1634.
- Yang, Q., Diamond, M. P., and Al-Hendy, A. (2016). The Emerging Role of Extracellular Vesicle-Derived miRNAs: Implication in Cancer Progression and Stem Cell Related Diseases. *J. Clin. Epigenetics* 2. Available at: <https://clinical-epigenetics.imedpub.com/abstract/the-emerging-role-of-extracellular-vesicle-derived-mirnas-implication-in-cancer-progression-and-stem-cell-related-diseases-8370.html> [Accessed May 15, 2020].
- Yanshina, D. D., Kossinova, O. A., Gopanenko, A. V., Krasheninina, O. A., Malygin, A. A., Venyaminova, A. G., et al. (2018). Structural features of the interaction of the 3'-untranslated region of mRNA containing exosomal RNA-specific motifs with YB-1, a potential mediator of mRNA sorting. *Biochimie* 144, 134–143. doi: 10.1016/j.biochi.2017.11.007.
- Yao, L., Swartz, P., Hamilton, P. T., and Clark, A. C. (2021). Remodeling hydrogen bond interactions results in relaxed specificity of Caspase-3. *Biosci. Rep.* 41. doi: 10.1042/BSR20203495.
- Yin, T. C. T. (2002). “Neural Mechanisms of Encoding Binaural Localization Cues in the Auditory Brainstem,” in *Integrative Functions in the Mammalian Auditory Pathway* Springer Handbook of Auditory Research. (Springer, New York, NY), 99–159. doi: 10.1007/978-1-4757-3654-0\_4.

- Yin, Y., Yan, P., Lu, J., Song, G., Zhu, Y., Li, Z., et al. (2015). Opposing Roles for the lncRNA *Haut* and Its Genomic Locus in Regulating HOXA Gene Activation during Embryonic Stem Cell Differentiation. *Cell Stem Cell* 16, 504–516. doi: 10.1016/j.stem.2015.03.007.
- Zamaraev, A. V., Kopeina, G. S., Prokhorova, E. A., Zhivotovsky, B., and Lavrik, I. N. (2017). Post-translational Modification of Caspases: The Other Side of Apoptosis Regulation. *Trends Cell Biol.* 27, 322–339. doi: 10.1016/j.tcb.2017.01.003.
- Zappulli, V., Friis, K. P., Fitzpatrick, Z., Maguire, C. A., and Breakefield, X. O. (2016). Extracellular vesicles and intercellular communication within the nervous system. *J. Clin. Invest.* 126, 1198–1207. doi: 10.1172/JCI81134.
- Zhang, H., Freitas, D., Kim, H. S., Fabijanic, K., Li, Z., Chen, H., et al. (2018). Identification of distinct nanoparticles and subsets of extracellular vesicles by asymmetric flow field-flow fractionation. *Nat. Cell Biol.* 20, 332. doi: 10.1038/s41556-018-0040-4.
- Zhao, H., Zhang, X., Frazão, J. B., Condino-Neto, A., and Newburger, P. E. (2013). HOX antisense lincRNA HOXA-AS2 is an apoptosis repressor in all Trans retinoic acid treated NB4 promyelocytic leukemia cells. *J. Cell. Biochem.* 114, 2375–2383. doi: 10.1002/jcb.24586.
- Zhao, L., Luo, H., Li, X., Li, T., He, J., Qi, Q., et al. (2017). Exosomes Derived from Human Pulmonary Artery Endothelial Cells Shift the Balance between Proliferation and Apoptosis of Smooth Muscle Cells. *Cardiology* 137, 43–53. doi: 10.1159/000453544.
- Zhao, Y., Yin, L., Zhang, H., Lan, T., Li, S., and Ma, P. (2018). Eph/ephrin family anchored on exosome facilitate communications between cells. *Cell Biol. Int.* 42, 1458–1462. doi: 10.1002/cbin.10968.
- Zhou, G., and Chen, X. (2019). Emerging role of extracellular microRNAs and lncRNAs. *ExRNA* 1, 10. doi: 10.1186/s41544-019-0012-2.
- Zhu, A., Srivastava, A., Ibrahim, J. G., Patro, R., and Love, M. I. (2019). Nonparametric expression analysis using inferential replicate counts. *Nucleic Acids Res.* 47, e105. doi: 10.1093/nar/gkz622.
- Zuccotti, A., Lee, S. C., Campanelli, D., Singer, W., Satheesh, S. V., Patriarchi, T., et al. (2013). L-type CaV1.2 deletion in the cochlea but not in the brainstem reduces noise vulnerability: implication for CaV1.2-mediated control of cochlear BDNF expression. *Front. Mol. Neurosci.* 6, 20. doi: 10.3389/fnmol.2013.00020.